University of Nevada, Reno

A Comparison of Geochemistry, Carbonate Mineralogy, and Argillic Alteration between the Dome Prospect and the Main Au Resource of the Donlin Creek Project in Southwest Alaska

A thesis submitted in partial fulfillment of the
requirements for the degree of Master of Science in Geology

By

Heidi L. Drexler

Dr. Tommy B. Thompson/Thesis Advisor

Ralph J. Roberts Center for Research in Economic Geology

May, 2010

ProQuest LLC
789 East Eisenhower Parkway
P.O. Box 1346
Ann Arbor, MI 48106-1346

We recommend that the thesis
prepared under our supervision by

HEIDI L. DREXLER

entitled

A Comparison of Geochemistry, Carbonate Mineralogy, and Argillic Alteration between the Dome Prospect and the Main Au Resource of the Donlin Creek Project in Southwest Alaska

be accepted in partial fulfillment of the
requirements for the degree of

MASTER OF SCIENCE

Tommy B. Thompson, Ph.D., Advisor

Alan R. Wallace, Ph.D., Committee Member

Victor R. Vasquez, Ph.D., Graduate School Representative

Marsha H. Read, Ph.D., Associate Dean, Graduate School

May, 2010

Abstract

The Donlin Creek project, located in southwestern Alaska, contains a measured and indicated resource of ~35 Moz of Au, with an inferred resource of 4 Moz. This district is spatially associated with a base-metal prospect at Dome, 6 km to the north-northeast. Previous studies indicated differences in salinities, temperatures, and some isotopic signatures at Dome compared to the resource area. A paragenetic sequence showing the temporal relationship of through-going veins, sulfide and carbonate mineralogical associations, and sulfur, carbon, and oxygen isotopic analyses demonstrate the genetic relationship between these two dissimilar ore deposit types.

The precious-metal mineral assemblage is composed of auriferous arsenopyrite-pyrite ± stibnite, realgar, and native arsenic intimately associated with Fe-dolomite. Crystallization of euhedral arsenopyrite on porous pyrite-marcasite ± pyrrhotite grain boundaries, mainly in the resource area, demonstrates the late timing of the precious-metal minerals compared to the base-metal mineral assemblage. The base-metal district is noted for pyrrhotite-sphalerite-chalcopyrite-pyrite-marcasite ± tetrahedrite stockwork veins. Relative vein ages exhibited in this study further subdivide and identify the vein assemblages currently logged in the resource area. Diagrams of trace elements obtained from LA-ICP-MS indicate four carbonate phases within veins that formed before, during, and after gold deposition. These include an early calcite phase, which has only been observed at Dome; a pre-

mineralization manganiferous calcite event; Fe-dolomite, which is consistently found with auriferous arsenopyrite; and a late-stage post-mineralization ankerite phase. Diagrams of trace elements from LA-ICP-MS data also show two quartz phases that formed before and after gold deposition.

Previous studies have indicated overlapping sulfur ($\delta^{34}S$ -8 to -16‰) and carbon ($\delta^{13}C$ –4.6 to -13.4‰) isotopic data from the ACMA/Lewis resource area and the Dome prospect. Additional carbon ($\delta^{13}C$ 1.8 to -16.7‰) and oxygen ($\delta^{18}O$ 2.2 to 24.9‰) isotopic analyses completed in this study also show overlapping data. These data suggest similar origins and evolution patterns for the carbonate and sulfide mineralogies associated with the through-going veins, and they further imply a genetic relationship between the precious- and base-metal districts at Donlin Creek.

Carbonate staining methods show broad associations between manganiferous calcite ± ankerite and higher gold grades. Previous studies demonstrated that NH_4-illite alteration is strongly associated with gold intervals. These mineral indicators provide methods for gold exploration at Donlin Creek. Fifty-meter elevation maps illustrate kriging of gold grades and clay alteration data and they show NNE- and NW-trending spatial patterns consistent with the orientation of dikes and sills in the district.

The geochemical and mineralogical analyses completed prior to and in this study demonstrate the lateral relationship between the precious and base-metal districts. In addition, these methods provide information for further classification of this district. As such, this study concludes that the Donlin Creek precious-metal resource and closely located Dome base-metal assemblage fall into the high-level intrusion-related ore deposit-type that is characteristic of the Kuskokwim Mineral Belt.

Acknowledgements

This project is made possible by the Center for Research in Economic Geology (CREG) program directed by Tommy Thompson at the University of Nevada, Reno and by Donlin Creek, LLC under the supervision of Rich Harris. Many thanks are given to Tommy Thompson and Rich Harris for their guidance and patience. To committee members Alan Wallace and Victor Vasquez, I would like to thank for their guidance and advice. Wes Sherlock, a PhD student in the CREG program provided tremendous assistance and guidance throughout this project and I was fortunate to be able to work with him, thank you Wes. A special thanks to Shelley Harvey and Deborah Fisher for taking care of the CREG students at UNR. To my colleagues in the geology department at UNR, geologists and friends at Donlin Creek, and Dan McNeil and Karl Rittger I give many thanks for their support, ideas, discussions, and distractions. A special thanks to my family and my non-geology friends for their continuing encouragement, attempt to understand, and enthusiasm for my career.

Table of Contents

List of Figures

List of Tables

Chapter 1: Introduction

1.1 Introduction

Located 480 km west-northwest of Anchorage and 20 km from the Kuskokwim River (Fig. 1), the world-class porphyry-style gold deposit of Donlin Creek is a low-grade, high-tonnage deposit. As of April 2009, the deposit contains a proven and probable reserve estimate of 383.3 Mt at 2.37 g/t Au (29.27 Moz Au), a measured and indicated resource of 94.6 Mt at 1.98 g/t Au (6.01 Moz Au), and an inferred resource of 54.5 Mt at 2.29 g/t Au (4.02 Moz Au) (Nova Gold website 1/22/10). The property is jointly owned by Barrick Gold Corporation (50%) and NovaGold (50%) in a limited liability company called Donlin Creek, LLC. Ten mineralized areas have been defined in the current resource area: the ACMA (American Creek Magnetic Anomaly) region is comprised of five such areas, including the ACMA, East ACMA, 400 zone, Aurora, and Akivik prospects. The Lewis region includes the other five mineralized areas, including the North Lewis, South Lewis, Rochelieu, Vortex and Queen prospects. These two main regions cover the current resource area at Donlin Creek (Fig. 2) and are referred to as ACMA/Lewis for the remainder of this paper.

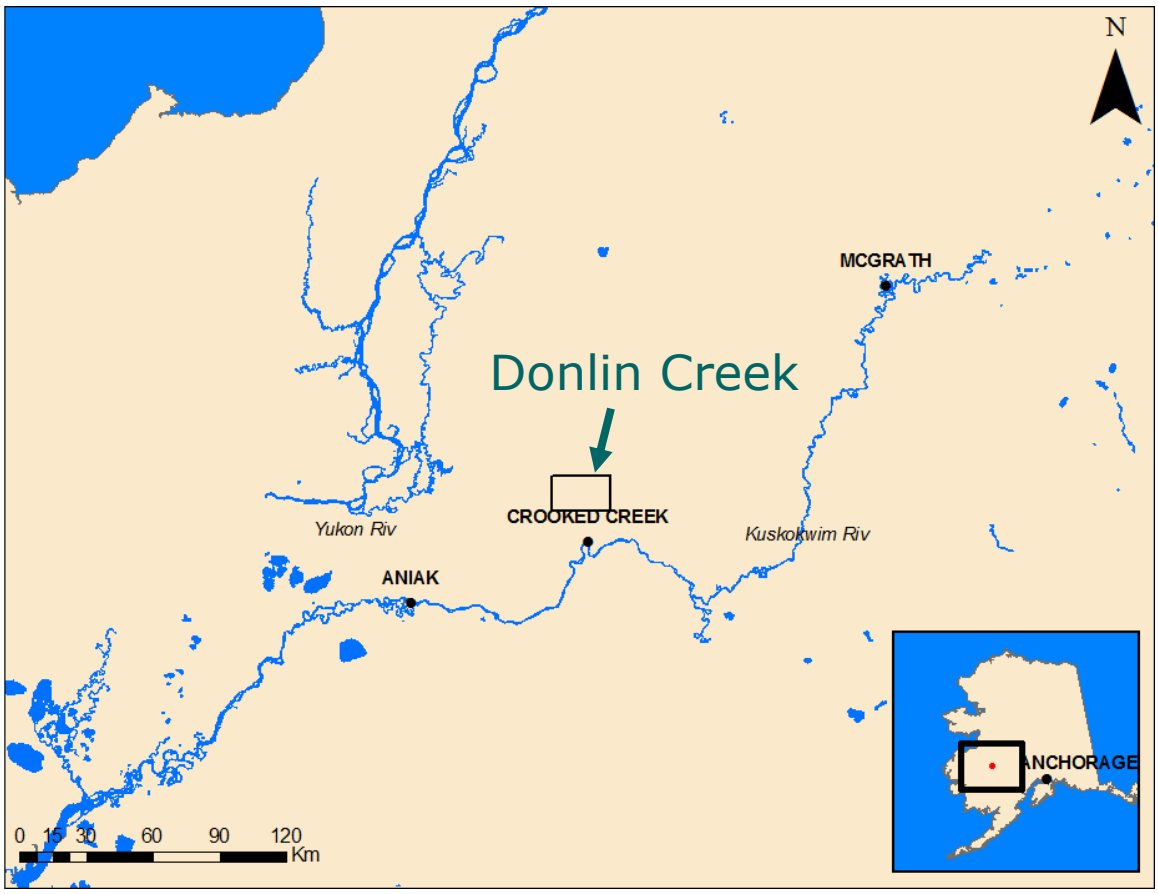

Figure 1. Location map of the Donlin Creek project in Alaska.

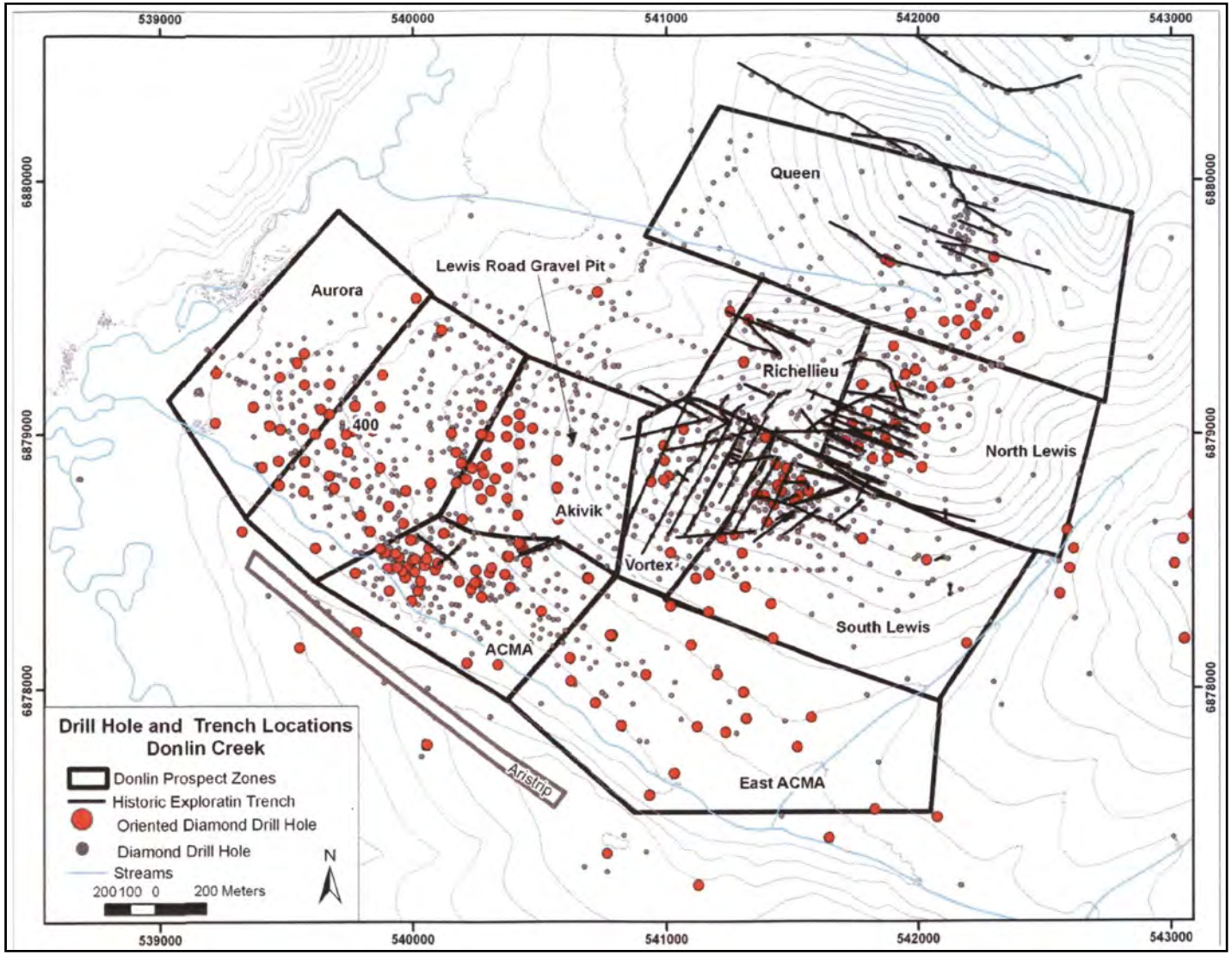

Figure 2. Map of the resource area showing the ten mineralized zones at Donlin Creek (MacNeil, 2009).

The ACMA/Lewis mineralization style has been classified as a low-temperature, low-sulfidation epithermal system in the NI-43-101. Goldfarb *et al.* (2004) argue for an orogenic origin of the system, Szumigala *et al.* (1999) suggest an intrusion-related system, and Ebert *et al.* (2003b) propose a reduced sub-epithermal deposit type for the resource area and a reduced porphyry Au classification for the Dome prospect. An Au-Ag-As-Hg-Rb-S-Se geochemical signature characterizes the higher grade zones at ACMA/Lewis, which commonly contains stibnite, realgar, and native arsenic (NI-43-101; this study). Gold occurs in the lattice structures of arsenopyrite and to a lesser extent in pyrite and marcasite grains (NI-43-101; Hillier, 2007). Arsenopyrite is disseminated within sheeted quartz and sulfide-rich veinlets and is present adjacent to veinlets and veinlet zones as well as in fractures or at structurally related contacts.

A higher temperature porphyry style system called Dome is located 6 km north-northeast of the ACMA/Lewis resource (Fig. 3). Dome has an early fracture-controlled stockwork system containing a deeper seated Te, Hg, Bi, As, and locally native gold signature (NI-43-101; this study). This prospect occurs along the same mineralized trend and the mineralized zones are contained within the same intrusive units as the resource at Donlin Creek. Salinity, temperature, ore formation age, base-metal content, and stable isotope differences have been reported by Goldfarb *et al.* (2004) and Piekenbrock *et al.* (2003), but the geologic association is still equivocal, particularly in light of their proximity. These geologic and genetic

differences and similarities provide preliminary evidence that either Dome is located closer to a shared common heat source or is a product of a different system not associated with the Donlin Creek deposit. Geochemical, carbonate mineralogy, and alteration patterns researched through this study will aid in establishing if the hydrothermal fluids associated with the gold deposition at ACMA/Lewis are also related to the emplacement of the base and precious-metals at Dome. These patterns will improve the current understanding of the epizonal system on a district scale and provide some empirical guides for exploration.

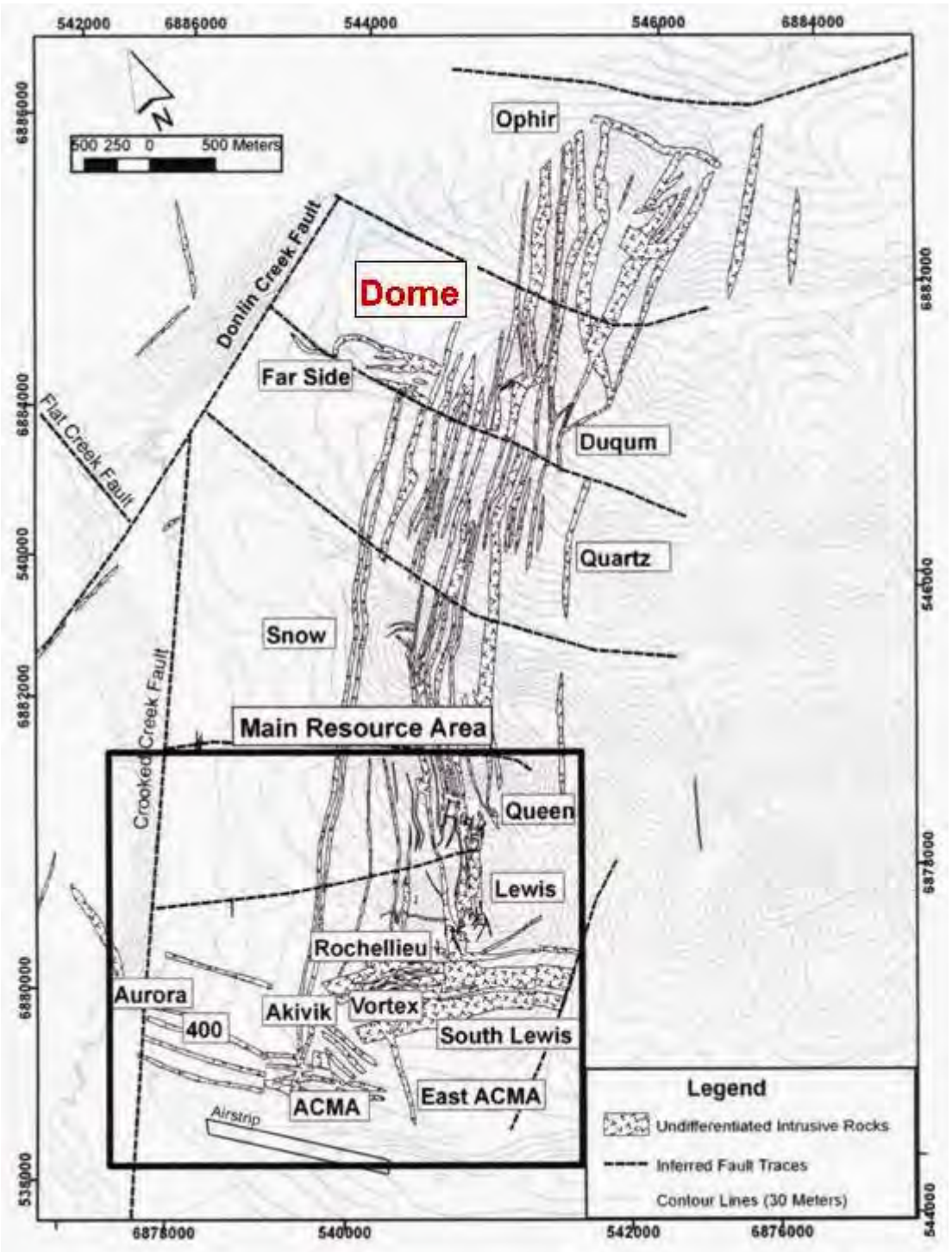

Figure 3. Location of Dome relative to the main resource area at Donlin Creek (modified from MacNeil, 2009).

1.2 Project History

The following paragraphs are summarized from the NI-43-101 provided by Nova Gold. Placer gold was discovered in the Donlin Creek district in 1909. Various prospectors and placer miners recovered approximately 30,000 ounces of gold from 1909 to 1956 outside the current ACMA/Lewis resource area by hand, underground, and hydraulic methods. Although the Lyman family continues to conduct placer mining in the area, the amount of gold recovered has not been recorded (Lyman, personal communication 07/2008). Resource Associates of Alaska, Westgold, Teck Exploration Ltd, and Calista Corporation conducted soil, rock, and trench sampling programs from 1974 to 1995 and identified anomalous gold values ranging from 2 to 20 ppm gold throughout the current resource area. Airborne geophysics, mapping, additional sampling, and the commencement of a drill program in the late 1980s identified eight prospects. Intense core drilling between 1995 and 2006 resulted in 242,256 meters of core and 29,477 meters of reverse circulation (RC) chips. This drilling led to the discovery and delineation of ACMA, expanded the resource initially discovered at Lewis, and uncovered a local calcium carbonate resource. Currently there are over 1800 core and RC drill holes on the property that support geological, metallurgical, geotechnical, engineering, and hydrological studies.

1.3 Project Objectives

The present study has two major goals. The first is to determine if the ACMA/Lewis and Dome deposits are parts of the same intrusive and mineralizing system possibly as distal and proximal end members, respectively, or if they are related to two

different intrusive and mineralizing systems. To answer that question, this study compares the geochemical, carbonate, and alteration patterns and associations with the metal deposits found at the ACMA/Lewis and Dome prospects. The results, both at each deposit and in the district as a whole, answer the original question about the genetic relationship, if any, between the two areas. The second major goal of this study is to use the geochemical and mineralogical trends to potentially develop district scale exploration guides.

1.4 Methodology

A series of drill holes were selected to represent district geology, styles and types of mineralized rocks, carbonate mineralogy, and argillic alteration along a transect that extends northeast of Dome to southwest of the ore resource at Donlin Creek (Fig. 4). One linear set of drill holes parallels the structural control of the districts mineralized zone and three other perpendicular linear sets of drill holes transect this structural control at Dome, Queen-Lewis, and ACMA. Past studies on hydrothermal systems reveal that argillic and sericitic alteration changes are commonly associated with these systems (Tommy Thompson, personal communication 2008). As such, this study may provide additional exploration tools that document the changes that took place within and around the mineralized zones at Donlin Creek.

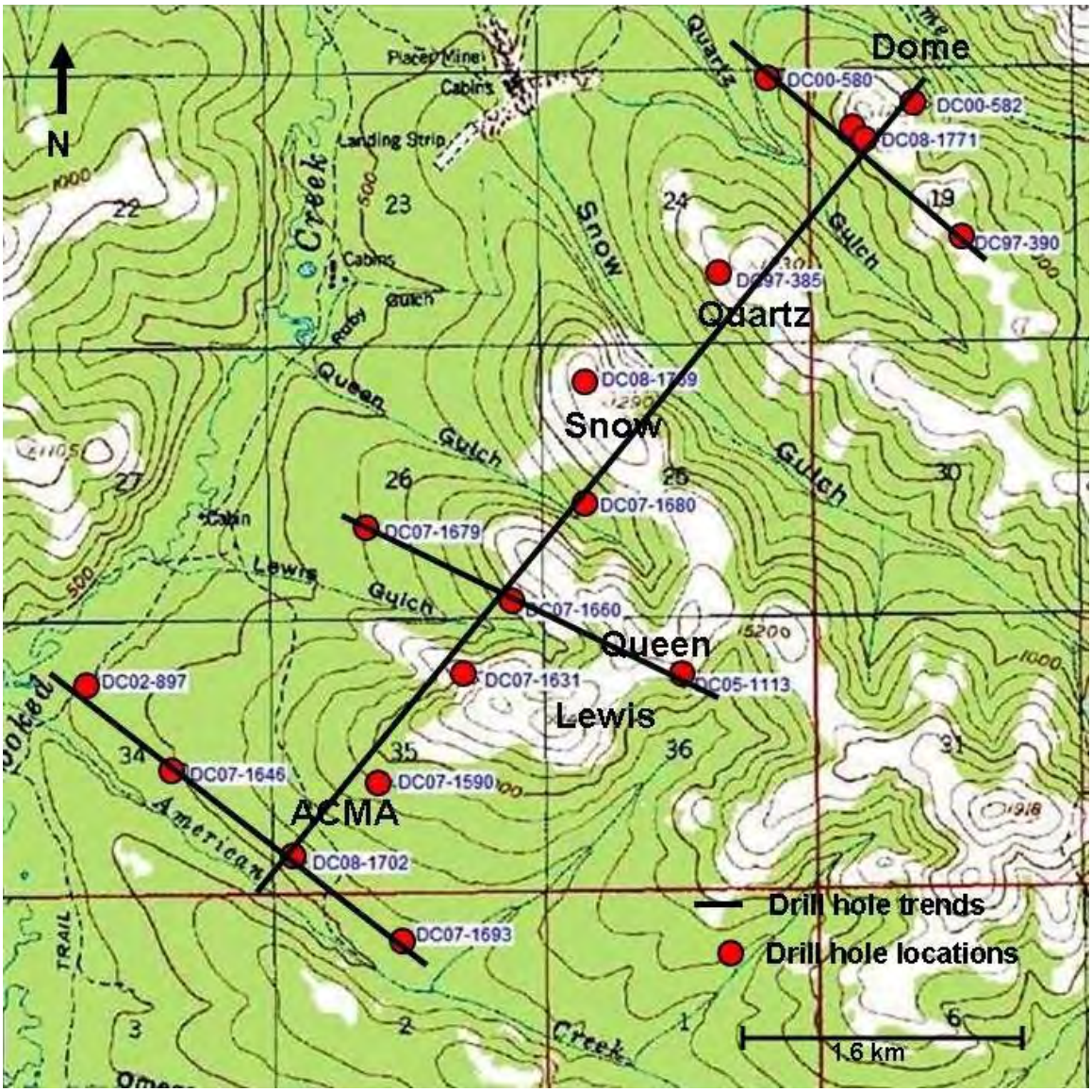

Figure 4. Drill holes selected for this project to represent the property from ACMA to Dome. The NE-SW transect is parallel to the intrusive units in the area and the other three transects are perpendicular to this trend to better understand the system along strike and its lateral extent.

1.4.1 Carbonate Mineralogy

Carbonate staining determines general carbonate mineralogy. A combination of alizarin red S, potassium ferricyanide, and 2% hydrochloric acid were "painted" along the length of drill core on fifteen of the seventeen (Fig. 4) representative drill holes. A blue stain reaction of veins, groundmass, and/or phenocrysts indicates the

presence of ferroan dolomite (Hitzman, 1999). A red signature depicts nonferrous calcite or aragonite, and purple implies ankerite (Fig. 5; Hitzman, 1999). Drill core sections were assigned a stain reaction color based on their groundmass and phenocrysts carbonate alteration. A section containing a strong blue stain reaction to the groundmass and phenocrysts is labeled blue. A section labeled red indicates a red reaction to the groundmass and the phenocrysts. A blue reaction to the groundmass and a red to purple reaction to the phenocrysts are labeled purple. Sections that exhibit a purple reaction to the groundmass with red or purple (rare) phenocrysts are also labeled purple. The stain reactions to any mineral containing iron are a shortcoming of this method and, locally, determining the carbonate composition within veins was difficult at a megascopic scale.

Figure 5. Pictures illustrating the reaction of alizarin red S, potassium ferricyanide, and hydrochloric acid on igneous and sedimentary rocks. Purple and red stain reactions (upper left) indicate ferroan-calcite and calcite and blue reactions (right) refer to ferroan dolomite or high Fe in sedimentary rocks.

Representative core hand samples were brought back to the University of Nevada, Reno (UNR) lab where binocular microscopy was used to observe cross-cutting

relationships between vein phases at a megascopic scale so representative samples could be chosen for further petrographic analysis. Detailed drawings (Appendix B) show the stain color reactions and cross cutting vein relationships.

Sixty-two thin sections were prepared from the core hand samples brought back from the project site. These samples included each of the different stain reaction colors, samples within and outside of high grade zones, and cross-cutting veins exhibiting different carbonate alterations. Reflected and transmitted light petrographic analyses were completed on these sections using an Olympus BX51 microscope. Photomicrographs illustrating the variety of carbonate textures and mineralogy were captured using an Olympus DP10 camera attached to the microscope. Thirteen representative samples of different carbonate textures and mineralogy were then analyzed using the JEOL 840A scanning electron microscope (SEM) on the UNR campus. These same samples were also analyzed by cathodoluminescence (CL) using a Nikon Labophot-pol and Luminoscope lab set up. This method was used as an alternative method of study during the time the UNR laser ablation system was impaired. Both the SEM and to a lesser extent the CL showed differences between carbonate phases, and further quantitative analyses were necessary to distinguish between the ferroan carbonates. Forty carbonate examples of different textures and mineralogy within vein phases, which included the 13 analyzed by the SEM and CL, and nine quartz vein samples, which were analyzed using a Photon Machines 193 excimer laser coupled to a Nu Instruments

"Attom" single collector inductively coupled plasma mass spectrometer (LA-ICP-MS) at the University of California, Santa Barbara. The data obtained through LA-ICP-MS methods were analyzed using correspondence analyses, correlation matrices, and regression analyses. Correspondence analyses represent the data spatially by choosing the two most important factors which show the highest percentage of data available. Regression analyses are a statistical analysis illustrating the elements that are statistically associated with the element of value, in this case gold.

Twenty-nine of the forty samples used for LA-ICP-MS analyses were used for carbon and oxygen isotope analysis. These samples were analyzed using the phosphoric acid reaction method described by McCrea (1950), with the exception of using a 90°C temperature. Analyses were performed using a Micromass MultiPrep preparation device interfaced with a Micromass IsoPrime stable isotope ratio mass spectrometer in dual inlet mode. $\delta^{13}C$ results are reported in units of ‰ vs. VPDB, and $\delta^{18}O$ results are reported in units of ‰ vs. VSMOW. An error of ±0.1‰ is used for both $\delta^{13}C$ and $\delta^{18}O$ values.

1.4.2 Geochemistry

Seventeen drill holes located on the transect between ACMA-Lewis and Dome and those transects perpendicular to these regions were resubmitted for "near-total" digestion method ME-MS61m, completed by ALS Chemex. These data were manipulated using correspondence analyses, correlation matrices, and regression analyses as described above. The remaining drill holes on the property that were

not chosen for the ME-MS61m analytical method were analyzed by fire assay with an atomic absorption finish for gold and by LECO induction furnaces for sulfur. Both of these methods were completed by ALS Chemex. Immobile element data obtained by the ME-MS61m method were plotted in scatter diagrams using Microsoft Excel to identify the relationship between the ACMA-Lewis and Dome districts.

1.4.3 Argillic Alteration

ASD TerraSpec Short Wave Infrared Spectrometer (SWIR) data were used to interpret igneous rock hosted clay alteration suites in drill core. Every 2 to 3 meters through the full length of the drill hole a relatively large phenocryst is chosen to represent the alteration within that interval. The sedimentary host rocks are too dark to be used effectively by the ASD-SWIR, as a consequence only the igneous units are analyzed with this method. These igneous units have been analyzed throughout the drilling history of the project from 1997 to 2008. These data were interpreted through an outside Barrick consultant and are currently available for analysis.

Ordinary quantile kriging methods using exponential semivariograms were used to interpret the gold data throughout the Donlin Creek district at 50 meter intervals. Clay alteration data collected by the ASD-SWIR were also plotted on these maps at 50 meter intervals illustrating the correlation of high gold grade zones and NH_4-illite.

2 Chapter 2: Regional and District Geology

2.1 Kuskokwim Mountain Geology

The Kuskokwim Mountain topography of southwestern Alaska is characterized as rolling hills, gentle slopes and highlands upwards of 1000 to 3000 feet above mean sea level (Wahrhaftig, 1994). This mountain range lies within a post-accretionary 70,000 km^2, southwest-oriented basin-fill flysch belt (Decker *et al.,* 1994; Silberling *et al.,* 1994; Kirschner, 1994; NI-43-101). Paleozoic to Mesozoic metamorphic rocks, an ophiolite sequence, and volcanic and sedimentary units crop out on the western side of the basin, and a continental margin sequence on the eastern edge of the basin, comprises the basement to the Kuskokwim Mountains (Miller *et al.,* 2002; Decker *et al.,* 1994). The 10-12 km thick Upper Cretaceous Kuskokwim Group sediments, with minor volcanic sequences overlie the basement and are largely composed of turbiditic, shallow marine sandstone and shale, and fluvial clastic deposits (Decker *et al.,* 1994; Goldfarb *et al.,* 2004; Miller *et al.,* 2002). Fossils within this sequence range in age from Cenomanian to Campanian or Maastrichtian (Late Cretaceous) (Miller *et al.,* 2002). Movement along the Iditarod-Nixon Fork fault from ~88 to ~71 Ma caused folding and steeply dipping NNE-trending normal faults and fractures in the Kuskokwim Group (Piekenbrock *et al.,* 2003; MacNeil, 2009). This structural preparation event allowed Late Cretaceous to Tertiary volcanic and plutonic sequences to intrude and overlie the Kuskokwim Group sediments (Bundtzen and Miller, 1997; Miller *et al.,* 2002; Piekenbrock *et al.,* 2003; Szumigala, 1996). Sub-alkaline to alkaline volcanic-plutonic complexes, subaerial calc-alkaline to alkaline andesitic to rhyodacitic volcanic fields, felsic to intermediate calc-alkaline

dikes, sills, and stocks, and minor intermediate to mafic dikes are the four main igneous rock types within these sequences (Bundtzen and Miller, 1997; Miller *et al.,* 2002; Piekenbrock *et al.,* 2003; Szumigala, 1996). Subsequent movement along the Iditarod-Nixon Fork fault forms additional NNE-trending fractures and microfractures within these igneous units again preparing the rocks for mineral deposition. Approximately 20 dikes, sills, and subarial volcanic units ranging from 8-650 km^2 occur along a northeast-trending orientation (Ebert, 2000; Goldfarb *et al.,* 2004, Miller *et al.,* 2002). Major and trace element data depict a typical arc-related calc-alkaline igneous rock series and suggest a common source for these volcanic-plutonic sequences (Szumigala, 1996). Petrographic and geochemical data suggest that the plutonic rocks within the Kuskokwim Mountain belt are both ilmenite series and I-type granites (Szumigala, 1996; Szumigala *et al.,* 1999).

2.2 Tectonic Evolution of SW Alaska

Satellite images, topographic maps, and aerial photos depict NE-striking NW-dipping structures that bracket the central Kuskokwim basin (Fig. 6; Goldfarb *et al.,* 2004; Piekenbrock *et al.,* 2003). To the north, the Iditarod-Nixon fork dextral fault forms a broad belt that extends 10-20 km wide. This fault shows an offset of >90 km (Goldfarb *et al.,* 2004; Piekenbrock *et al.,* 2003). South of Donlin Creek is the Denali-Farewell dextral fault, which exhibits an offset of 134-150 km (Goldfarb *et al.,* 2004; Piekenbrock *et al.,* 2003). These strike-slip faults were active between 90 and 58 Ma (Goldfarb *et al.,* 2004) and were accompanied by magmatism and ore deposition at ~70 Ma and ~58 Ma (Miller *et al.,* 2002). Magmatism and ore deposition also

occurred at ~30 Ma (Miller *et al.,* 2002). Dating of interbedded ash layers and igneous rocks within the Donlin Creek resource area constrain the deposition of the Kuskokwim Group sedimentary package to ~88 to ~71 Ma (MacNeil, 2009). Reactivation of the deep seated Iditarod-Nixon Fork and the Denali-Farewell faults divided the Kuskokwim Group sedimentary sequence into three basins: the Iditarod, the central Kuskokwim, and the Nashagak from the NW to the SE (Decker *et al.,* 1994; Goldfarb *et al.,* 2004; Piekenbrock *et al.,* 2003). A post-sedimentation NNE-SSW regional compression event resulting from subduction of the Kula plate beneath the North American plate created E-W folds and northward-directed thrust belts (Piekenbrock *et al.,* 2003; MacNeil, 2009). The Iditarod-Nixon Fork fault reactivated around 88 to ~71 Ma folding the Kuskokwim Group sedimentary rocks in the resource area to the NNE with SSW dips of 10-50° (Piekenbrock *et al.,* 2003; MacNeil. 2009). In addition to folding, NNE-oriented SE-dipping normal faults developed (MacNeil, 2009). Numerous Late Cretaceous rhyodacite dikes are parallel to and cut by the NE-striking Donlin fault zone, a steeply dipping strike-slip structure that is a splay off the much larger Iditarod-Nixon Fork fault (Goldfarb *et al.,* 2004; MacNeil, 2009). Gold mineralization dated around 71 Ma was deposited in steeply dipping, NE-striking fractures and is interpreted to be related to the intrusive events (MacNeil, 2009). Faults that were active after mineralization strike NE and NW and dip steeply to the NW and NE, respectively.

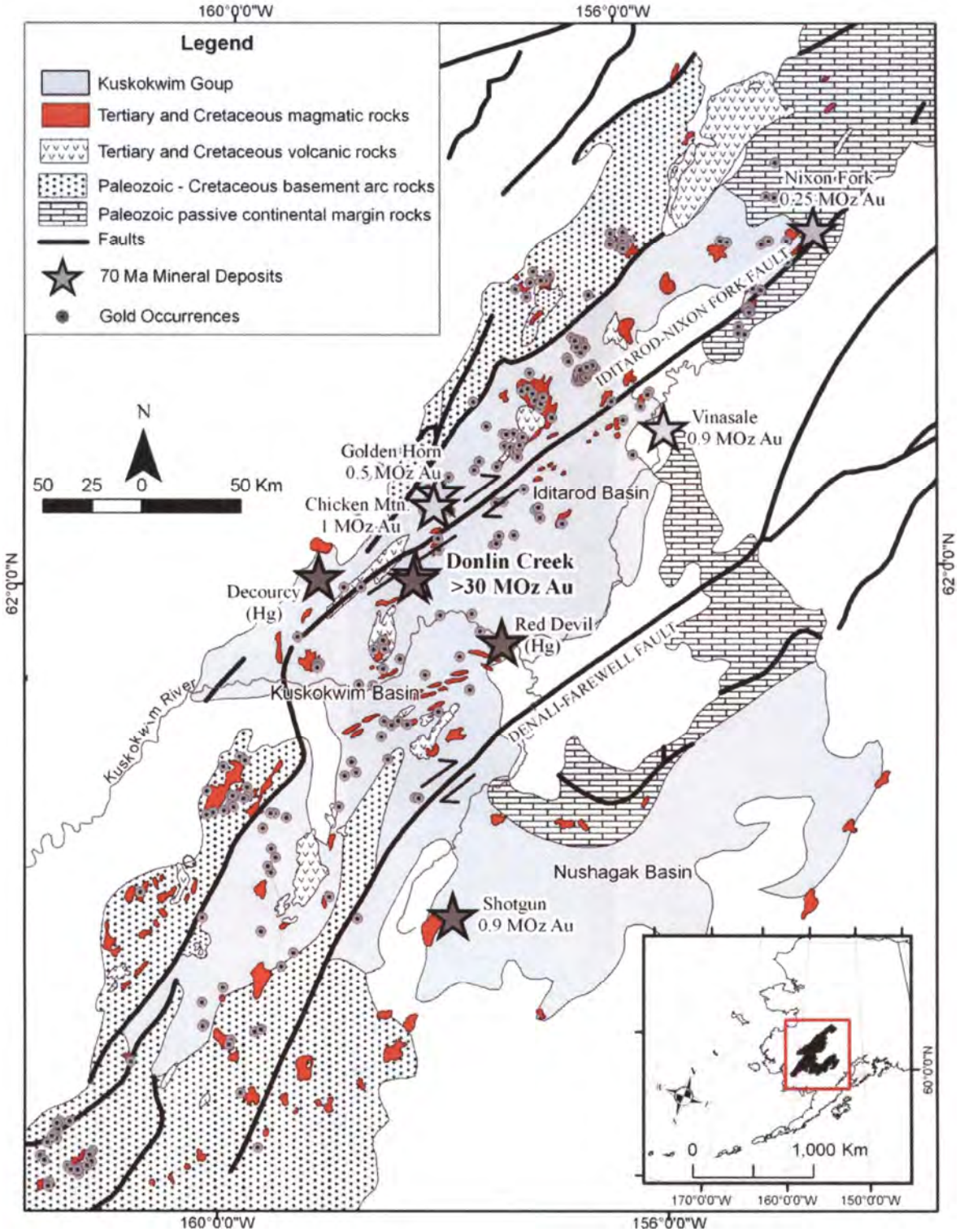

Figure 6. Location of the Iditarod-Nixon Fork fault and Denali-Farewell fault in comparison to Donlin Creek. Diagram also illustrates 70 Ma mineral deposits and other gold occurrences (MacNeil, 2009).

2.3 Kuskokwim Mountains Mineral Belt

A northeast-trending, 900 km by 200 km magmatic arc, also known as the Tintina Gold Belt (Fig. 7), formed in the Late Cretaceous with the collision of the Kula plate and the North American Plate (Goldfarb, 1997; Goldfarb *et al.,* 2000). Compression with local extension and magmatism largely shaped the Kuskokwim basin during this time. This magmatic event lasted ~20 m.y. and produced five deposit types: (1) copper-gold polymetallic stockwork, skarn, and vein deposits; (2) gold polymetallic bodies; (3) intrusion-related, boron-enriched silver-tin polymetallic breccia pipes and replacement bodies; (4) epithermal gold and silver veins; and (5) gold, polymetallic heavy mineral placer deposits in the Kuskokwim region (MacNeil, 2009; Fig. 6). Ten deposits related to Late Cretaceous-Early Tertiary intrusion event have an inferred gold reserve of 35.23 Moz, 6.46 Moz silver, 12,160 metric tons of tin, and 28,088 metric tons of copper with byproduct mercury, tungsten, and antimony (Bundtzen and Miller, 1997).

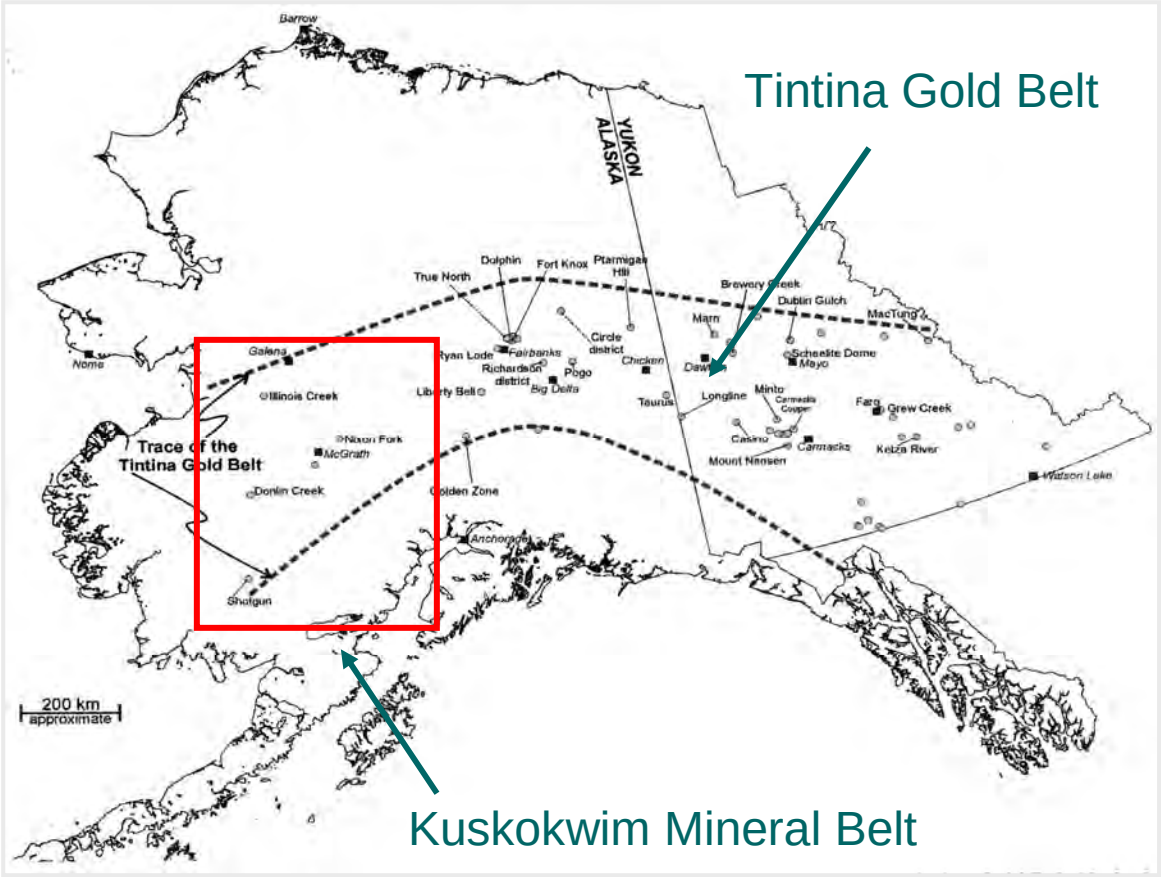

Figure 7. The Kuskokwim Mineral Belt within the Tintina Gold Belt (modified from Flanigan et al., 2000).

Szumigala (1996) studied gold deposits and their genetic relationship with spatially associated plutonic rocks in the Kuskokwim region. This region, termed the Kuskokwim Mineral Belt, is a sub-region of the Tintina Mineral Belt (Fig. 7). The ~1000 km long Tintina belt continues along the North American/Canadian Cordillera (Goldfarb *et al.,* 2000). The mineral deposits located in Canada are predominantly mesothermal vein systems with no clear link to magmatism, whereas the deposits in the Kuskokwim region are genetically associated to igneous intrusions and currently not classified as mesothermal systems (Goldfarb *et al.,* 2000). Szumigala's study (1996) concluded that hydrothermal systems within the

Kuskokwim region are vertically zoned, but can be laterally zoned at depths less than 3 km. Epithermal mercury vein deposits represent the upper portion, antimony deposits are at intermediate depths, followed downward by gold-rich systems, and into a base-metal-rich sequence at depth. Geochemically, the upper regions contain As, Sb, Ba, F, Hg, B and Tl signatures, while the lower regions have Cu, Pb, Zn, Mo, Au, Ag, Bi, Te, and Co (Fig. 8). An example of the upper portion of the zoning pattern can be observed at the Red Devil Mine, located along the Kuskokwim River in SW Alaska. This mine produced 35,000 flasks of mercury through the processing of cinnabar from 1923 to 1971, becoming the largest mercury producer in Alaska (AK Dept of Environmental Conservation March, 2009).

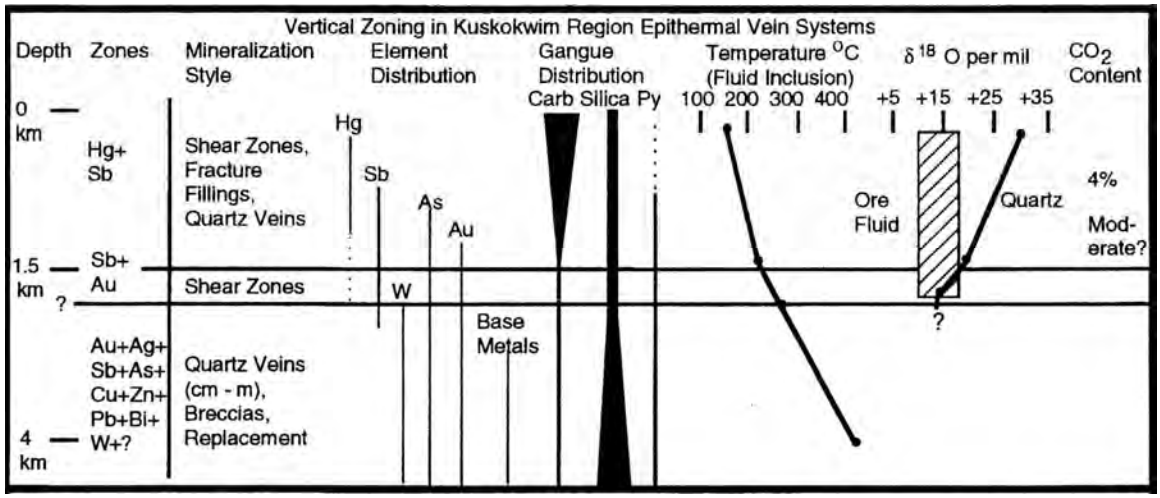

Figure 8. Vertical zoning characteristics of the Kuskokwim region epithermal vein systems (Szumigala, 1996).

Placer deposits have led to the discovery of most of the intrusion-related deposits in Alaska (Szumigala, 1996). In the Iditarod district (Golden Horn and Flat) alone, 48.5

tons of gold has been recovered and many of these deposits are spatially associated with igneous bodies (Goldfarb, 1997).

2.4 District Geology

2.4.1 Kuskokwim Group sedimentary rocks

The Donlin Creek mineralized trend includes an area 8 km long by 3 km wide. The host rocks are composed mainly of greywacke, shale, siltstone, and rhyodacitic and mafic intrusive units (Table 1; NI-43-101; Ebert, 2000). The sedimentary host rocks consist of interbedded shales, greywacke, and locally sandstone and siltstone units; they are locally laminated, graded, and contain coal seams, shell fossils and fragments, and rarely relict leaves or branches. The depositional environment is currently interpreted as a consequence of turbidites (NI-43-101). However, a few geologists currently working on the property argue for a shallower shelf environment due to the presence of the sandy layers, plant debris, and shell fragments (personal communication 6/2008). The greywacke at Donlin Creek is light to dark gray and consists of 1-2 mm sand and silt grains cemented together with carbonate. The shales and siltstones both contain clay- and silt-size particles and are dark gray to black in color. The shales are distinctive by their fissile nature, whereas the siltstones are characterized by semi-conchoidal to conchoidal fractures. Locally, ash beds up to 5 cm thick, and conglomerate units comprised of shale and siltstone clasts within a greywacke host, are found throughout the property. Generally, greywacke is dominant in the northern part of the resource area (Lewis, Rochelieu, Akivik, and Queen), shale is dominant in the south (ACMA and South Lewis), and the Main Shale unit thins to the west as the Upper Siltstone thickens (NI-

43-101). These sedimentary host layers strike NW across the property and dip 10-50° to the SW.

Assigned Nomenclature	Principal Rock Type	Apparent Thickness
Upper Greywacke	Greywacke	100+ meters
Upper Siltstone	Siltstone/Shale	50 meters
Main Greywacke	Greywacke	80 meters
Main Shale	Shale/Argillite	To 140 meters
Basal Greywacke	Greywacke	200+ meters, open at depth

Table 1. Sedimentary units that make up the Kuskokwim Group sediments in the resource area at Donlin Creek (modified from Piekenbrock *et al.,* 2003).

2.4.2 Intrusive units

Several temporally related, but texturally and spatially distinctive, igneous units intruded the Kuskokwim Group at Donlin Creek. The five rhyodacite intrusive rocks occur as dikes in the greywacke-rich Lewis region of the deposit. These dikes extend 6 km north along the NE-striking Donlin fault zone (Ebert, 2000) through the Dome prospect and to the south as sills in the shale-rich AMCA region. These sills parallel the previously folded sedimentary rocks within the hanging walls of regional thrust faults (MacNeil, 2009). The dikes and sills within the resource area range from 3 to 60 meters wide and exhibit irregular and sharp contacts with the country rock (Goldfarb *et al.,* 2004). The rhyodacitic intrusions associated with the gold mineralization have a zircon SHRIMP date of 71.6 ± 0.6 Ma (K. Daniel MacNeil, personal communication 1/20/2009)

The following intrusive rock descriptions are based on the author's observations and work completed by Piekenbrock *et al.* (2003). The rhyodacites are broken out

into five petrographic units based on textures: RDXB, RDA, RDXL, RDX, and RDF. The temporal association of these intrusive units can be established through cross-cutting relationships (Table 2).

Rhyodacite Description	Nomenclature	Relative Age
Blue porphyry – graphitic component	RDXB	Youngest
Aphanitic flow banded porphyry	RDA	
Lath-rich porphyry	RDXL	
Crystalline (crowded) porphyry- most abundant	RDX	
Fine-grained porphyry	RDF	
Mafic Dike	MD	Oldest

Table 2. Rhyodacite intrusive units at Donlin Creek and their relative age relationships (modified from Piekenbrock *et al.,* 2003).

2.4.2.1 Mafic Dike

The oldest intrusive unit (MD) is the mafic dike unit, which has an intermediate to mafic composition. This unit occurs as dikes that fill NNE- and EW-striking structures and dip SE and N, respectively, and form sills throughout the sedimentary sequence (Piekenbrock *et al.,* 2003). Fresh or unaltered examples of this intrusive are rarely found on the property, but where observed, this intrusion has a grey colored groundmass. The altered version of this intrusion has a light green groundmass color and contains a moderate to intense chromium-rich mineral referred to as fuchsite or mariposite and carbonate alteration. Carbonate altered biotite grains are also common within this unit. These intrusions range in width from 1-3 meters and may show flow-banded margins. Locally, these mafic intrusions contain large (up to 2 inches wide) graphitic clots and high-grade gold.

2.4.2.2 Fine-grained Porphyry

The least common and oldest of the rhyodacite intrusive units is the RDF or fine-grained rhyodacite. This intrusive differs from the RDA due to the fine-grained nature of the feldspar crystals and aphanitic groundmass. The RDA exhibits medium to coarse grained phenocrysts within an aphanitic groundmass. The RDF is characterized by the feldspar grain size in correlation to the distinctive blue to dark gray groundmass. These dikes range from 5-10 meters wide, fill NNE, ENE and E-striking structures, and dip 10-25 degrees to the north.

2.4.2.3 Crystalline (crowded) Porphyry

RDX is the most common intrusive rock type on the property and is phenocryst-rich with porphyritic and locally equigranular textures. Contacts with other rhyodacite intrusions and the sedimentary host rocks are sharp, irregular, with minimal to absent chill margins. On the northeast side of Lewis extending southward are two major RDX dikes ranging from 50-100 meters wide. The sills are located in the southern portion of the resource area stratigraphically below RDXL and RDA intrusive units. These RDX sills follow the folds that dominate the ACMA region to a near-overturned position. This unit, which exhibits variably intense and locally texturally destructive NH_4-illite, illite, and kaolinite ± carbonate alteration of feldspar phenocrysts, is commonly misinterpreted as RDA.

2.4.2.4 Lath-rich Porphyry

The lath-rich crystalline rhyodacite is labeled RDXL. This unit contains distinctive, locally crowded, lath-shaped or elongate phenocrysts of plagioclase up to 1 centimeter in length with adjacent fine- to medium-grained potassium feldspar

phenocrysts. The groundmass within this unit is generally gray to dark gray, arguably blue. The graphitic content within this unit is much lower to nonexistent when compared to the RDXB intrusions. In the Akivik area, two major dikes trend southward into ACMA. Few, smaller dikes are found in Lewis. ACMA also hosts a RDXL sill located stratigraphically below the RDX sill package which continues to the west and pinches out to the east. Locally, relict potassium feldspar and coarser-grained biotite with less carbonate and illite occur within this unit. Feldspar grains exhibit NH_4-illite, illite, kaolinite, and carbonate alteration.

2.4.2.5 Aphanitic Flow-Banded Porphyry

The RDA nomenclature represents an aphanitic rhyodacite with a salt and pepper texture of fine grained crystals of biotite, quartz, and potassium feldspar within an aphanitic groundmass. Up to 3 mm wide anhedral quartz grains are characteristic of unit. The groundmass color ranges from gray/light gray to grayish-tan and the percent of phenocrysts varies gradationally throughout this unit. At contacts between sedimentary or igneous rock, this porphyry exhibits a flow banded texture. As many as eight dikes have been found extending from Rochelieu to ACMA/East ACMA. Two major sill packages have also been noted. One is located in ACMA, stratigraphically above a package of RDX sills, and the other is found south of the American Creek (AC) fault in the Aurora area on the west side of the property. The potassium feldspar phenocrysts alter to NH_4-illite, illite, kaolinite, and locally to Fe-carbonate.

2.4.2.6 Blue Porphyry

The RDXB intrusive unit or Blue Porphyry is the youngest intrusive phase. Lewis Blue Porphyry and Vortex Blue Porphyry are the two major dikes on the property located within the Lewis and Vortex prospect areas, respectively. Largely, RDXB sills occur in the southern portion of Lewis and ACMA where they occur as individual intrusions or associated with RDA. Contacts with other intrusive units and sedimentary host rocks are commonly sharp and irregular, and locally faulted. Gold is found locally within the RDXB unit as high-grade disseminated grains within arsenopyrite. The RDXB contains very distinctive coarse-grained equant to blocky porphyritic feldspar grains within a blue groundmass. The blue appearance is due to the high graphitic and sulfide content. Locally, the color appears to be an alteration product, showing intensities near fault contacts, fractures, and veinlets. Alteration of the feldspar grains consists of NH_4-illite, illite, montmorillonite, kaolinite, and locally Fe-carbonate.

2.4.3 Vein Types

This study recognized six vein assemblages (Fig. 9). The veins occur throughout the property from Dome to ACMA-Lewis and trend 024°/071° (MacNeil, 2009). Sheets and zones of sulfide rich vein assemblages within the resource area range from 2-35 meters long and were believed to occur within larger, high-grade 100-350 meter mineralized corridors (Piekenbrock *et al.,* 2003). Six km northeast at the Dome prospect, disseminated and stockwork high-temperature sulfide-rich veins cross-cut the porphyries and the surrounding hornfels (Goldfarb *et al.,* 2004; Ebert, 2000; this project). V1 veins refer to any vein containing massive sulfides; V2 veins contain an

abundant amount of quartz ± minor sulfides; V3 indicates a vein with any amount of stibnite, realgar, or native arsenic; and V4 veins are carbonate veins. The detailed vein study completed in this study identifies the actual number of veining events and their temporal relationship. LA-ICP-MS analyses of carbonate and quartz phases suggest that five of these vein assemblages extend from Dome to ACMA. Limited amounts of LA-ICP-MS data suggest that ankerite is presence only at Dome; however, petrographic and detailed logging show stringer veins containing ankerite cross-cut older vein assemblages throughout the district. These assemblages include a pre-mineralization quartz vein sequence with a sugary texture (noted in the drill logs as V2), a pre-mineralization calcite phase located predominantly at Dome (V4a), a base-metal sulfide-rich phase (V1), a quartz-pyrite-auriferous arsenopyrite ± realgar, stibnite, and arsenic assemblage associated within a dolomitic-rich matrix (V3), a post-mineralization quartz phase (V2b), and a post-mineralization massive ankerite phase (V4b). These stages are described here, and illustrative photographs are provided in Appendix A.

Figure 9. Paragenetic sequence for the minerals deposited at Donlin Creek and at the Dome prospect. The veinlet assemblages defined by Donlin Creek staff and are currently being logged at Donlin Creek are designated as V1 through V4. The relative ages from this study further subdivide and identify their paragenetic relationships. Au in this system is associated predominantly with arsenopyrite and to a lesser extent pyrite. See Appendix A.

The barren quartz vein assemblage (V2a) occurs with a sugary texture at Dome and as euhedral quartz within open spaced veins in the resource area (Figs. A-5, A-9, A-40). These veins range from less than a few mms to several cm wide and are cross cut and overprinted by subsequent veining events. V4a or early calcite phase occurs with the base metal assemblage replacing along the grain boundaries and along cleavage planes. This phase only occurs at Dome. The vein phase associated with sphalerite, chalcopyrite, pyrrhotite, pyrite, marcasite, arsenopyrite, and locally tetrahedrite, and graphite (V1) occurs throughout the property; however, the sphalerite, chalcopyrite, and pyrrhotite occurrences are much more prevalent at Dome and decrease southwestward towards ACMA-Lewis. Property wide, these base-metal sulfide veins are only a few mms wide. The precious-metal sulfide mineralogy associated with Fe-dolomite (V3) is dominant at ACMA/Lewis, although it also occurs on the western side of Dome. This assemblage which ranges from a few mms to several cm includes pyrite, marcasite, auriferous-arsenopyrite, stibnite, native arsenic, realgar, local tetrahedrite, and sphalerite with chalcopyrite disease. These veins are strongly associated with dolomite (Figs. A-42 and A-44 through A-48). The late stage silica-rich vein (V2b) phases replace the pre-mineralization carbonate grains and exhibit a siliceous to sugary texture. Massive ferroan-calcite (ankerite) stringers and veins (V4b) occur throughout the property (Figs. A-4, A-14, A-15, A-50, A-51). These late veins cross-cut the previous vein assemblages and have thicknesses up to 2 cm at Dome. In the resource area ankerite veins are

generally on the order of a few mms wide and locally fill remaining open spaces of previous vein assemblages.

2.4.4Mineralogy

The main gold resource at Donlin Creek is located at the southern end of the Lewis dike complex where ACMA sills are dominant (Goldfarb *et al.,* 2004). The mineralized areas are vein dominant with local disseminated haloes. The resource occurs primarily within felsic dikes and sills, cross-cuts greywacke-dominant stratigraphic layers, and is present at fault contacts and along intrusive-sedimentary contacts (Piekenbrock *et al.,* 2003; NI-43-101). Previous studies reported contradictory cross-cutting field relationships and geochronological data between the ACMA/Lewis and Dome's mineralizing events. These studies did not provide photo documentation to confirm the field relationships. Petrography also shows that the mineralization at Dome predated the mineralizing event at ACMA/Lewis (this study). $^{40}Ar/^{39}Ar$ dates of illite at Dome depict younger (68.0 ±1.0 and 65.1 ± 0.9 Ma) ages than the illite dated at ACMA/Lewis (Goldfarb *et al.,* 2004). Goldfarb *et al.* (2004) interpreted these data to record hydrothermal activity at Dome from >74 to 68 Ma that produced argon loss and thus younger ages in older minerals. However, it is possible that the micas at Dome may have annealed through subsequent hydrothermal activity, which would also indicate a younger age than the initial depositional event.

2.4.4.1 ACMA-Lewis

The observations discussed below include the Queen, Lewis, and ACMA regions. The igneous rock units have weakly to intensely resorbed quartz grains (Fig. A-54)

that range from 0.3 to 4 mms wide and are rounded to subrounded in shape, and relict feldspar and biotite grains. Alteration-related illite, with local kaolinite, carbonate, and alunite replace euhedral to subhedral feldspar grains (Fig. A-59, A-60, and A-61). The pattern of alteration within the feldspar grains suggests that the latter were initially zoned. The edges of feldspar contain illite with local alunite in the mid-center to center with or without interstitial kaolinite. Relict biotite grains up to 1 mm are now composed of primarily illite associated with various percentages of sphalerite, pyrite ± marcasite, carbonate, and hematite (Figs. A-56, A-57, and A-58). Pyrite is subhedral, <0.1 mms wide, and makes up 1% of the groundmass. Sphalerite occurs as anhedral grains <0.1 mms wide, and comprises <1% of the groundmass. Euhedral arsenopyrite grains comprise up to 5% of the groundmass and occur as grains up to 0.1 mms wide.

Subangular to subrounded quartz grains are the only remaining primary grains (Fig. A-7 and A-8) within the sedimentary units of the ACMA/Lewis district. The groundmass occurs with varying percentages of quartz as siliceous alteration, illite, kaolinite, carbonate, sphalerite, pyrite, and locally hematite. Hematite replaces the cement between sedimentary grains. Pyrite, sphalerite, arsenopyrite are the dominant sulfides that are disseminated in the sedimentary unit. Pyrite occurs as euhedral to anhedral grains where locally the texture is interpreted to be a rock replacement texture, but also observed as framboidal and zoned. Pyrite makes up 2-4% of the matrix. Sphalerite weakly replaces mica grains, is anhedral, occurs as

grains up to 0.1 mm wide, and makes up 1% of the matrix. Arsenopyrite has euhedral grains up to 0.1 mms wide and ranges from 2-7% within a sedimentary matrix.

In the precious-metal vein assemblage located primarily at ACMA-Lewis, euhedral arsenopyrite was deposited largely on pyrite grain boundaries and overprinted and infilled between euhedral quartz grains (Fig. 10, A-37 and A-38). Euhedral to subhedral blocky pyrite grains generally 0.3 mms wide occur within the dolomite-sulfide vein assemblage and appear to have locally co-precipitated with arsenopyrite. Botryoidal pyrite occurs with or without individual grains of arsenopyrite in local channelized flows. This sequence is associated with graphite and illite that formed during later alteration. Arsenopyrite occurs as euhedral to subhedral grains that locally replaced pyrrhotite (Figs. A-17, A-19, A-20, and A-23), rimming pyrite and marcasite, or as individual euhedral grains making up 2-25% of the vein mineralogy. These grains occur in two sizes (Fig. A-49), one ranging from 0.1 to 0.2 mm wide and the larger grains up to 1 cm. Szumigala (1996) reports both of these grains as structural hosts for gold; however, the finer-grained arsenopyrite can contain 5-10% more gold than the larger grains. Stibnite is found as small euhedral needle-like or fibrous grains. Realgar occurs within veins associated with strong silica content and also within the adjacent groundmass where it locally replaced the intrusive unit's phenocrysts. Botryoidal native arsenic grains occur at the edge of euhedral quartz grains (Fig. A-40).

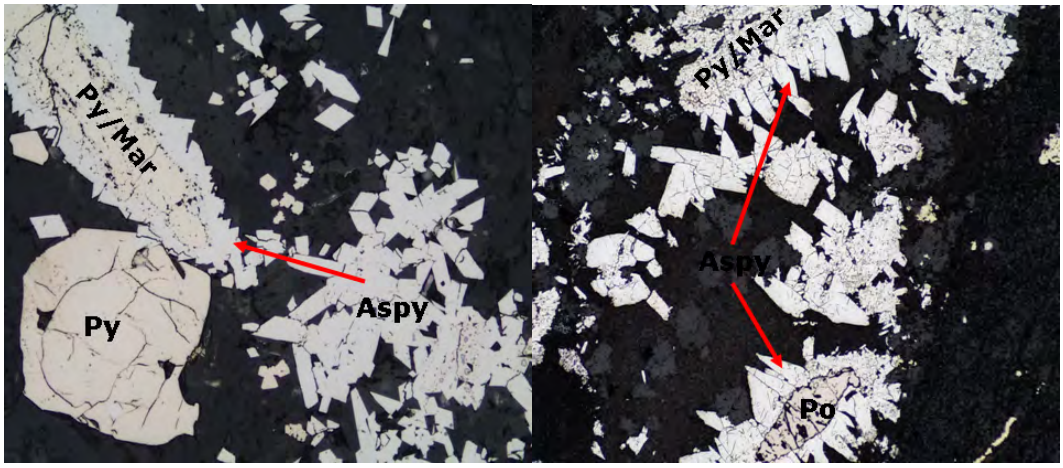

Figure 10. Base-metal minerals pyrite/marcasite (py/mar) and pyrrhotite (Po) with crystallization of precious-metal minerals arsenopyrite and pyrite at base-metal mineral boundaries. Left: photomicrograph from ACMA, 2.2mm, reflected light; right: photo from Dome, 2.2mm, reflected light.

2.4.4.2 Dome

The regions discussed here refer to the Dome, Snow, and Quartz sections of the district (Fig. 3). The intrusive rock units at Dome are composed predominantly of quartz and relict feldspar and biotite phenocrysts within a siliceous groundmass associated with varying percentages of illite, alunite, carbonate, sphalerite, chalcopyrite, pyrite, marcasite, and pyrrhotite. Rarer minerals in the groundmass include biotite, kaolinite, hematite, rutile, chlorite, and arsenopyrite. The magmatic quartz phenocrysts range from 0.5 mms to 4.5 mms wide, are subangular to rounded, and locally show a minor resorbed texture at the edges of the grains (Figs. A-55 and A-56). At Snow and Quartz regions, quartz phenocrysts range from 0.2 to 4 mms and show a greater intensity of resorbed edges of the anhedral grain boundaries compared to those at Dome. Relict feldspar phenocrysts are composed of illite along the margins of the grains with varying degrees of quartz, carbonate, kaolinite, and rarely alunite in the center of the grains at Dome. Locally, the

precipitation of sericite/illite in relict euhedral to subhedral, 1-4 mms wide feldspar grains is wide spread. Euhedral to subhedral relict biotite grains are also present and are composed of dominantly illite with varying degrees of pyrite and sphalerite replacement ranging from 1-3 mms wide. Rutile occurs within quartz grains (Figs. A-1 and A-2), in biotite and potassium feldspar coinciding with the potassic alteration zone, in illite, and rarely in alunite. Chalcopyrite, pyrrhotite, and arsenopyrite are present in the groundmass, where they locally are associated with carbonate. Rare chlorite (Fig. A-3) formed prior to the final sericitization stage within the groundmass.

The sedimentary rock layers contain a similar mineralogy as the groundmass of the intrusive rocks with differences in mineral percentages. Silica replacement is the predominant alteration within the sedimentary matrix with illite, hematite, carbonate, sphalerite, pyrite or marcasite, arsenopyrite and kaolinite. Locally hematite comprises up to 30% of the matrix in samples located to the north and northeast of the property. The sedimentary matrix is commonly laminated and can be poorly sorted to equigranular. Sulfides within the matrix occur at shallower depths to the east and west, and at greater depths to the north. The sedimentary rock units located south of Dome at the Snow and Quartz regions show an increase in hematite and precious-metal mineral overprints when compared to those at Dome.

Within the base and precious-metal-rich vein assemblage, sphalerite occurs with and without chalcopyrite disease. It is locally iron-rich and zoned (Fig. A-25), and it precipitated prior to and coeval with pyrite. Locally, tetrahedrite is replaced by sphalerite (Figs. A-25, A-26, A-27, A-28, A-29, and A-33). Sphalerite with chalcopyrite disease (Figs. A-26, A-27, A-28, A-33, A-34, and A-35) occurs as blebs 0.1 to 0.3 mms wide, and can be alone within the vein assemblage or within pyrite grains. Chalcopyrite occurs as anhedral very fine grains, and most commonly it occurs within sphalerite as chalcopyrite disease (Figs. A-16, A-17, and A-18). Pyrrhotite occurs at depths greater than 107 meters only in drill hole DC00-582, the farthest north drill hole. Porous pyrite grains are interpreted to represent rock replacement textures (Fig. A-31). The pore spaces within these grains and the subsequent phases of pyrite are moderately to intensely filled in, altered to (locally as pseudomorphs), and cemented by marcasite (Fig A-30). Pyrite precipitated as euhedral to anhedral grains, locally with a rock replacement texture, forms a blocky, porous (Figs. A-33, A-34, A-37, and A-38), botryoidal, or framboid texture, locally zoned, (Fig. A-32) and range in size from <0.1 to 1.5 mms. Pyrite ranges in percent from 3 to 10% within the vein and locally up to 50-80%. The blocky grains appear to occur pre- and post-rock replacement and post-porous pyrite textures.

At depths greater than 96 meters to the west and at 239 meters depth below the top of Dome, sphalerite-chalcopyrite and pyrite-marcasite are fractured into jigsaw puzzle pieces that were cemented by quartz. Occurrences of stibnite are rare,

suggesting its precipitation near the end of or after the faulting or fracturing event (Fig. 11). Stibnite occurs only in the western portion of the district (DC00-580) at depths of >100 meters. The fractured grains and silica precipitated around carbonate grains and cut across initial sugary quartz, stringy sulfide, and carbonate veinlets.

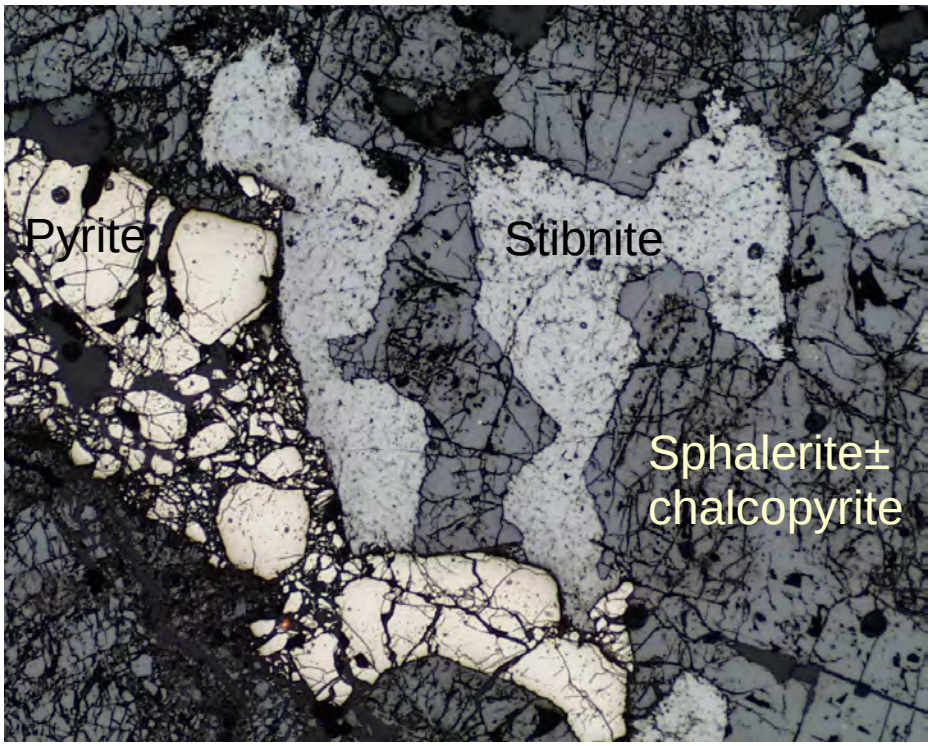

Figure 11. Photomicrograph of fractured sphalerite ±chalcopyrite and pyrite with over print by stibnite. FOV = 4.4mm, reflected light.

2.4.5 Alteration

2.4.5.1 ACMA-Lewis

High-grade, 100-350 meter wide mineralized "corridors" were discovered by Piekenbrock *et al.* (2003) and are defined by a distinctive ammonia-illite alteration assemblage in rhyodacite intrusive units (Fig. 12; NI-43-101). Outboard of this

high-grade zone is an illite-kaolinite alteration halo where the grade is low to barren (NI-43-101). Prior to this study, these corridors were only identified within the resource area and the extent of mineralized rock is open at depth within the ACMA area.

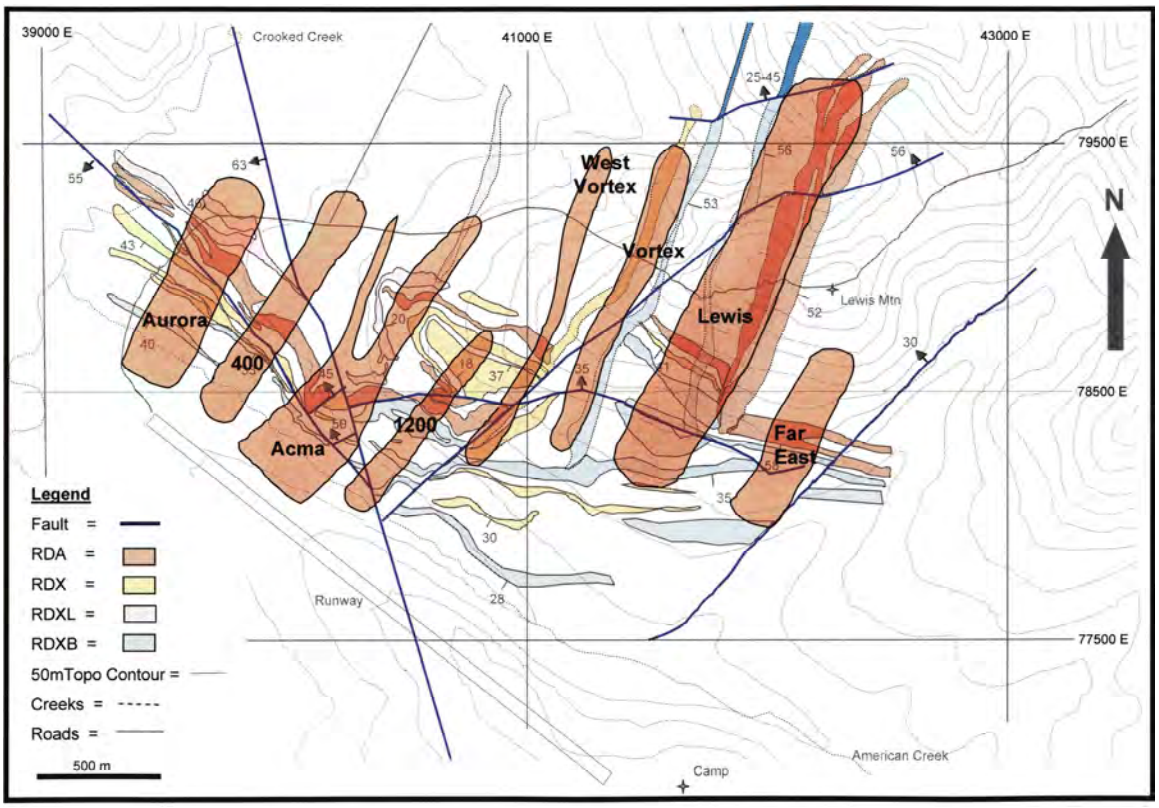

Figure 12. Mineralized corridors outlining high grade zones associated with ammonia-illite - illite alteration and haloed by kaolinite-smectite alteration (diagram from by Piekenbrock *et al.*, 2003).

The Lewis and Queen regions (Fig. 3) of the northern resource area are dominated by illite alteration. This alteration style is followed by varying degrees of silica, sulfides, and alunite and kaolinite alteration. Hematite, carbonate, and graphite locally halo or replace sedimentary and igneous grains. Cross-cutting relationships

suggest silica is the primary alteration event followed by sulfides; sericite and carbonate overprinted those alteration products, with subsequent illite, kaolinite, and hematite supergene alteration. In contrast, ACMA at the south end of the resource area (Fig. 3) is dominated by silica with various amounts of illite, sulfide, carbonate, alunite (Fig. A-60) with local kaolinite (Figs. A-59 through A-62) and illite (Fig. A-64) supergene alteration. Silica alteration produced grains <0.1 mms wide.

2.4.5.2 Dome

The regions of Dome, Snow, and Quartz are included in the description discussed below where hornfelsing is prominent. Silicification is the dominant alteration process throughout the intrusive and sedimentary rock units. This alteration style produced less than or equal to 0.1 mm subrounded to rounded grains, which occur in the groundmass of the intrusive rocks and within the matrix of the sedimentary units. Cross-cutting relationships suggest the silica alteration of these rock units was the first alteration event followed by illite. Illite is present between quartz grains and strongly replaced relict feldspar and biotite grains. Grains of illite are also seen lining the margins of veins and occurring between quartz and sulfide grains within the veins, suggesting a later sericitization event. In drill hole DC97-390 on the east side of Dome, kaolinite is dominant at and below a depth of 195 meters. Hematite, in drill holes DC00-582 and DC97-393 located on top of and to the north of Dome, becomes predominant around 123 meters and extends to a depth of 248 meters only within sedimentary units. Carbonate is present intermittently throughout the Dome district; however, its presence is variable below depths of 123 meters within both rock units. Biotite occurs at depths of 33-70 m in

the farthest north drill hole, DC00-582 (Fig. A-63). Chalcedony is rare and found north of Dome (Fig. A-53). Most notably, kaolinite, hematite, carbonate, and biotite alteration occur below depths of 123 meters from the top of Dome and to the east, whereas to the west, these alteration styles are noted at shallower depths (74-126 meters). Locally south of the Dome region, the predominant alteration phase is sulfidation followed by carbonate and illite in lesser degrees. Illite occurs throughout the six square kilometer district, and textures and fluid inclusions indicate boiling of fluids in all the drill intervals at Dome and Snow and down the top of and to the west of the hills through Lewis and into ACMA. To the east of the Lewis and Queen hilltops, definitive features to indicate boiling were not observed.

3 Chapter 3: Previous Work

3.1 Previous Work

Several previous technical studies have focused on various classification aspects, isotopes, fluid inclusions, and petrography at ACMA/Lewis where the Dome prospect was briefly examined. In general, the intrusive units that extend from the ACMA/Lewis resource through Dome are classified as evolved, peraluminous hypabyssal bodies containing high silica (74.1% SiO_2) and aluminum (14.5% Al_2O_3) contents (Bundtzen and Miller, 1997). When plotted on a compositional diagram, the dikes and sills are classified as alkali-quartz granite (Goldfarb *et al.,* 2004) or rhyolite to rhyodacite. These reduced, ilmenite series intrusive units are associated with volcanic-arc tectonic settings.

3.1.1 Geochronology

Goldfarb *et al.* (2004) determined K-Ar, U-Pb, and $^{40}Ar/^{39}Ar$ ages that range from 70.9 ± 2.1 to 65.1 ± 2.0 Ma for intrusive units throughout the property. Goldfarb *et al.* (2004) interpreted this range of dates as either a prolonged period (3-5 million years) of magmatism or a cooling of mica closure temperatures after a much shorter lived intrusive period. A structural based thesis by MacNeil (2009) reported a Zircon SHRIMP date for one of the intrusive units as 71.6 ± 0.6 Ma, which is comparable with the earlier results reported by Goldfarb *et al.* (2004). The mineralizing event at ACMA/Lewis is defined by a $^{40}Ar/^{39}Ar$ dates of 72.75 ± 0.52 Ma to 71.09 ± 0.38 Ma on hydrothermal illite that is spatially and genetically associated with the Au mineralization at Donlin Creek (MacNeil, 2009). Mineralization is therefore temporally related to the emplacement of intrusion units

and the NNE faults. $^{40}Ar/^{39}Ar$ and U-Pb dates for illite within mineralized veins at Dome reveal ages of 68 ± 1.0 and 65.1 ± 0.9 Ma (Goldfarb *et al.,* 2004). Goldfarb *et al.* (2004) interpreted these dates to represent a continuation of magmatism that led to an argon loss and resetting of the hydrothermal micas. They therefore interpreted the original age of the hornfels at Dome to be ≥ 74 to 68 Ma. The geochronological data of the dikes at Dome are comparable to the dike and sill events at ACMA/Lewis, suggesting that the mineralizing and intrusive events in both districts were contemporaneous.

3.1.2 Fluid Inclusions

3.1.2.1 Salinities and CO_2 Contents

A fluid inclusion study completed by Ebert *et al.* (2003b) consists of 32 double polished thin sections and 16 heating and freezing measurements both of which represent the district in its entirety and are discussed below. All measurements and observations were from quartz grains associated with Au-bearing veins. Four fluid inclusion types were identified: low-salinity liquid-rich with no daughter minerals and low-salinity vapor-rich with no daughter minerals in the ACMA/Lewis, Queen and Snow zones; and hypersaline liquid-rich with up to 4 daughter minerals, and vapor-rich low salinity inclusions with rare CO_2 double bubbles were found at Dome. Specifically, the fluids associated with the Dome mineralizing event averaged 39 wt% NaCl equivalent and 8.3 wt.% CO_2 compared to the average of 2.5 wt.% NaCl equivalent and 4.5 wt.% CO_2 at ACMA/Lewis (Goldfarb *et al.,* 2004; Ebert *et al.,* 2003b). Cross-cutting relationships of veins and inclusion trails observed by Ebert *et al.* (2003b) suggest the inclusions found at Dome are contemporaneous and

are cut by the later low-salinity inclusions in the resource area. These later inclusion types show equivocal temporal relationships with one another.

3.1.2.2 Mineralization Temperatures and Depth of Formation

ACMA/Lewis formation temperatures of ore and gangue minerals, interpreted from fluid inclusion analyses, and for auriferous arsenopyrite are interpreted to range from 275°C to 300°C (Szumigala *et al.,* 1999; Goldfarb *et al.,* 2004) at a depth of 1-2 km under lithostatic conditions (Goldfarb *et al.,* 2004; Ebert *et al.,* 2003b). Fluid inclusion data from the Dome area suggest higher mineralization temperatures of 400°C to 450°C (Szumigala *et al.,* 1999; Goldfarb *et al.,* 2004) Ebert *et al.* (2003b) interpreted the mineralizing depth at 1.5 to 3 km at Dome, under hydrostatic conditions.

3.1.3 Stable and Radiogenic Isotopes

3.1.3.1 Sulfur

Fifty mineral separates from gold-bearing veins were analyzed for sulfur isotope ratios and represent the Donlin Creek District from the main resource area to Dome (Goldfarb *et al.,* 2004). In addition, 9 gold-associated sulfide and 10 whole rock igneous and sedimentary host rock samples were analysed by Ebert *et al.* (2003b). $\delta^{34}S$ values for the diagenetic pyrite in greywacke units of the Kuskokwim Group sediments range from 0 to -16 per mil, whereas the diagenetic pyrite in shale units range from -5 to -27 per mil (Gray *et al.,* 1997; Goldfarb *et al.,* 2004). $\delta^{34}S$ values for the igneous rocks located at Dome range from -10 to -15 per mil and the intrusive units at ACMA/Lewis yield $\delta^{34}S$ values of -8 to -16 per mil. $\delta^{34}S$ values from Au-associated sulfides range from -7.3 to -27.2 per mil, with most values between -8

and -16 per mil (Goldfarb *et al.,* 2004; Ebert, 2000; Ebert *et al.,* 2003b). A late stibnite-rich phase contains sulfur values of -16 to -27 per mil. Geochronological data suggest that the igneous and mineralization events in the Donlin Creek district were contemporaneous (MacNeil, 2009). In addition the $\delta^{34}S$ values of the intrusive units and sulfides overlap, suggesting a similar sulfur evolution for the sulfides within the productive veins and igneous units. The -8 to -27.2‰ $\delta^{34}S$ data obtained from the igneous units and associated Au-bearing sulfides indicate that the sulfur in both suites could have been derived from greywacke or shale sequences within the Kuskokwim Group sediments.

3.1.3.2 Oxygen and Deuterium

Measured oxygen isotopic analyses for 21 whole rock rhyodacite units, 12 mineralized vein samples, and 2 biotite separates in the Donlin Creek district produced $\delta^{18}O$ values of 11 to 25 per mil (Goldfarb *et al.,,,* 2004; Ebert *et al.,* 2003b). $\delta^{18}O$ values from Dome are less than 17.4 per mil, whereas ACMA/Lewis values are between 18 and 25 per mil (Ebert, 2003b). The vein samples yielded $\delta^{18}O$ values that overlap those of the dikes, sills, and Kuskokwim Group sedimentary rocks in the district. Data obtained from hydrothermal fuchsite, chlorite, and illite for hydrogen isotope analysis produced δD values of -150 to -80 per mil (Goldfarb *et al.,* 2004; Szumigala *et al.,* 1999; Ebert *et al.,* 2003b). The micas for that study were collected along the margins of gold-bearing veins.

Calculated fluid compositions, using fractionation curves and temperatures obtained from fluid inclusion analyses indicate -90 to -110‰ δD values and 7 to

11‰ $\delta^{18}O$ values for Dome, -115 to -130‰ δD values and 4 to 6‰ $\delta^{18}O$ values for ACMA/Lewis, and -130 to -135‰ δD values and 5 to 11‰ $\delta^{18}O$ values for the late stibnite phase (Ebert *et al.,* 2003b). Dome fluid inclusion data partially overlap the data δD and $\delta^{18}O$ values for the rhyodacite dikes and sill at ACMA/Lewis indicating a predominantly magmatic origin. The fluids at ACMA/Lewis contain lighter δD and $\delta^{18}O$ values and are interpreted to be a mix of Dome fluids and meteoric waters, and the late stibnite phase containing the heaviest δD and $\delta^{18}O$ values is interpreted to have the most meteoric water involvement (Ebert *et al.,* 2003b). A plot of δD and $\delta^{18}O$ values obtained from Szumigala's (1999; Goldfarb *et al.,* 2004) study illustrates a meteoric and organic influence, which plot near other Hg-Sb deposits within southwestern Alaska.

3.1.3.3 Carbon

Ebert *et al.* (2003b) measured 12 fluid inclusion samples containing CO_2 and analysed them for $\delta^{13}C$. The Dome (-4.6 to -12.8‰) and ACMA/Lewis (-5.6 to -13.4‰) $\delta^{13}C$ values overlap and are interpreted to have originated from the same source. In addition the late stibnite-rich phase contains $\delta^{13}C$ values of -13.5 to -21.2‰ and is interpreted to have a sedimentary source.

3.1.3.4 Neodymium and Strontium

ε_{Nd} values of the rhyodacite dikes representative of five prospects throughout the property yield values of -8.7 to -3.1 (Goldfarb *et al.,* 2004). These negative values are consistent with the values obtained from other hypabyssal dikes within the Kuskokwim basin (Goldfarb *et al.,* 2004) and suggest crustal contamination within

the melt. These data agree with Szumigala's (1999) I-type igneous classification and the $^{87}Sr/^{86}Sr$ ratios of 0.70559 to 0.70850 (Goldfarb *et al.,* 2004).

3.1.3.5 Lead

The $^{206}Pb/^{204}Pb$ (18.760-19.306), $^{207}Pb/^{204}Pb$ (15.554-15.616), and $^{208}Pb/^{204}Pb$ (38.364-38.817) values from whole rock lead compositions of SW Alaska's granitic porphyries, and Donlin Creek rhyodacites and sulfides were compared. Data from the Donlin Creek rhyodacite and sulfides overlap significantly and are indistinguishable. Ten sedimentary samples were also analyzed for lead isotopes and plot within the vicinity of the rhyodacites and sulfides analyzed from Donlin Creek (Goldfarb *et al.,* 2004).

3.1.4Petrography

A detailed petrographic and paragenetic study was completed by Thompson (2007) of eleven samples within the ACMA/Lewis resource area. Thompson's study identified a predominantly quartz feldspar porphyry that contains abundant sphalerite, pyrite, and arsenopyrite, which occur as replacement, open-space, brecciated, and deformed textures. Moderate to large amounts of quartz, illite, rutile, lesser chalcedony, kaolinite, and albite alteration minerals were observed.

4 Chapter 4: Results

4.1 Analytical Results

The chemical relationship between the ACMA/Lewis resource area and the Dome prospect has been shown in previous studies (Ebert *et al.,* 2003b; Goldfarb *et al.,* 2004). They conclude that overlapping $\delta^{34}S$ (-10 to -15‰), $^{206}Pb/^{204}Pb$ (18.9 to 19.0), and CO_2 (-5 to -13‰) isotopic values of sulfur and lead from sulfides and carbon from fluid inclusions within vein assemblages, respectively, indicate similar evolution patterns in both areas. A paragenetic sequence completed during this study (Fig. 9) shows continuity between and within the 6 km long district. These events include deposition of pre-mineralization quartz (V2a) and calcite (V4a) phases, a base-metal assemblage (V1), a precious-metal assemblage (V3), followed by post mineral deposition of quartz (V2b) and ankerite (V4b) in veins. In addition, immobile element analyses of fresh igneous rocks show overlapping data, which suggests a genetic association between the igneous phases throughout the district (Fig. 13). Therefore, because these two dissimilar ore deposit types show possible igneous and hydrothermal patterns, further analysis of the carbonate mineralogy, geochemistry, and argillic alteration will determine how they may be related.

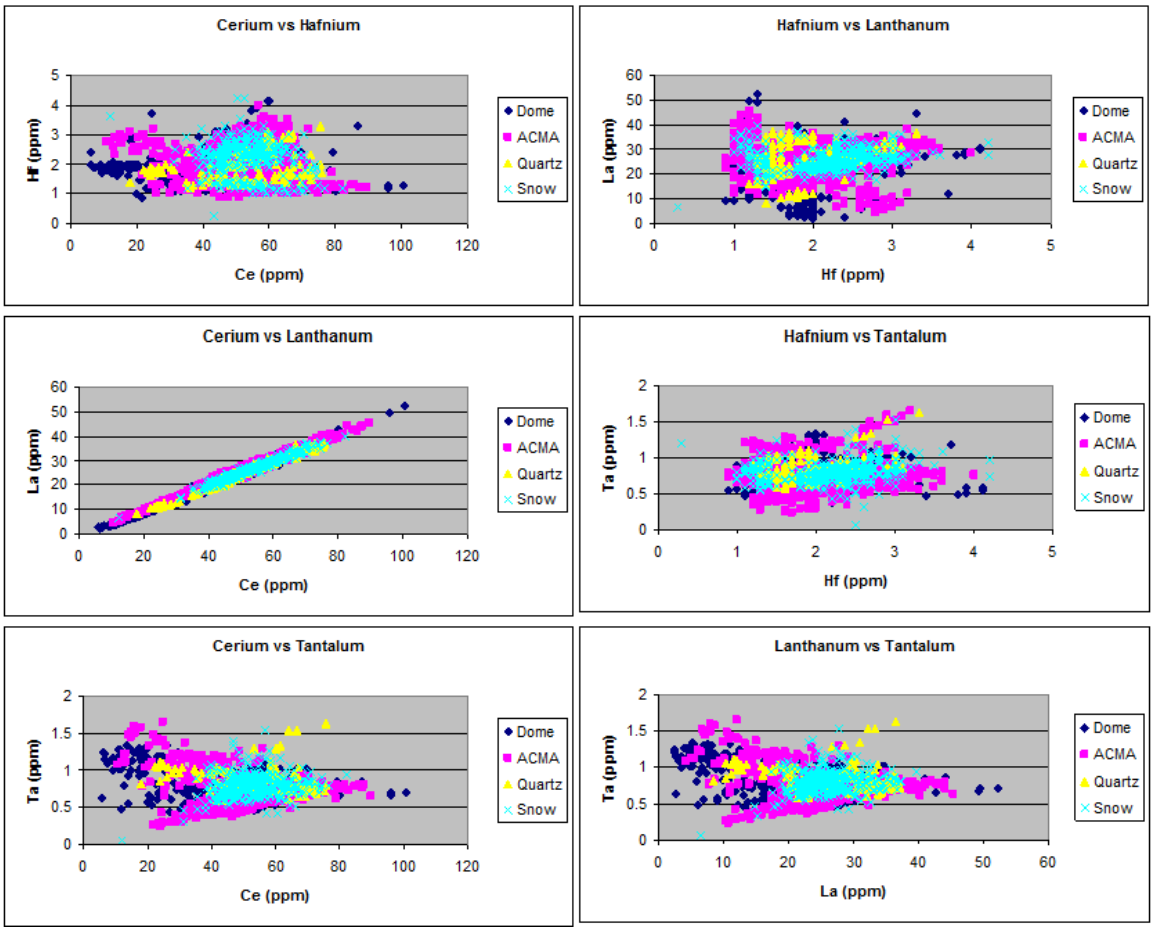

Figure 13. Ce, Hf, La, and Ta immobile element diagrams illustrate overlapping data points suggesting that the igneous host rocks and multiple veining events originate from the same source and therefore show a genetic relationship between ACMA/Lewis, Dome, and the areas between these regions.

Two of the six vein phases connecting the dissimilar mineral deposit types in the two districts are quartz. The first quartz phase (V2a) occurs as a sugary texture in the Dome area and conversely as euhedral grains in the outer margins of fractures. This initial phase is enriched with As, Ba, Fe, Mg, Li, Rb, Sn, and Ti compared to the post-sulfide quartz phase (V2b; Fig. 14). The depleted late quartz phase commonly replaces carbonate.

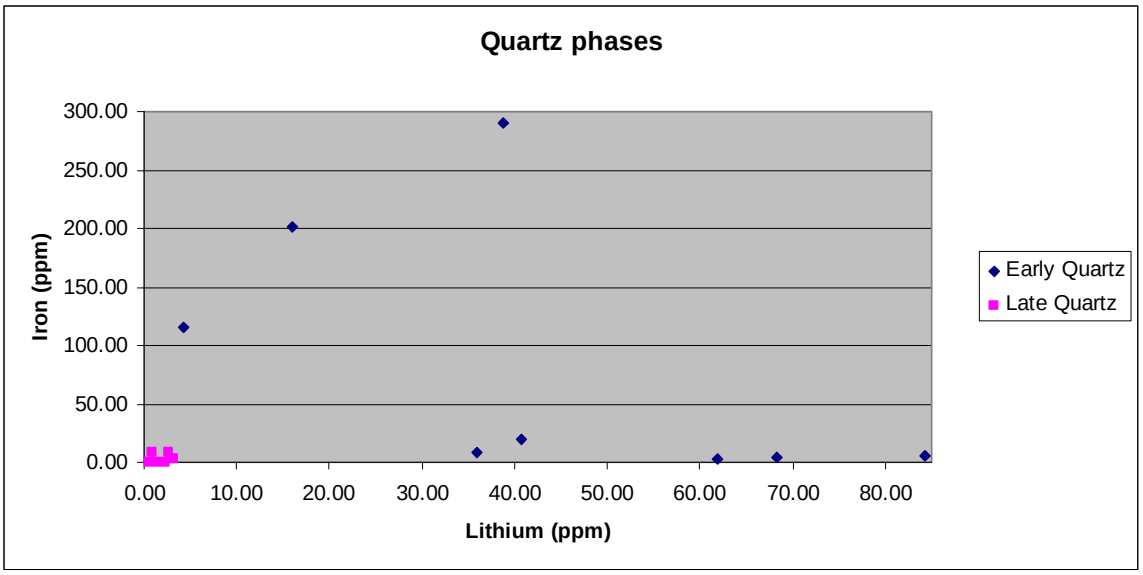

Figure 14. Iron-lithium scatter plot of analyses of the two quartz phases that connect the Dome and ACMA/Lewis Creek districts.

4.2 Carbonate Mineralogy

Carbonate alteration minerals are wide spread throughout the Donlin Creek property. The paragenetic sequence and LA-ICP-MS analyses provide evidence for four carbonate phases that were deposited before, during and after deposition of precious-metals. Carbonate staining was used to determine whether different compositions of carbonate existed within the system and if so to determine their temporal relationships with one another and to the base and precious-metal assemblages.

The blue colored reaction is strongly associated with the groundmass of sedimentary host rocks indicating a high presence of Fe. Additionally, purple and red reaction colors of the groundmass appeared to be correlated with higher gold grade sections and NH_4-illite alteration in the resource area (Figs. 15 & 16;

Appendix C). At this time the cause for the green stain reaction that occurs near the base-metal assemblage is undefined; however, it is found in areas of high silicification.

Textures and cross-cutting relationships between vein phases reveal five vein relationships (Appendix B). These relations include a sugary quartz phase over printed by ankerite and calcite veins (Figs. B-1, B-2, and B-3); sugary quartz veins overprinted by sulfide-rich veins (Fig. B-2); sulfides associated with calcite and ankerite (Figs. B-4 and B-5); euhedral quartz grains with calcite infill ± sulfides (Figs. B-6, B-7, and B-8); and quartz/sulfide veins cut by calcite veins (Fig. B-9). These relationships were supported and confirmed with the use of SEM, LA-ICP-MS, and CL techniques.

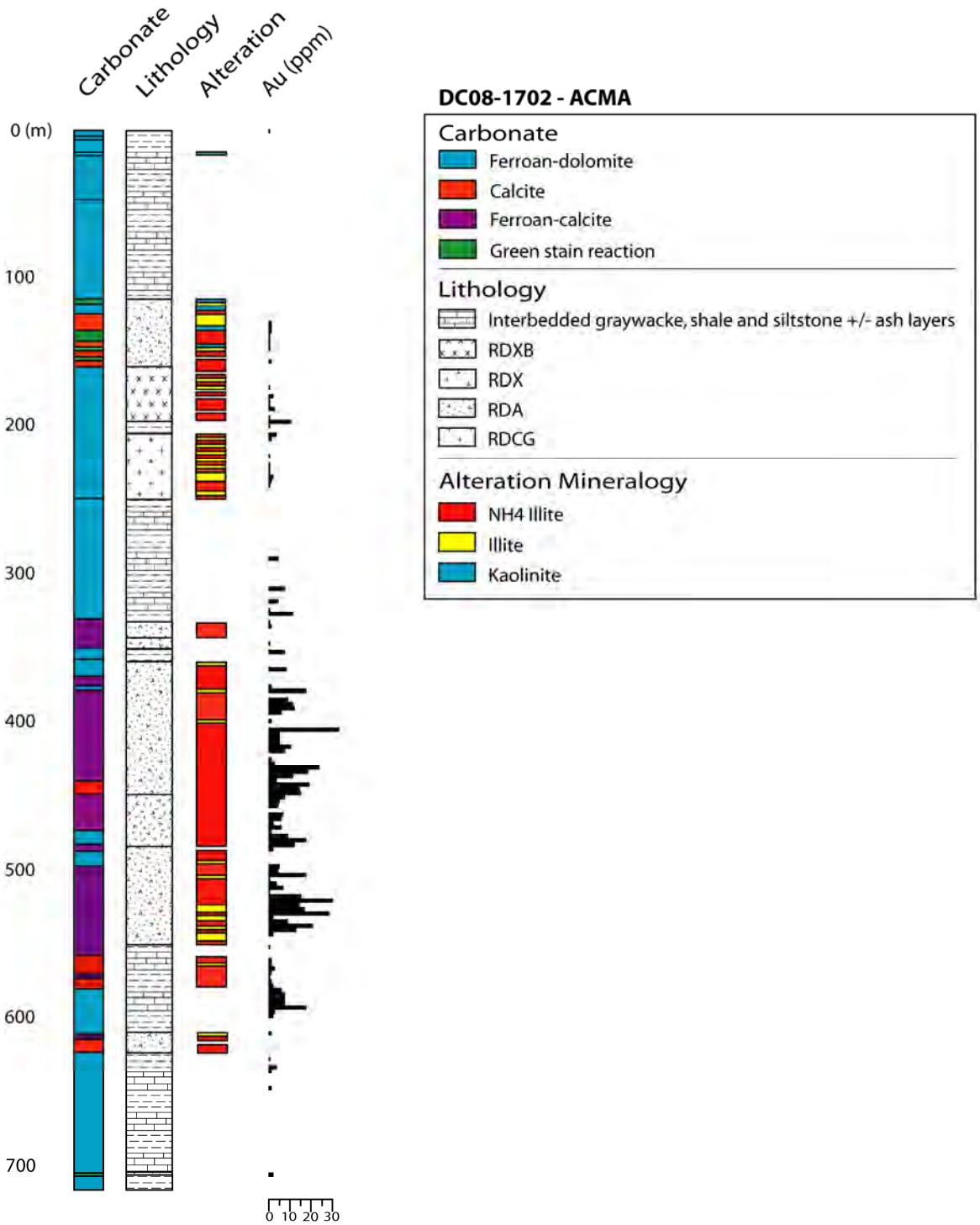

Figure 15. Drill hole DC08-1702 from ACMA illustrating the relationship between lithology, Au grade (ppm), and carbonate mineralogy. Note the carbonate color change associated with areas of increased gold content. The green stain reaction is currently undefined.

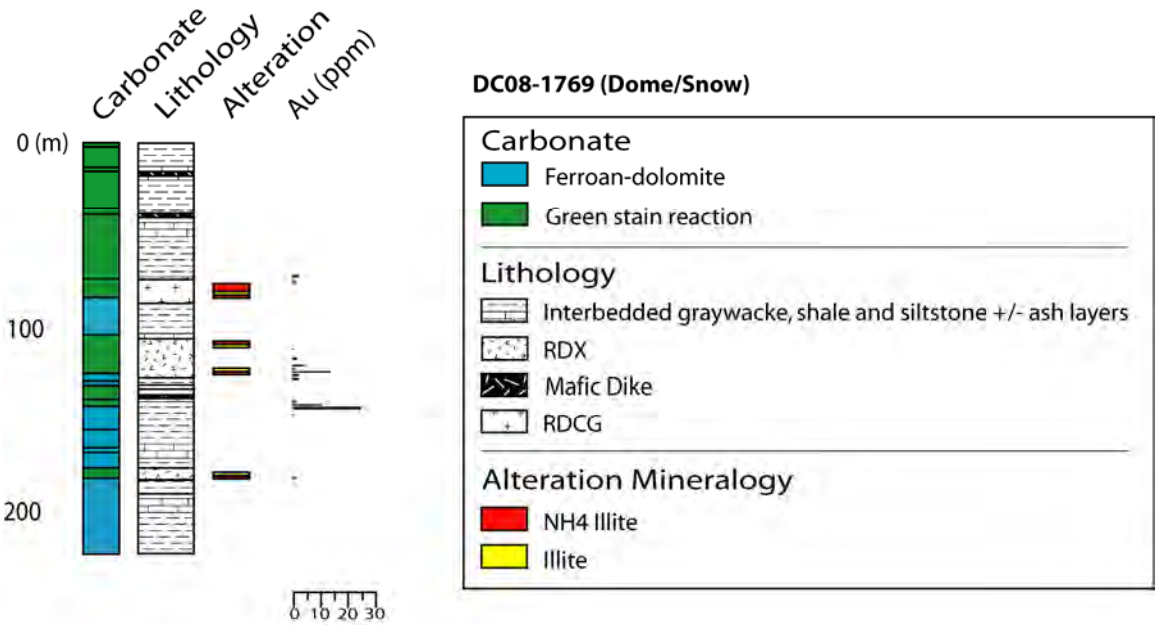

Figure 16. Drill hole DC08-1769 located at the Snow property represents the closest drill hole located to Dome that has carbonate staining data. Note that the staining technique does not appear to work well compared to ACMA-Lewis drill holes. The green stain reaction is currently undefined.

Thirteen carbonate minerals were analyzed using the SEM. These data showed strong peaks for calcium and varying peak heights for magnesium, iron, and locally manganese and was useful for determining calcite from non-calcite phases (Figs. 17, 19 & 20). The same samples were analyzed using CL which demonstrated three carbonate phases based on their illumination; with the addition of cross-cutting relationships, four carbonate phases were identified. Early calcite shows a bright orange illumination (Fig. 21) in comparison to the more iron-rich carbonate phases. The luminescence between these two Fe-rich phases is slight; however, one appeared darker than the other (Figs. 18 & 21). A total of fifty-one carbonate minerals were evaluated by the LA-ICP-MS. When evaluated by their cross-cutting relationships these data also illustrate four carbonate phases. These phases include

an early massive calcite phase found only at Dome (Figs. 17 (left), A-10, and A-11), Mn-calcite phase that exhibits platy and massive textures (Figs. 17 (right), 19, 20, 22, A-43, A-44, A-45, and A-53), a "grungy" (Figs. 17 (left), 19, 20, A-42, A-43, A-44, A-45, A-47, and A-48) and locally platy Fe-dolomitic phase associated with the precious-metal assemblage found predominantly at ACMA/Lewis Creek, and a massive ankerite phase (Figs. 22, A-4, A-6, A-7, A-14, A-50, A-51, and A-53). The latter three phases are found throughout the district.

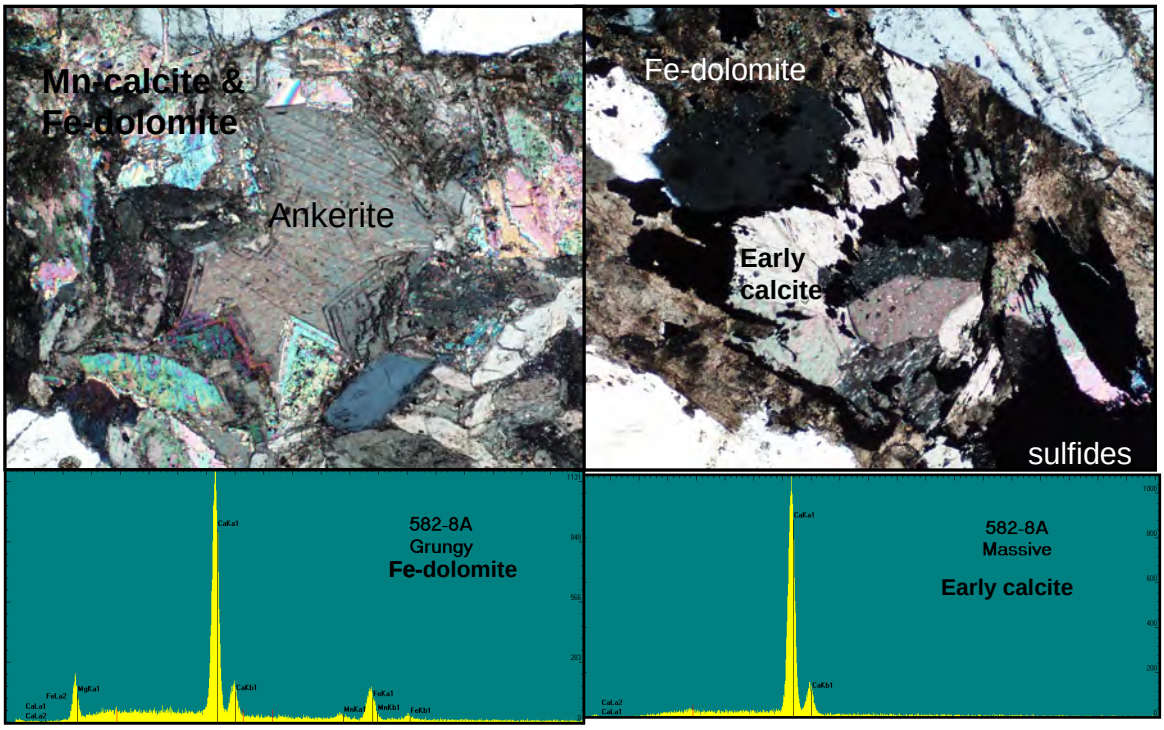

Figure 17. Samples from DC00-582 at Dome. Left: Ankerite filling in between euhedral Mn-calcite and Fe-dolomite grains. FOV 4.4mm, XPL. Right: Early calcite replaced by sulfides and Fe-dolomite. FOV=4.4mm, XPL.

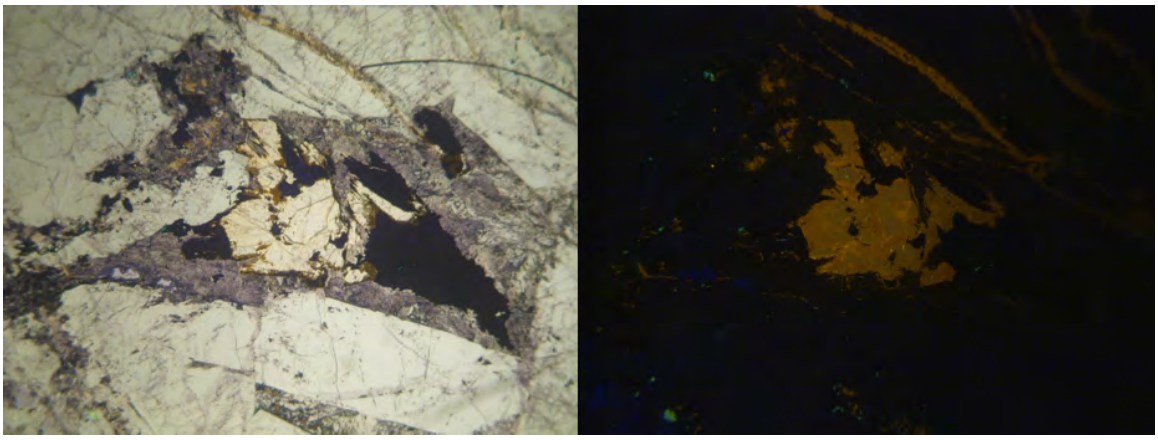

Figure 18. CL images of the same minerals as XPL and SEM images in figure 17, illustrating the illumination differences between calcite, Mn-calcite, Fe-dolomite, and ankerite. STD and PPL, 5X.

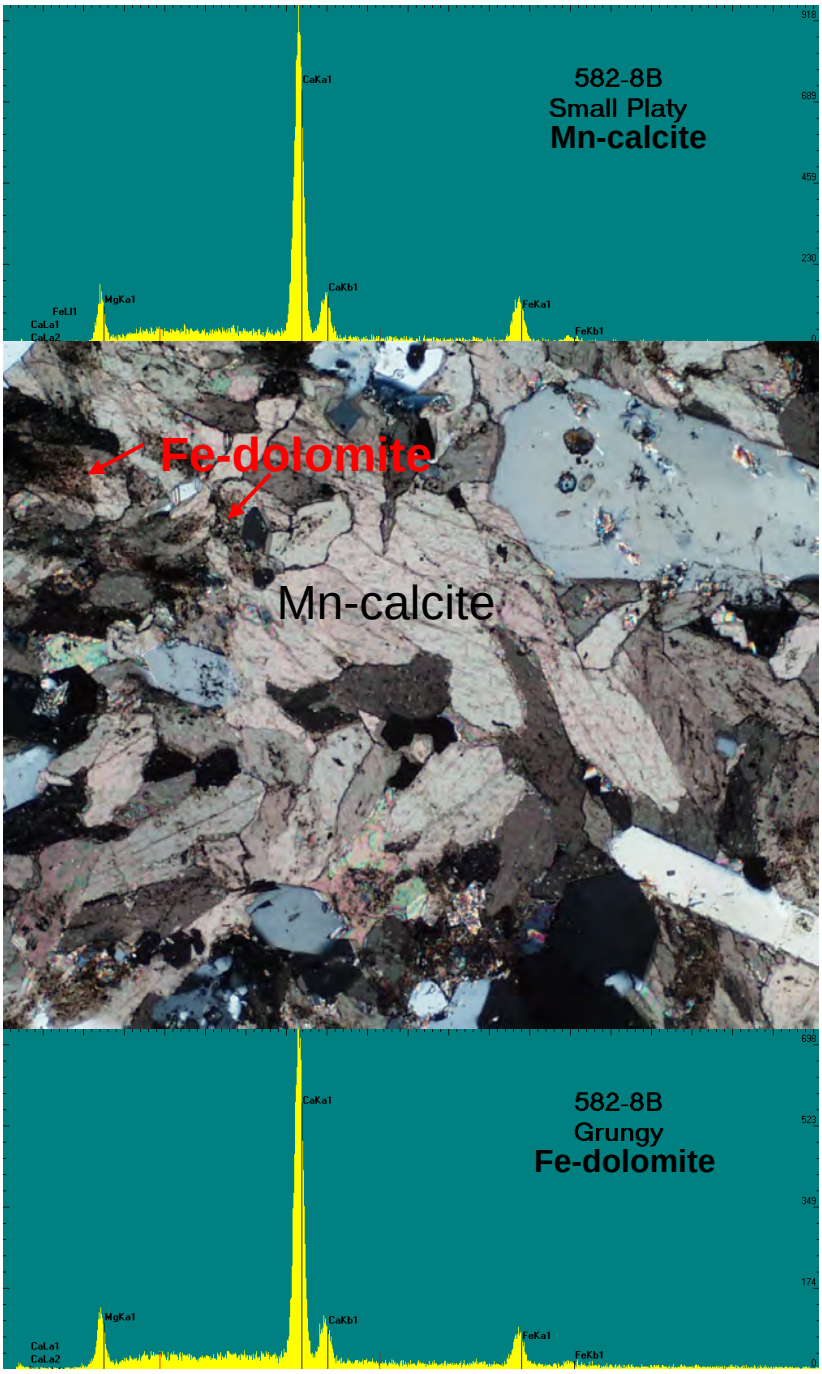

Figure 19. Mn-calcite being replaced by grungy Fe-dolomite in Dome drill hole DC00-582; FOV=4.4mm, XPL.

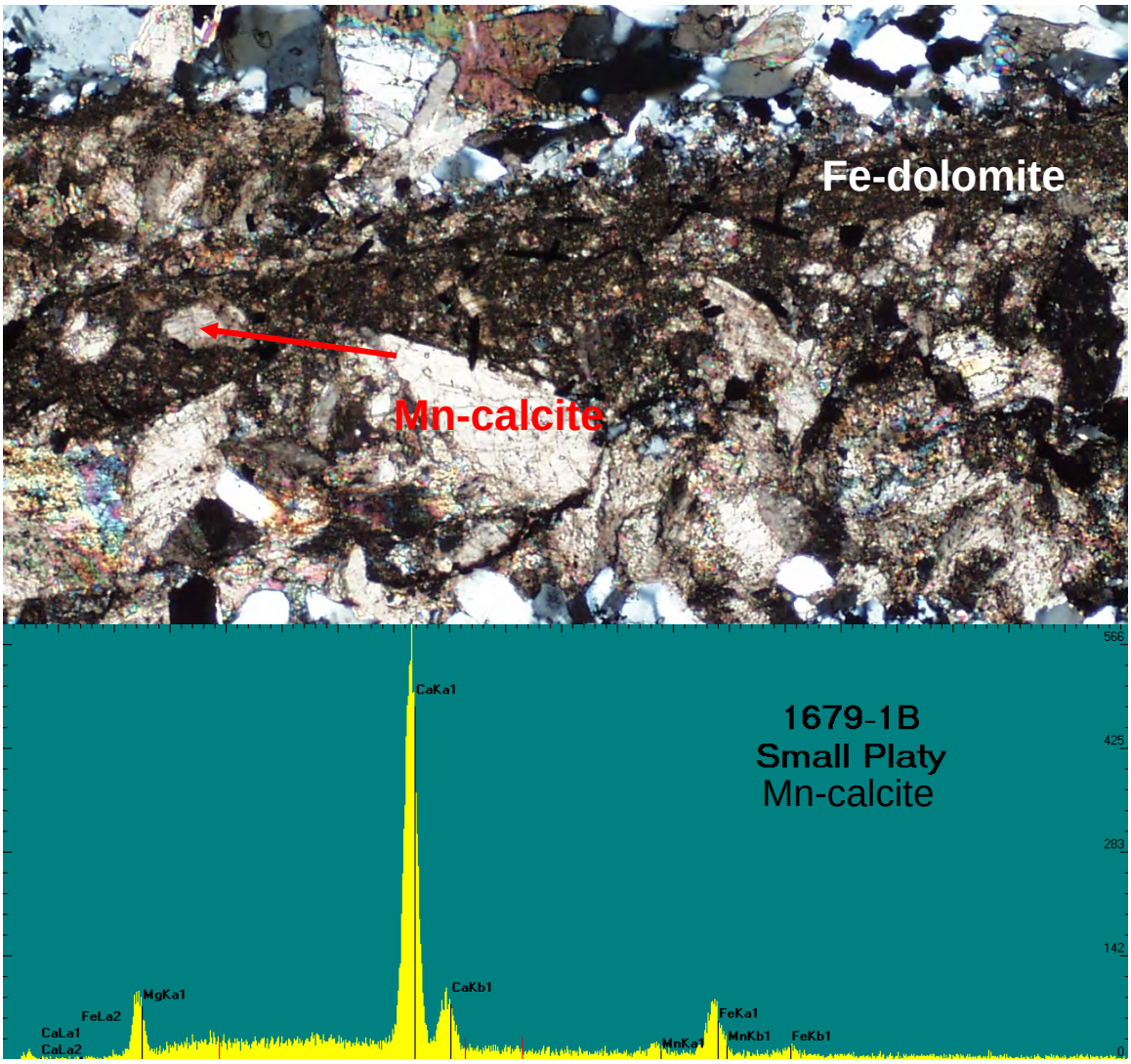

Figure 20. Fe-dolomite replacing Mn-calcite in ACMA, drill hole DC07-1679; FOV=4.4mm, XPL.

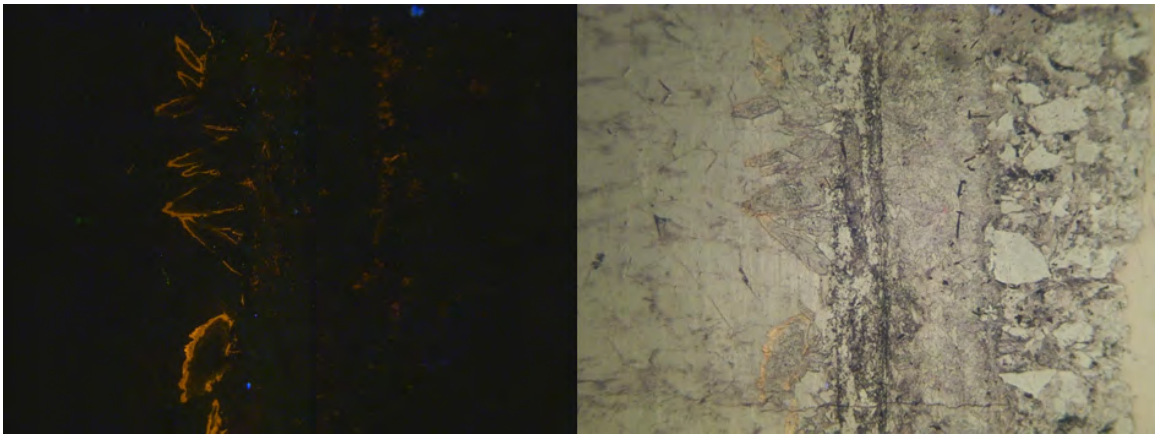

Figure 21. CL images of drill hole DC07-1679 showing minor to no illumination differences between Mn-calcite and Fe-dolomite. Note the late calcite phase that rims euhedral Mn-calcite grains and produces the brighter illumination seen in the left image. PPL and STD, 5X.

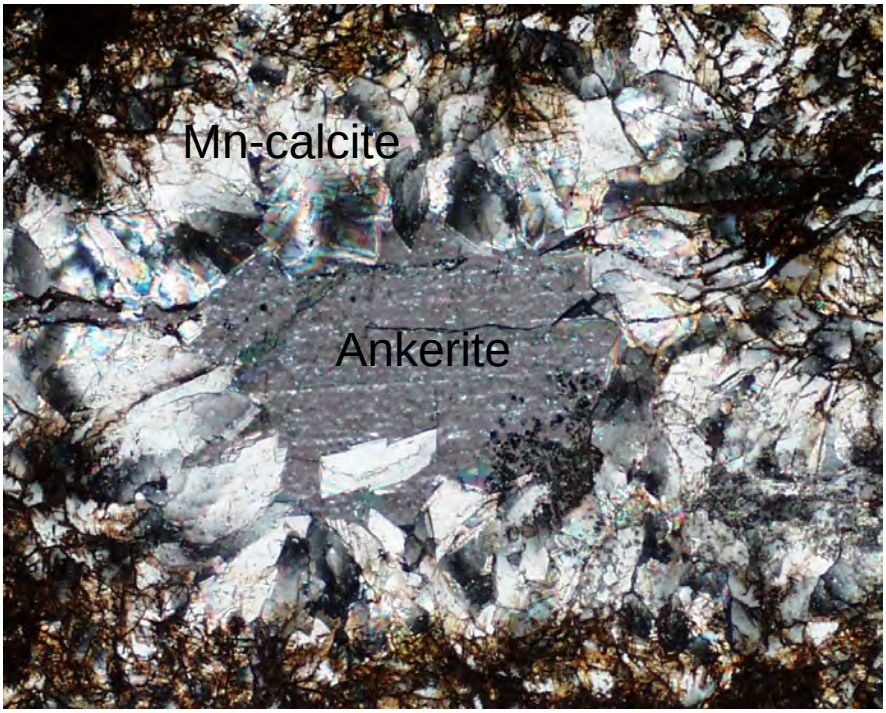

Figure 22. Ankerite in drill hole DC08-1769 that fills pores between euhedral Mn-calcite grains; FOV=4.4mm, XPL.

Plots compare Fe, Mg, and Mn concentrations of carbonate ICP data and show four distinct phases (Fig. 23). These plots show the chemical distinction between: the early calcite phase (V4a) with minor amounts of Fe and Mg; a Mn-calcite phase with similar Mn concentrations but distinct Fe and Mg concentrations from Fe-dolomite,

which is associated with the precious-metal minerals (V3); and a Fe-rich, low Mn, and comparable Mg- to Mn-calcite, ankerite phase (V4b). Based on the chemical relations (Fig. 24), pre-gold Mn-calcite and gold associated Fe-dolomite phases are present throughout the district. The intimate spatial relationship and optical properties suggest that these phases formed during the same veining event (V3) and show significant textural and Fe, Mg, and Mn concentration distinctions (Fig. 25). Paragenetically, the early calcite phase (V4a) lacks significant Fe and Mg. Later carbonates include comparatively Mn-rich calcite and Fe-dolomite (V3), and a later stage calcite phase (V4b) enriched in Fe ± Mg. Ankerite filled in the open spaces of the quartz veins and locally overprinted mineral phases formed during the earlier mineralizing events.

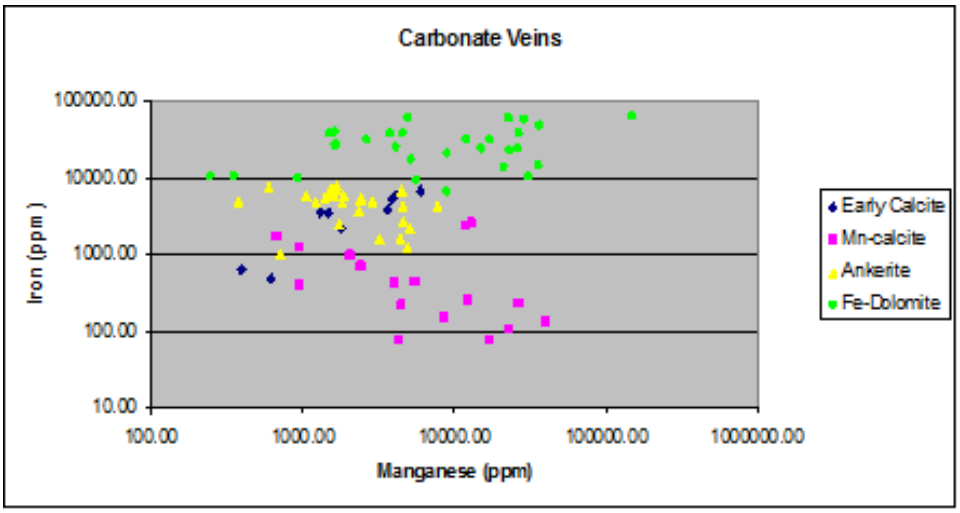

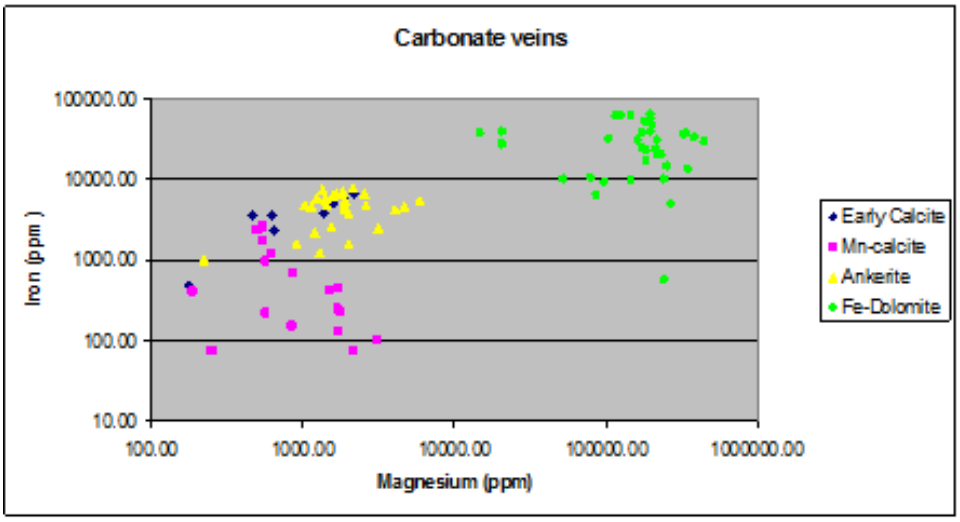

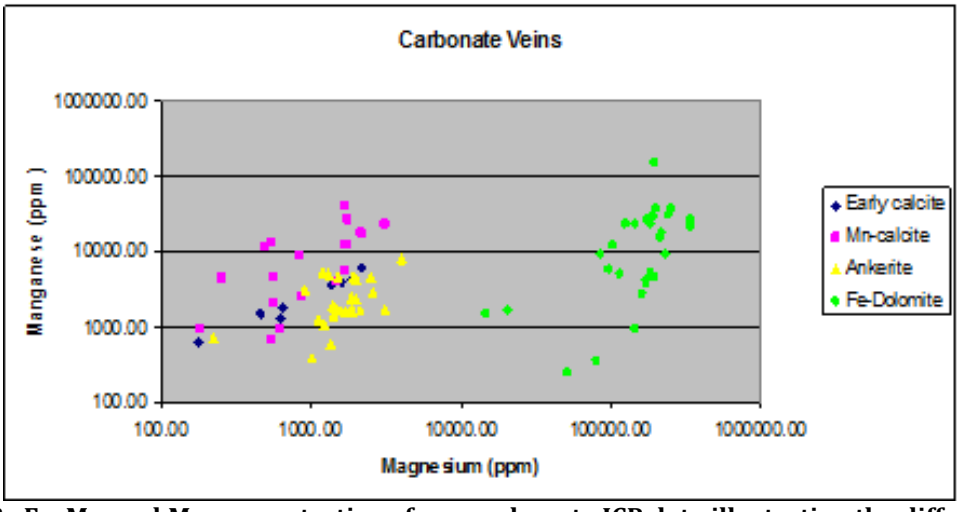

Figure 23. Fe, Mg, and Mn concentrations from carbonate ICP data illustrating the differences between the four carbonate phases. Note the overlapping early calcite phase on the Mn-calcite and ankerite phase.

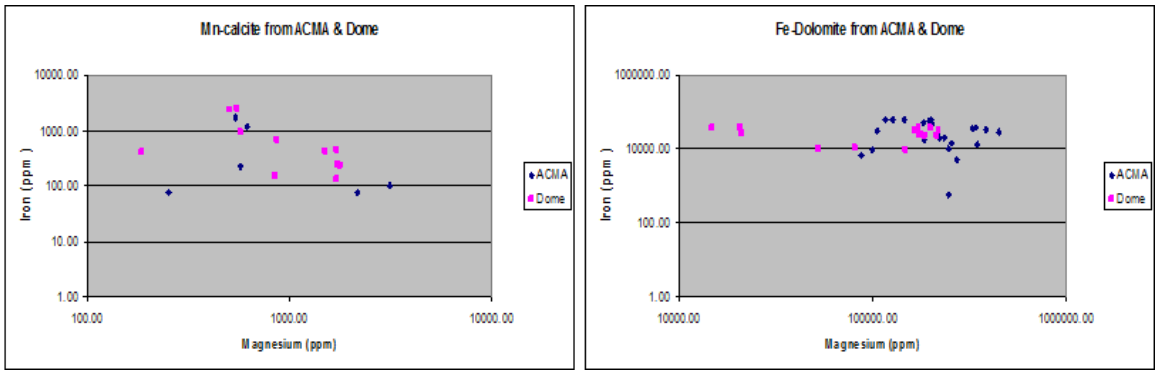

Figure 24. Fe-dolomite and Mn-calcite data from ACMA and Dome. These data points illustrate that the carbonates temporally associated with gold are found throughout the district, from ACMA/Lewis to Dome.

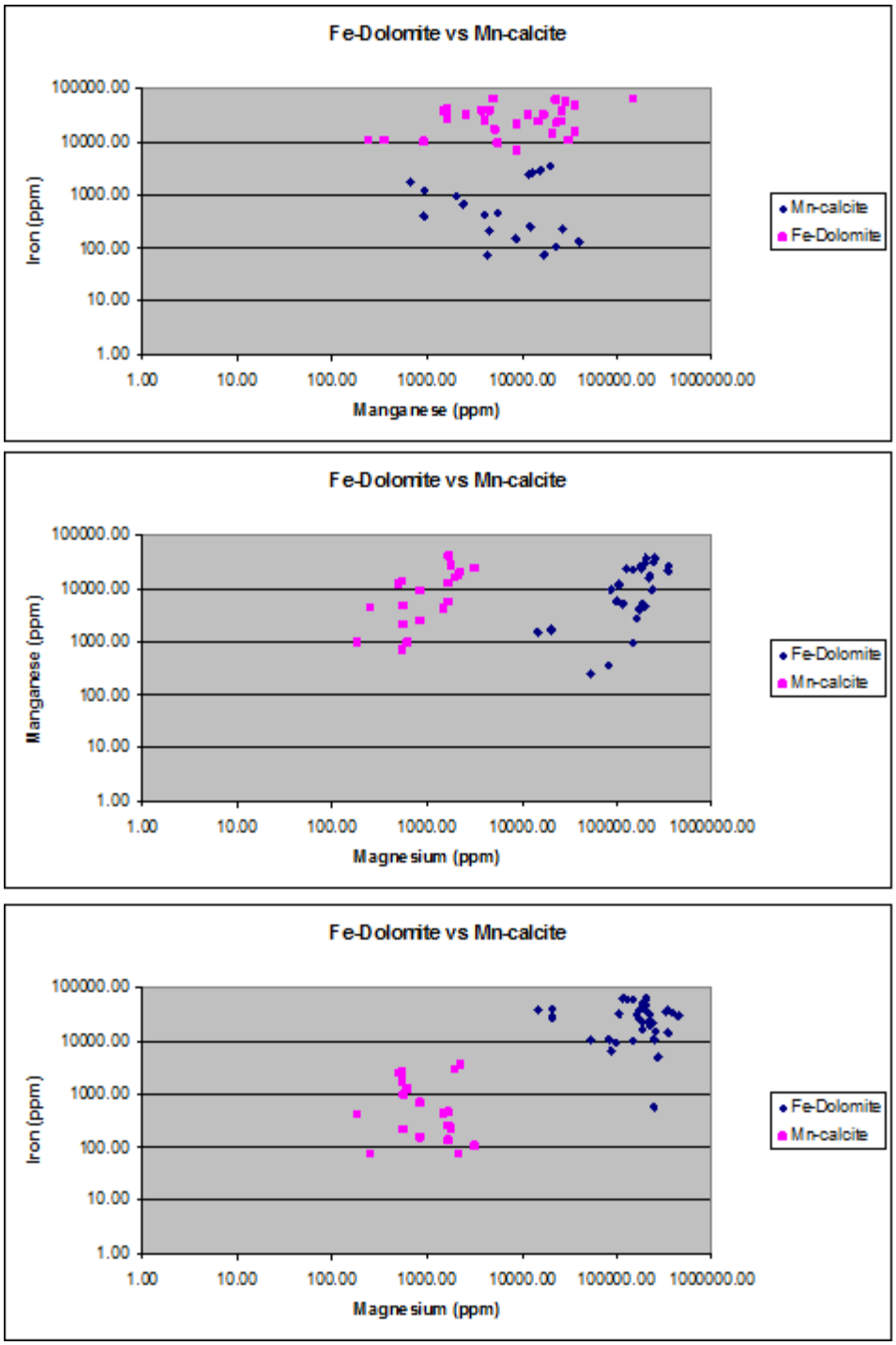

Figure 25. Fe, Mg, and Mn comparison between Fe-dolomite and Mn-calcite. Note the similar Mn values and very distinct Fe and Mg values.

4.2.1 Carbon and Oxygen Isotopes

The same carbonate samples used for SEM, CL, and LA-ICP-MS analyses were also analyzed for carbon and oxygen isotopes. The oxygen isotopes for all four vein phases contain $\delta^{18}O$ (VSMOW) values of 2.2 to 24.9‰ (Fig. 26). This study did not observe differences or trends between the phases or districts (Fig. 27) whereas work completed by Ebert *et al.* (2003b) found lighter $\delta^{18}O$ values (< 17.4‰) near Dome and heavier $\delta^{18}O$ values (18 to 25‰) in ACMA/Lewis suggesting a more meteoric involvement in the fluids associated with ACMA/Lewis. Szumigala *et al.* (1999) reported $\delta^{18}O$ values from sulfide-bearing quartz veins at ACMA/Lewis at 11 to 25‰. The $\delta^{13}C$ values for the four carbonate phases range from 1.8 to -16.7‰. These data are also consistent with values obtained from other Donlin Creek studies and from igneous rocks located in southwestern Alaska. No $\delta^{13}C$ values for Kuskokwim Group sediments have been determined (R. Harris, R. Goldfarb, T. Bundtzen, R. Newberry, and M. Miller, personal comm.). A plot of $\delta^{18}O$ and $\delta^{13}C$ values (Fig. 28) shows that data from this study (black circles) fall within a similar range as other isotopic samples taken from the property. These data are largely enriched in $\delta^{18}O$ and depleted in $\delta^{13}C$ values compared to regional igneous rocks. Since there are no $\delta^{13}C$ data for the Kuskokwim Group sedimentary host rocks only a range of $\delta^{18}O$ values can be shown (Fig. 28). The placement of Donlin Creek district data points between the regional igneous rock data and the Kuskokwim Group sedimentary rock $\delta^{18}O$ data suggest that the carbonates at ACMA/Lewis and Dome are from a mixture of local igneous and sedimentary sources.

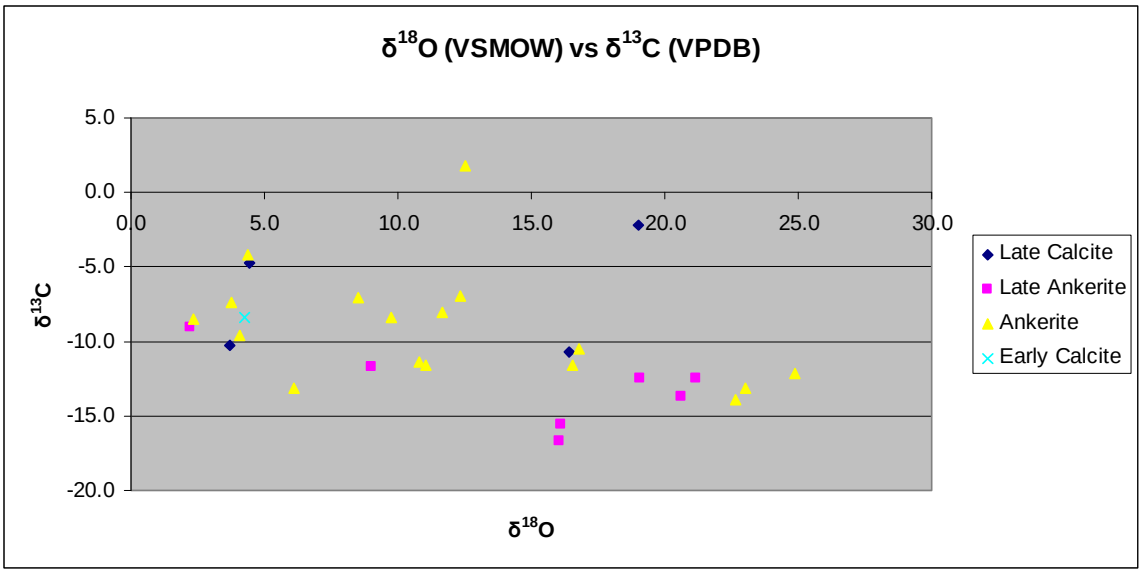

Figure 26. Diagram illustrating C and O isotopic data of the 4 carbonate phases within the Donlin Creek district. Note the wide spread data range of each carbonate phase.

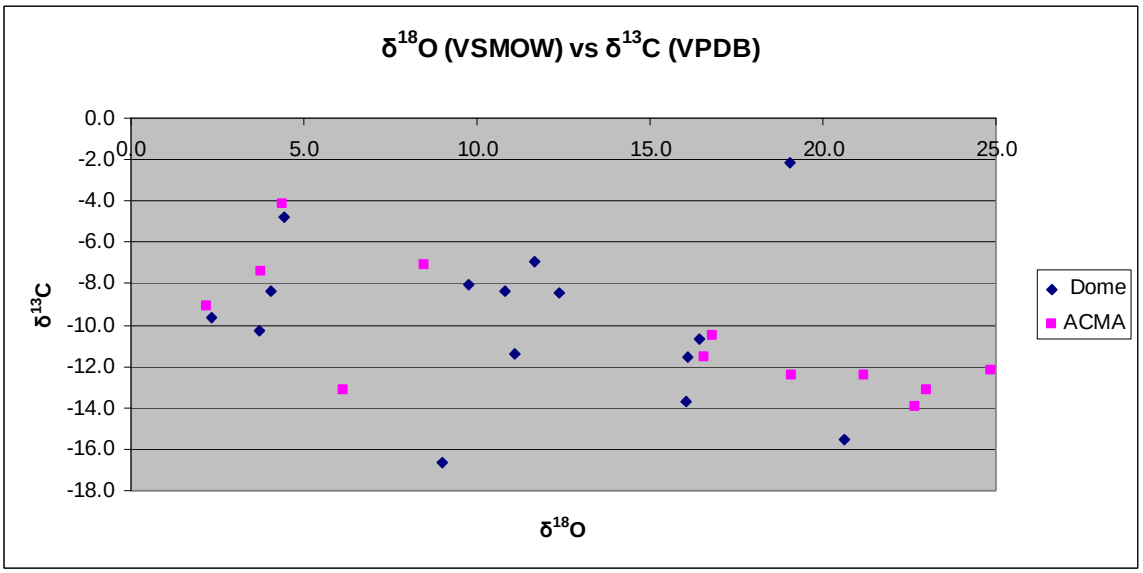

Figure 27. Diagram of C and O isotope data from ACMA and Dome illustrating the lack of trends or distinctive values between the two districts.

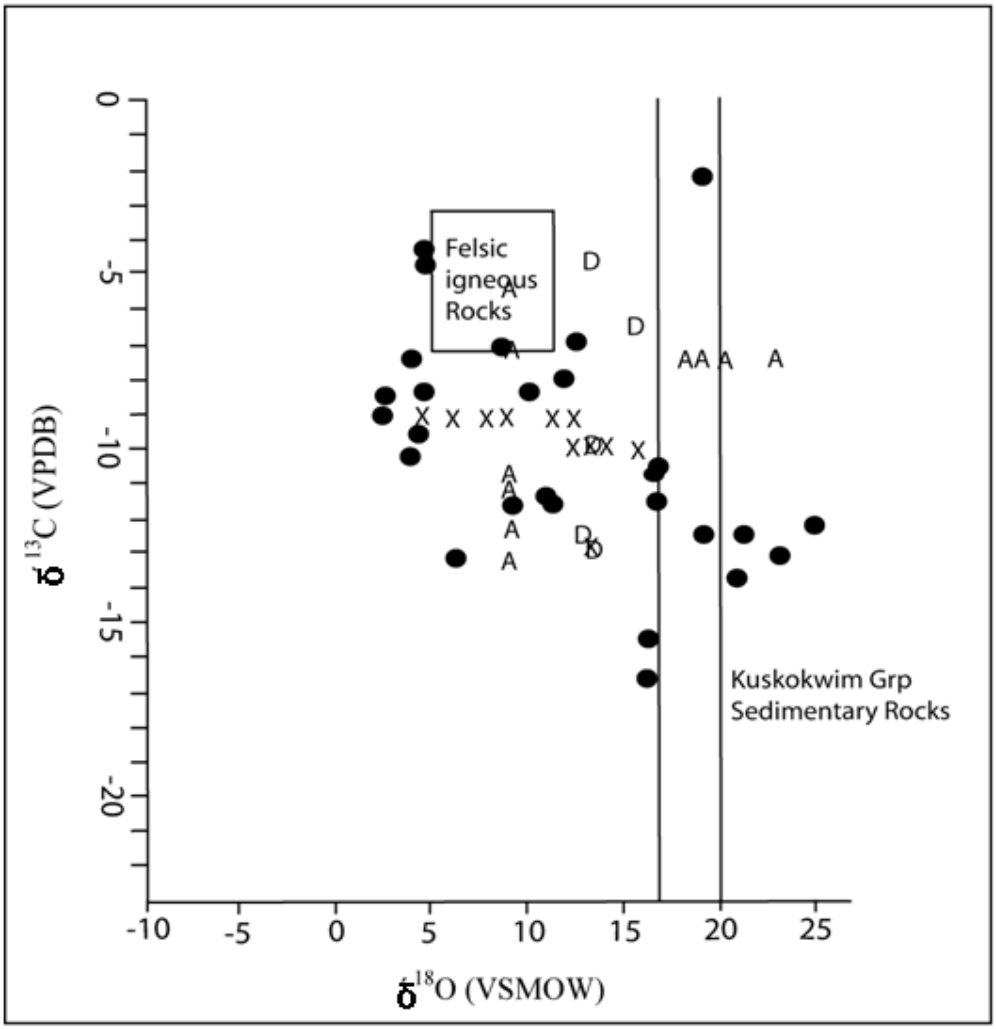

Figure 28. $\delta^{13}C$ and $\delta^{18}O$ isotopes (black circles) from the carbonates from ACMA/Lewis to Dome. A (ACMA), D (Dome), and X refer to other $\delta^{13}C$ and $\delta^{18}O$ isotopic data from a previous study (Ebert, 2002b). The felsic igneous rocks refers to isotopic compositions of local igneous intrusions, and the Kuskokwim Group sedimentary Rock area (two vertical lines) shows the range of $\delta^{18}O$ data for those units; however, no $\delta^{13}C$ isotope data from these rocks have been obtained (R. Harris, R. Goldfarb, T. Bundtzen, R. Newberry, and M. Miller, personal comm.).

4.3 Geochemical correlations

The whole rock samples selected for correspondence analyses, correlation matrices, and regression analyses were limited to igneous rock types containing gold grades greater then 1 gram per ton (gpt). Geochemical analysis of seven drill holes represents the ACMA/Lewis area. These data were analyzed with correspondence analyses and show a gold correlation with As, Hg, S, Ag, W, and Se (Fig. 29). These

same data analyzed using correlation matrices indicate an association of As and Rb with Au (Table 3). In addition, the regression analysis statistically illustrates the association of As, Rb, Se, Te, Tl, S, Be, P, Li, Na, Nb, Sb, Ta, In, Y, K, Ti, La, Ce, and Hg with gold (Fig. 30). The combined results indicate that As, Ag, Hg, Rb, S, Se, and W are the elements associated with gold in the ACMA-Lewis resource area. Two drill holes and eleven data points of igneous composition containing greater than 1 gpt gold were used to represent Dome in these geochemical analyses. These data indicate a correlation between Te, Hg, Bi, and As with Au using the correspondence analysis (Fig. 31). Correlation matrices show an association of As, Bi, Co, Hg, and Te with gold (Table 3). Statistical analysis indicates a gold correlation with Te, Bi, Nb, Hg, Ga, and Al (Fig. 32). The combined results suggests an association of Te, Hg, Bi, As, and Na with gold at Dome.

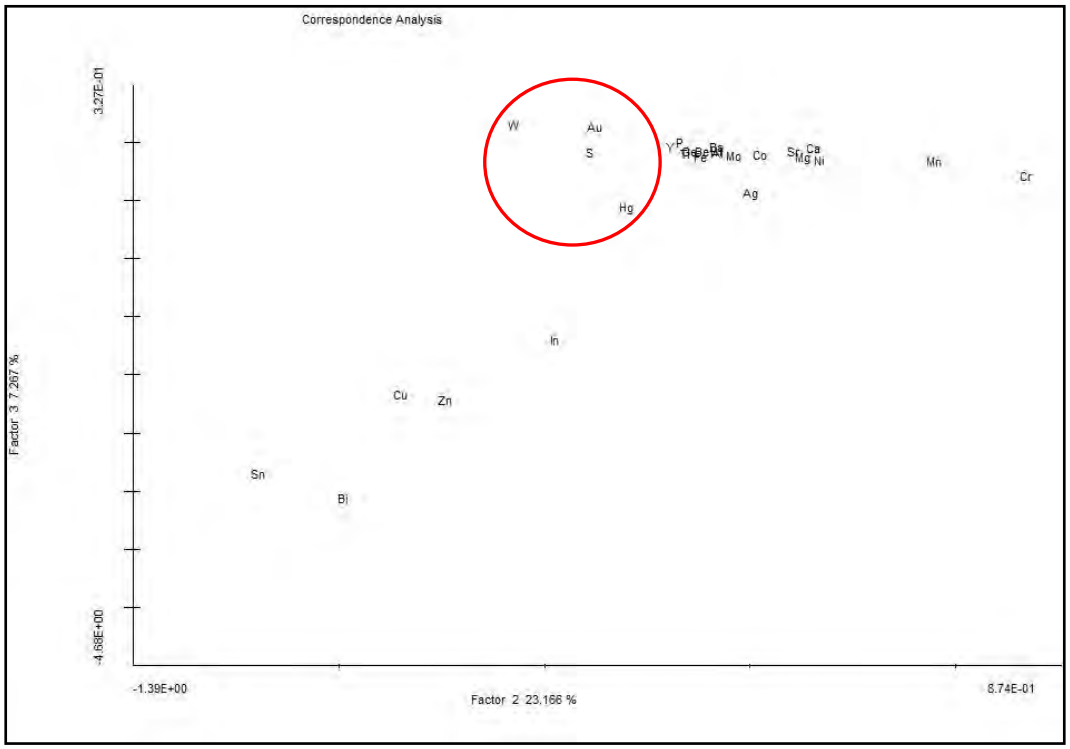

Figure 29. Correlation analyses representing the elements associated with gold in the ACMA-Lewis area. The red circle shows the close spatial relationship between gold and W, S, and Hg.

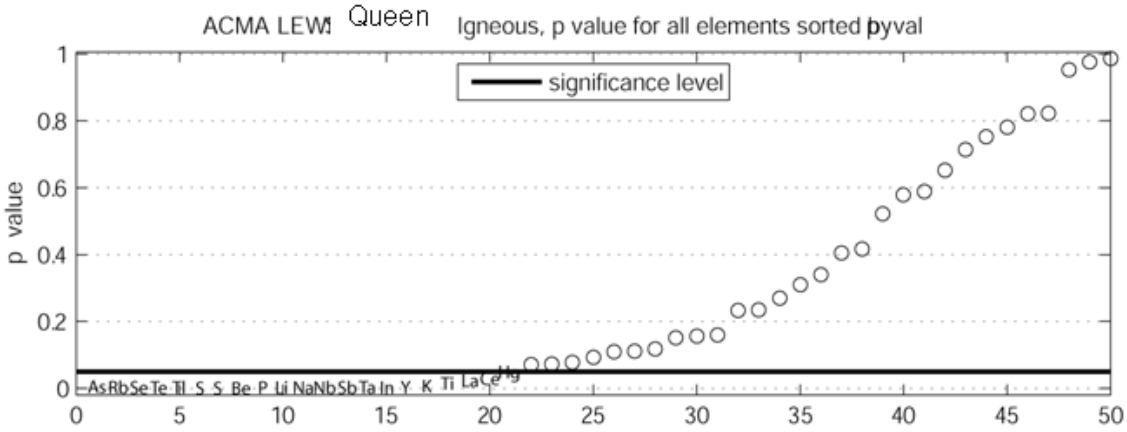

Figure 30. Regression analysis of composite geochemistry from a series of drill holes located in ACMA, Lewis, and Queen

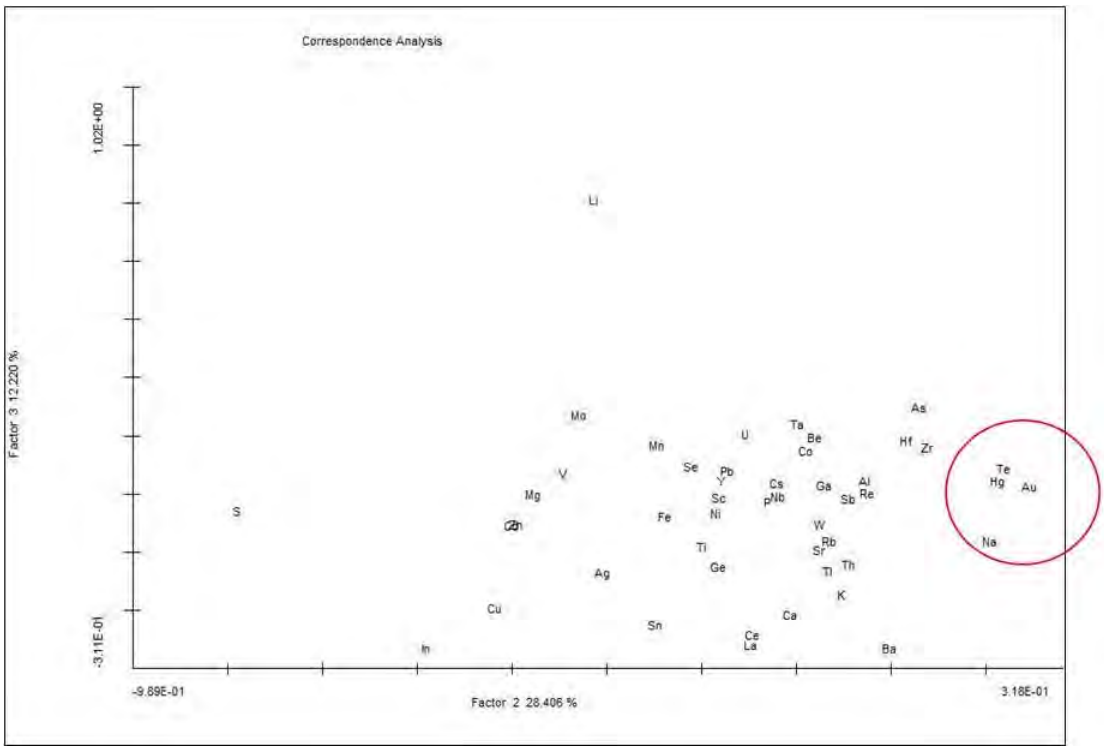

Figure 31. Correspondence analysis illustrating the elements associated with gold from the Dome region. The red circle indicates these elements.

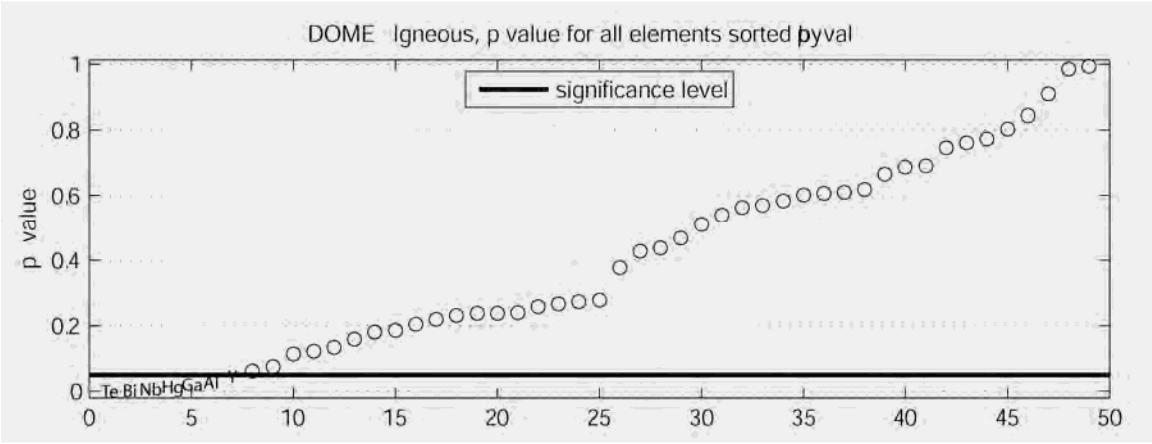

Figure 32. Regression analysis statistically correlating Te, Bi, Nb, Hg, Ga, and Al with gold in the Dome area.

Au	Dome	Snow	ACMA-Lewis
Au	1	1.000	1.000
Ag	-0.068	0.290	0.036
Al	-0.679	0.423	-0.133
As	0.494	0.664	0.550
Ba	0.039	0.634	-0.086
Be	-0.482	0.044	0.336
Bi	0.812	0.217	-0.043
Ca	-0.148	-0.547	-0.092
Cd	-0.170	-0.460	0.018
Ce	-0.389	0.600	0.143
Co	0.431	0.269	0.033
Cr	-0.266	0.804	-0.001
Cs	-0.436	0.199	0.011
Cu	-0.177	0.070	-0.011
Fe	-0.099	0.555	0.110
Ga	-0.692	0.104	-0.106
Ge	-0.295	-0.663	0.123
Hf	-0.003	-0.007	-0.079
Hg	0.730	0.477	0.102
In	-0.136	0.245	-0.039
K	-0.137	0.098	0.220
La	-0.359	0.579	0.151
Li	-0.187	-0.364	-0.298
Mg	-0.111	-0.047	0.052
Mn	-0.244	-0.282	-0.002
Mo	-0.393	0.531	-0.037
Na	-0.104	0.163	-0.232
Nb	-0.773	-0.182	-0.240
Ni	-0.373	0.345	-0.004
P	-0.505	0.581	0.289
Pb	-0.387	0.181	-0.122
Rb	-0.415	0.102	0.448
Re	0.000	0.000	0.089
S	-0.362	-0.535	0.314
S	-0.368	-0.552	0.307
Sb	-0.175	0.369	0.218
Sc	-0.402	0.507	0.111
Se	-0.557	0.071	0.365
Sn	-0.197	0.110	0.008
Sr	-0.193	0.576	-0.130
Ta	-0.580	-0.566	-0.219
Te	0.841	0.691	0.350
Th	-0.455	0.651	0.091
Ti	-0.086	0.550	0.164
Tl	-0.208	0.821	0.342
U	-0.388	0.170	-0.022
V	0.006	0.692	0.045
W	-0.223	0.305	0.115
Y	-0.613	0.123	0.192
Zn	-0.173	-0.158	-0.026
Zr	0.261	0.406	0.066

Table 3. The relationship of Au and other elements analyzed through correlation matrices. This diagram illustrates the correlation in the Dome, Snow, and ACMA-Lewis districts, respectively.

The samples discussed above represent ACMA/Lewis and Dome. Two drill holes are located at Quartz and Snow between ACMA/Lewis and Dome. Correspondence analyses of samples from these holes show correlation between Ba, Na, K, and Rb with gold (Fig. 33), whereas correlation matrices indicate an association with Al, As, Ba, Cr, Fe, Hg, La, Mo, P, Sc, Sr, Te, Th, Ti, Tl, V, and Zr (Table 3). The regression analysis does not demonstrate a statistical association between any elements and gold (Fig. 34). Due to the number of elements associated with gold using the correlation matrix, the random elements found with correspondence analysis, and the lack of relationship shown by the regression analyses this study concludes that there is no distinctive association between gold and any of the fifty other elements analyzed in the Quartz and Snow zones.

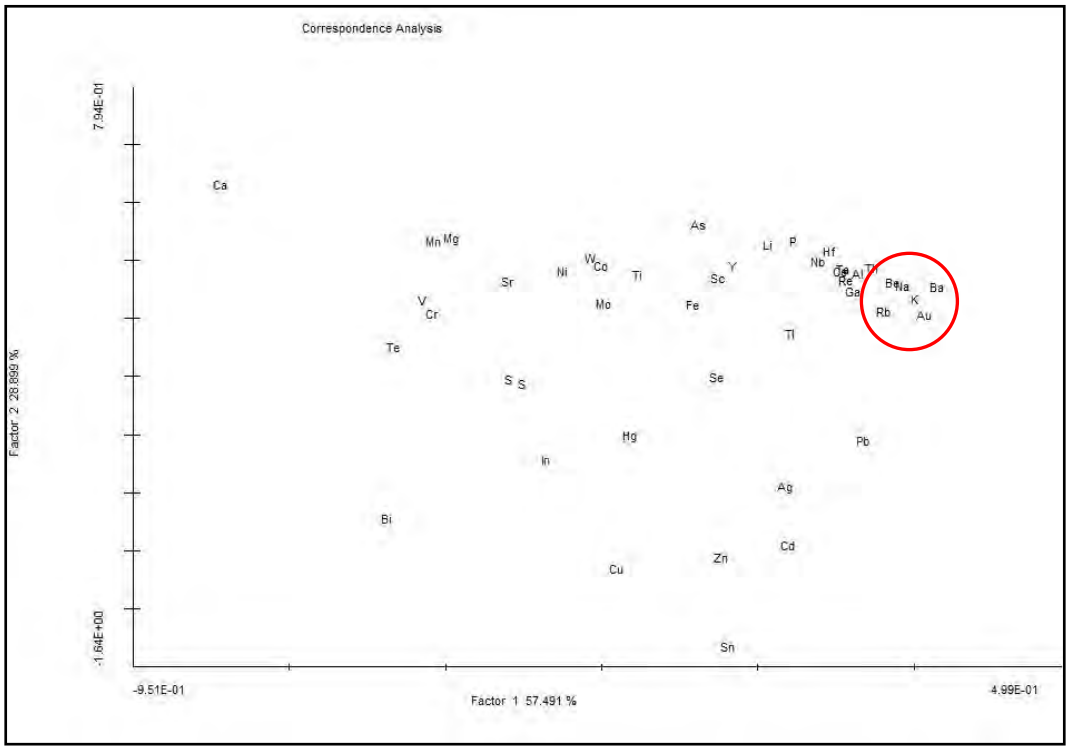

Figure 33. Correspondence analysis showing the elements associated with gold from the Snow and Quartz zones. The red circle highlights the relationship between gold and Ba, Na, Be, K, and Rb.

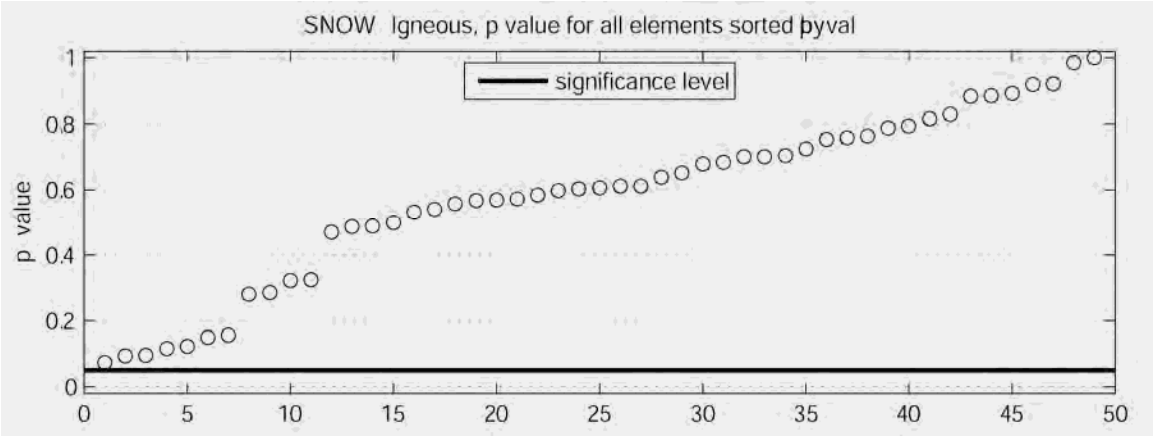

Figure 34. Regression analysis illustrating no statistical correlation between gold and other elements in the Snow and Quartz zones.

4.4 Argillic Alteration Mineralogy

Earlier studies identified an ammonia-illite alteration assemblage that is strongly associated with gold-bearing zones at ACMA/Lewis (Piekenbrock *et al.,* 2003). This

study also identified a similar pattern of gold and ammonia-illite alteration in the resource area (Fig. 15). Although the same alteration style exists at Dome, this alteration style apparently does not correlate to either of the mineralizing events in this area (Fig. 16).

4.5 Comparison of Gold and Argillic Alteration Mineralogy

Ordinary kriging methods of gold show the location of high grade gold zones in comparison to low grade gold zones (Appendix D). Clay alteration data including NH_4-illite, illite, and kaolinite, were also plotted on these 50 meter elevation maps. Previous modeling by Piekenbrock *et al.* (2003) proposed NNE trending mineral corridors illustrating the strong correlation between NH_4-illite and high gold grades. In comparison, the 50 meter elevation maps shown in this study also indicate NNE trend of high gold and clay alteration, but in addition show a SE trend that mimics sill orientation in ACMA. However, these NNE-trending "mineral corridors" proposed by Piekenbrock *et al.* (2003) do not occur in the sill-rich portion of the district (ACMA). Locally, the association between NH_4-illite and gold can be observed, but it can be better illustrated in the lithology-gold-alteration correlation models in Appendix C. Gold begins to decrease at depths greater than 500 meters and figures D-13 through D-16 show local gold occurrences on the east side of Dome and rarely on the west side of Dome.

5 Chapter 5: Discussion and Conclusion

5.1 Discussion

Prior to this study, the genetic relationship between the resource at Donlin Creek and the Dome prospect was equivocal and limited to their close proximities and a few chemical analyses. This study has shown through additional isotopic, petrographic, and immobile element analyses that ACMA/Lewis and Dome do have through going and likely genetically related base- (V1) and precious-metal (V3) vein assemblages. Further, carbonate mineralogy studies and geochemical analyses suggest that, although the systems are related, they differ in mineralogical make up, mineralizing events, and therefore geochemical signatures.

Pyrite, arsenopyrite, stibnite, realgar, and native arsenic form the predominant mineral assemblage in the ACMA/Lewis district. Conversely, sphalerite, chalcopyrite, pyrite, pyrrhotite, tetrahedrite, marcasite and minor arsenopyrite comprise the base-metal assemblage in the Dome region. Petrographic observations suggest the base-metal assemblage was over printed by the precious-metal assemblage as shown by the presence of arsenopyrite grains on the edges of pyrite, chalcopyrite, marcasite, and previously precipitated blocky arsenopyrite grains. Due to the lack of base-metal minerals in the resource area, the overprint is characterized by arsenopyrite that crystallized at the edges of pyrite grains with a rock replacement texture (porous), consistent with textures found at Dome, and local rare occurrences of pyrrhotite. Pyrite has a blocky, framboidal, or euhedral

grain shape in the resource area compared to the porous and locally blocky appearance at Dome.

Histogram-style diagrams show distinct Ag, Hg, Rb, S, Se, and W, and Te, Hg, Bi, As, and Na geochemical signatures likely reflecting an overprinting event (Figs. 35-38). Twenty elements are compared with gold values from two high-grade drill holes located in ACMA (DC08-1702) and Dome (DC08-1771). The ACMA figures (Figs. 35 -36) illustrate peaks at Au, Ag, As, Be, Hg, K, Rb, S, Sn, Tl, ± Pb around depths of 195 meters. The variety of element associations with Au may demonstrate different hydrothermal fluid events. In addition, peaks in the Dome drill hole (Figs. 37 - 38) at depths of 40, 130, and 360 meters show a stronger association between Au and Te, As, Rb, and Ag, As, Cu, Pb, ± S suggesting two hydrothermal fluid events. Geochemical peaks at 40 meters characterize the Dome mineralizing event. Additionally, the geochemical signatures at 130 and 160 meters are largely coincident with the resource area, with the addition of Cu and Pb. Cu and Pb may have been part of the same hydrothermal fluid, but were deposited at higher temperature locations, which is characteristic behavior for these elements. Fe, Mg, and Mn that are commonly found in the carbonate assemblages locally show a correlation with gold (Figs. 36 & 38).

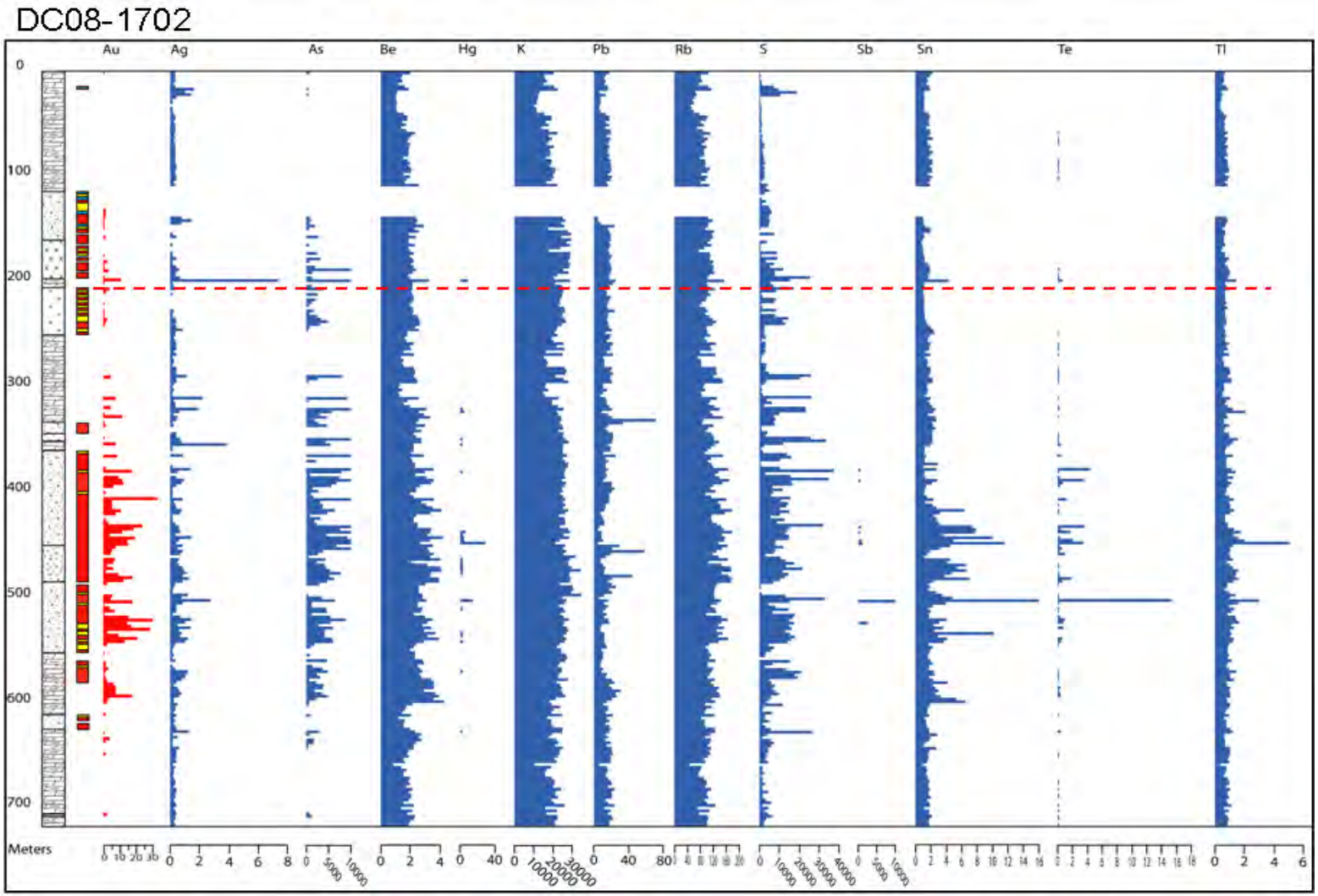

Figure 35. Elemental associations from drill hole DC08-1702 in ACMA. Note the peaks located above the red dashed lines indicating the Au-Ag-As-Be-Hg-Rb-S-Sn-Tl geochemical signature which characterizes the ACMA/Lewis area.

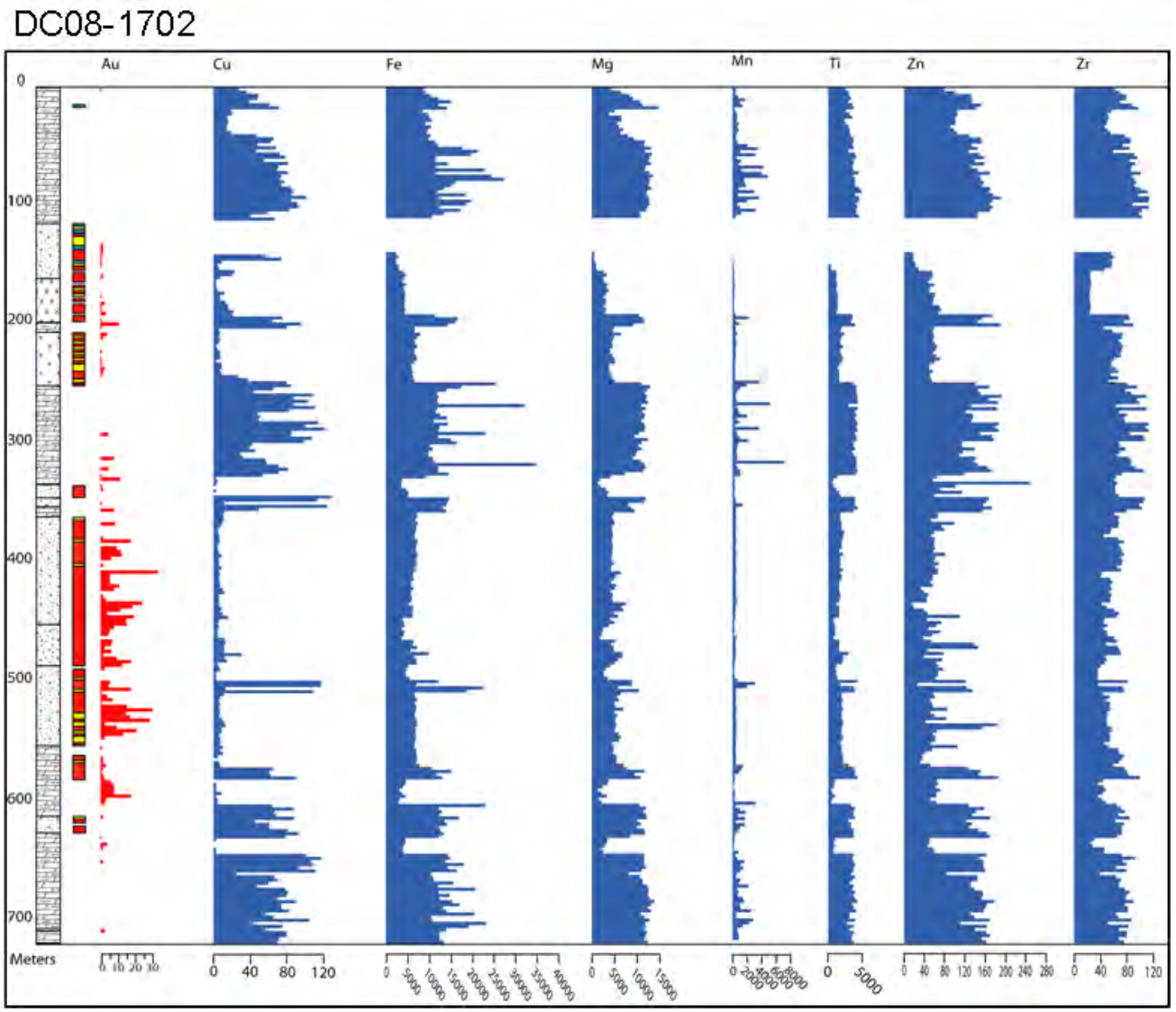

Figure 36. Continued elemental associations from drill hole DC08-1702 in ACMA.

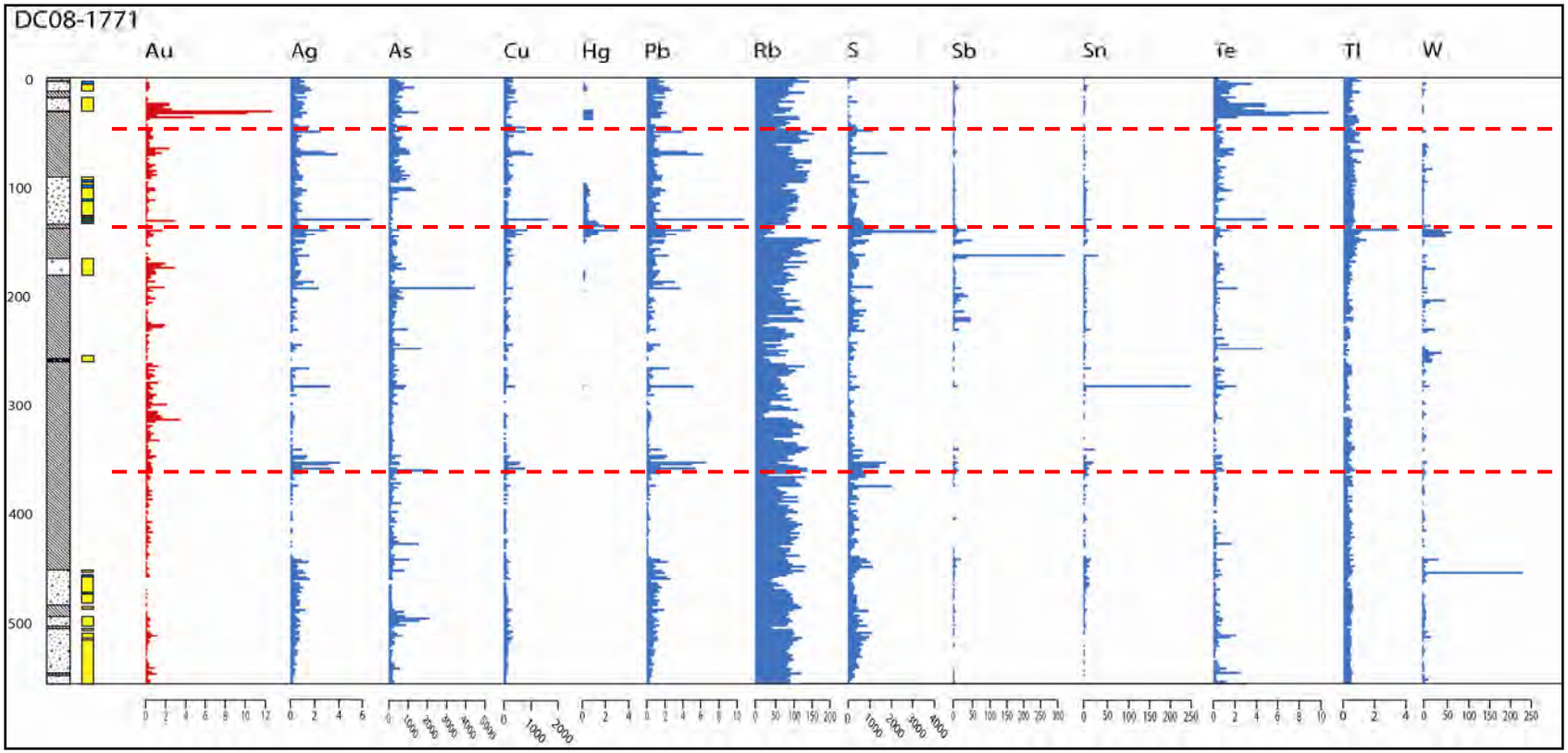

Figure 37. Composite geochemical data illustrating the association of elements in drill hole DC08-1771 from Dome. Note the two hydrothermal fluid events above the red dashed lines: on or around 40m, and the other two around 130 and 360m.

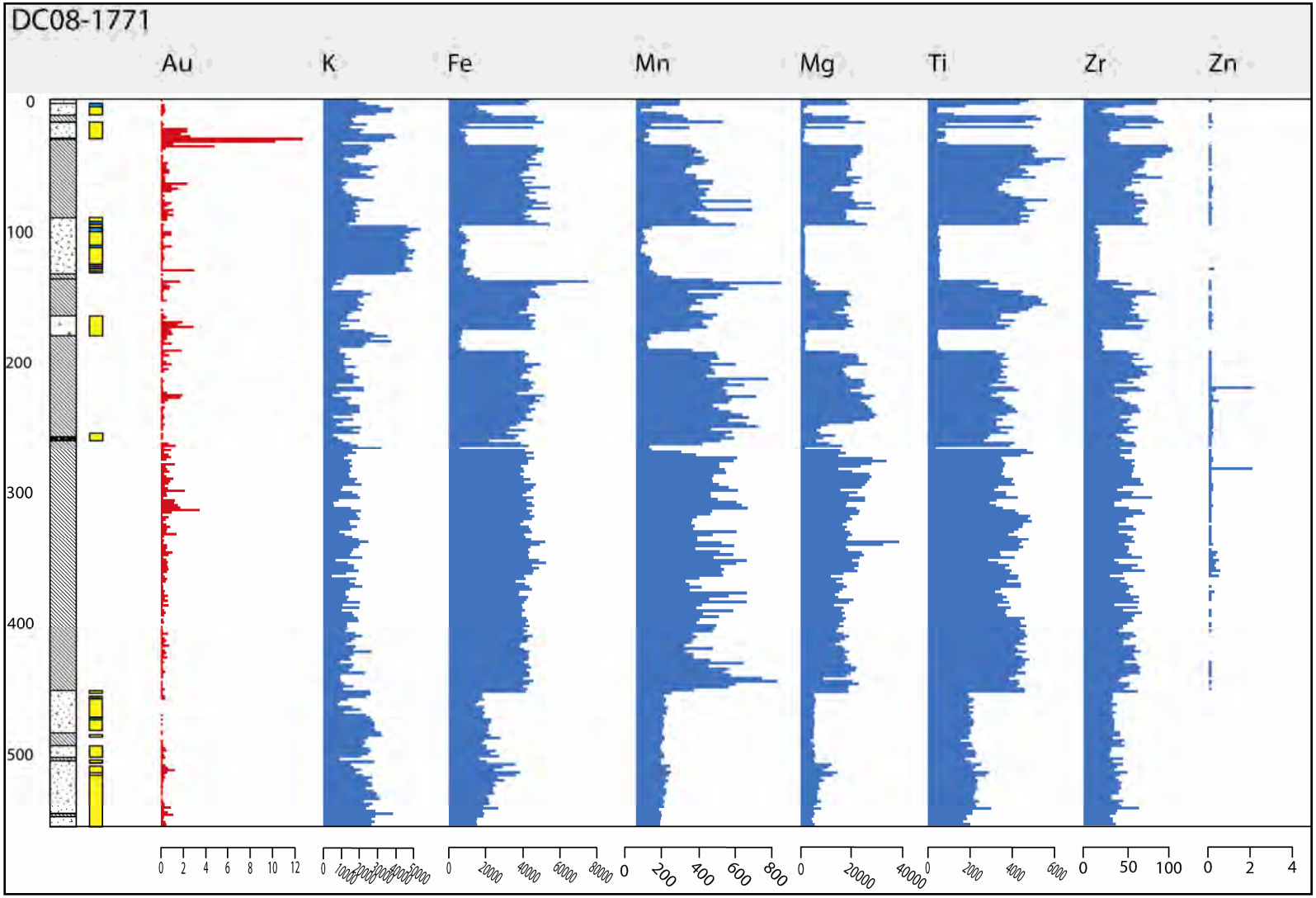

Figure 38. Geochemical data from Dome drill hole DC08-1771 showing that K has a positive correlation and Fe, Mn, Mg, Ti, Zr, and Zn have inverse correlations to gold.

In the gold grade versus alteration correlation diagrams, NH_4-illite is shown to strongly associate with the higher gold grades in the resource area (Fig. 15). Petrographically, this association has not been observed during the course of this study. The gold-NH_4-illite correlation is not found at Dome (Fig. 16). The predominant clay mineral in the base-metal region is illite; NH_4-illite is local and rare. In addition, the carbonate staining completed during this project shows the strong correlation between high grade zones and calcite- (Mn) ± ferroan-calcite-rich areas. However, LA-ICP-MS, SEM, and petrographic analyses indicate an intimate association between these high grade zones and ferroan-dolomite and Mn-calcite. Manganese-calcite is more wide spread throughout the district than are the calcite, Fe-dolomite, and ankerite phases. The widespread nature and its platy nature, suggesting deposition just prior to the deposition of Au, are likely the reasons for the association between high gold grades and Mn-calcite in the carbonate-lithology-alteration-Au models (Appendix C). High grade zones, NH_4-illite, and Mn-calcite coexist in the resource area and less so beyond Queen. The strong correlation between NH_4-illite and Mn-calcite and the limited amount of stained drill holes beyond Snow suggests the association between carbonate type and gold grade also does not exist NNE past Queen.

The geochemical signature at the Snow and Quartz zones is diffuse and appears random, and stibnite is more abundant here compared to the resource area and Dome. Petrographic analyses indicate intense post-mineralization fracturing of

precious and base metal minerals at ~100 meters depth on the west side of Dome and at ~240 meters deep beneath Dome. Limited evidence of this post-mineralization structure suggests an eastward dipping orientation. MacNeil (2009) discussed several parallel post-intrusion faults within the resource area that dip steeply to the NE. $^{40}Ar/^{39}Ar$ and U-Pb dates for illite within mineralized veins at Dome reveal an age younger than the mineralizing event at ACMA-Lewis (Goldfarb *et al.,* 2004). Reactivation and subsequent fluid introduction along this fault have annealed these micas producing an age that was younger than the actual mineralization age.

The presence of stibnite within the precious and base metal mineral fractures at Snow and Quartz suggests stibnite deposited paragenetically after the faulting or fracturing event by an influx of additional fluids. Previous isotopic studies show a distinct $\delta^{34}S$ (-16 to -27‰) and $\delta^{13}C$ (-13.5 to -21.2‰) values from this event compared to the overlapping ACMA/Lewis and Dome sulfur and carbon values ($\delta^{34}S$ -8 to -16‰ and $\delta^{13}C$ –4.6 to -13.4‰) in the resource area. The addition of this low temperature hydrothermal fluid along post-mineralization faults appears to have strongly disrupted the original geochemical signature in the Snow/Quartz zone and the timing of mineralization at Dome, but weakly disrupted the geochemical signature or the temporal relationship of the mineralizing events in the resource area.

Past studies concluded that the ACMA/Lewis precious-metal mineral assemblage formed in a low-sulfidation epithermal system (Ebert, 2000; 2003c); an orogenic or mesothermal assemblage based on geochemical signature, alteration, and oxygen isotopes (Goldfarb *et al.,* 2004); and an intrusion-related Au deposit similar to other intrusion-related systems in the Kuskokwim Mineral Belt in which Donlin Creek lies (Szumigala, 1996). Ebert *et al.* (2003b) proposed using the term "reduced sub-epithermal gold" deposit when referring to the resource area and "reduced porphyry Au" deposit in reference to the Dome prospect. The mineralogy and porphyry associations with intrusion-related gold deposits are also reduced in nature, suggesting that the terms "reduced intrusion-related gold systems" and "reduced porphyry Au" are describing the same systems with differing terminology. Some argue that the intrusion-related label "lacks descriptive implications" and is a catch-all term rather than a classification scheme.

The term "low sulfidation epithermal" does not fit the Donlin Creek district because of the predominant illite ± kaolinite alteration assemblage, the large magmatic water component in the fluids that produced the productive veins, and the calculated 0.1 water:rock ratios (Ebert *et al.,* 2003b). In addition, the vuggy nature of the district veins, (Fig. A-65) argues against a mesothermal origin for this system. Vuggy or open-spaced textures suggest formation at depths of 1-2 kilometers or less; in contrast, mesothermal systems develop at depths of 12-15 km. Although significant amounts of CO_2 can induce boiling and therefore form a vuggy texture at

greater depths, this reaction does not occur at the temperatures suggested to have deposited the minerals at Dome (Drummond and Ohmoto, 1985) where boiling textures are observed. Further, the sulfur isotope range for the district is markedly lower than those reported for orogenic systems (Goldfarb *et al.,* 2004). The fine grained nature of the rhyodacite host rocks at Dome also suggest shallow emplacement of a hot magmatic body that resulted in rapid cooling of the magma. A mesothermal classification could be plausible for the resource area alone due to the temperature constraints; however, the resource area is genetically related to Dome and should be categorized as a whole. The formation temperatures and boiling textures in this area suggest that the emplacement of the intrusion-related system at Donlin Creek is shallower than mesothermal ore deposit requirements.

The precious-metal geochemical signature of ACMA-Lewis and the more base-metal-rich assemblage at Dome suggest lateral zoning within a single mineralizing system. Szumigala (1996) discussed the characteristics of several intrusion-related deposits located along the Kuskokwim Mineral Belt. These characteristics include a genetic association with Late Cretaceous-Early Tertiary igneous intrusions, a zoned relationship between Au and smaller scale base-metals districts with significant As and less significant Hg and Sb, a predominant propylitic alteration with local ankerite and illite, structural control with local breccias, and a chalcopyrite-arsenopyrite-pyrite-tetrahedrite ore assemblage. Hart (2007) suggested that these reduced intrusion-related gold systems (RIRGS) “are a distinct class that lacks

anomalous Cu, have associated W, low sulfide volumes, and a reduced sulfide mineral assemblage, and are associated with felsic, moderately reduced (ilmenite-series) plutons." In addition Hart (2007) also suggests, the timing of the intrusive host rocks and the mineralization are contemporaneous and is a key characteristic component to this ore deposit systems. Figure 39 demonstrates the different types of ore deposits that are associated with intrusion-related Au systems. ACMA/Lewis and Dome fall into the high-level system still associated with igneous material outlined in red. The similarities and differences between the RIRGS within the Kuskokwim Mineral Belt and Donlin Creek are significant and are outlined in Table 3. Describing the ACMA/Lewis and Dome deposits as separate deposit types (i.e. reduced sub-epithermal and reduced porphyry Au) does not imply a genetic relationship between the two districts. As such, this study concludes that the Donlin Creek precious-metal resource and closely located base-metal assemblage fall into a relatively new classification scheme of high-level reduced intrusion-related gold vein system that is characteristic of the Kuskokwim Mineral Belt.

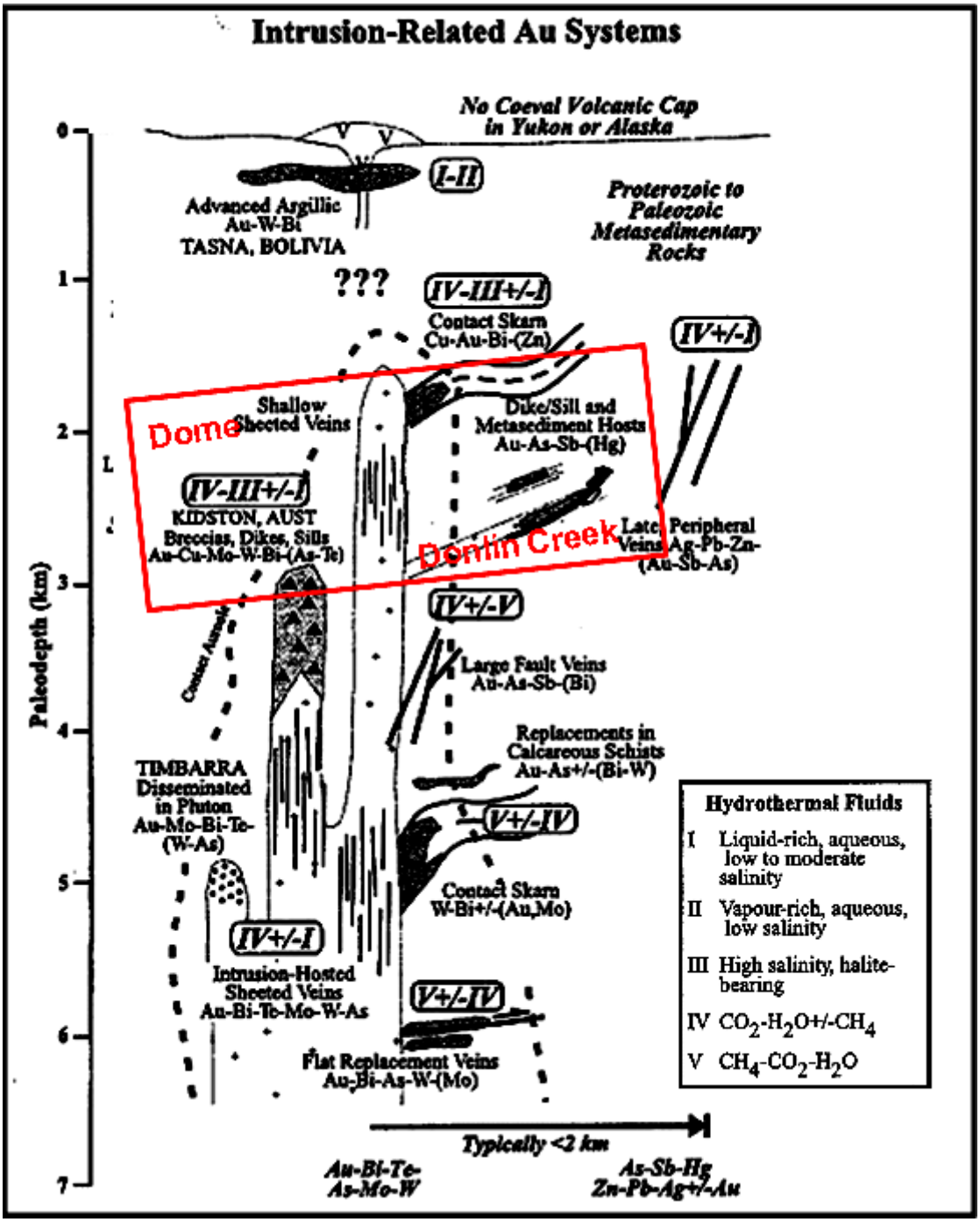

Figure 39. A model illustrating the variation of ore deposit types associated with intrusion-related systems. The ore types similar to ACMA/Lewis and Dome are shown in the red box (modified from Lang *et al.,* 2000).

Deposit Type/Location	Donlin Creek	Dome	RIRGS
Igneous composition	Rhyodacite	Rhodacite	Intermediate to felsic
Formation Depth	1 to 2 km	3 to 5 km	3 to 9 km
Formation T (°C)	275-300	400 to 450	250 to 650
Geochemical Signature	Ag,As,Hg,Rb,Se, W	Te,Hg,Bi,As,Na,Co,Mo	Bi,W,As,Mo,Te,±Sb
NaCl eq wt %	3-4 wt%	>>3-4 wt%	2 to 6 wt%
CO_2 concentrations	2-6.5 wt.%	3.1-14.6 wt.%	5-14%
Tectonic Setting	Subduction-related	Subduction-related	Convergent plate boundaries
Alteration	QSP-carb-il-kaol-dick-mont	Qtz-ser-sulf-carb-potassic	Prop-ankerite-sericite
Formation waters	Magmatic±meteoric	Magmatic±meteroic	Magmatic±meteroic
Sulfur ($\delta^{34}S$)	-27.2 to -7.3‰	-27.2 to -7.3‰	-11 to 0‰
Oxygen ($\delta^{18}O$; minerals)	2 to 25‰	2 to 25‰	13 to 20
Strontium ($^{87/86}Sr_{initial}$)	0.706 to 0.709	0.706 to 0.709	0.709-0.720
$^{206}Pb/^{204}Pb$	18.76 to 19.31	18.76 to 19.31	19 to 19.45
$^{207}Pb/^{204}Pb$	15.55 to 15.62	15.55 to 15.62	15.57 to 15.58
Tourmaline	Present	Present	Present
Quartz textures	Vuggy	Vuggy	
Vein morphology	Sheeted	Sheeted, stockwork	Shear, fracture fillings, qtz
Fe-Ti Oxides	Reduced, ilmenite	Reduced, ilmenite	Reduced, ilmenite
Base metal content	Low base metals	low base metals	Low base metals
Metamorphism	Rare	Hornfelsing	Hornfelsing
Ore minerals	Aspy-stibnite-native arsenic-realgar-pyrite-sphalerite	sphalerite-chalcopyrite-tetrahedrite-pyrite-pyrrhotite-marcasite±aspy	Chalcopyrite-arsenopyrite-pyrite-tetrahedrite

Table 4. Comparison of ACMA/Lewis and Dome to the reduced intrusion-related gold system (RIRGS) ore deposit type.

5.1.1 Mineralization History

The primary mineralogy within the five phases of rhyodacite intrusions consists largely of quartz, feldspar, biotite, and rutile. Three major events occurred relatively contemporaneously in the Donlin Creek district: emplacement of igneous dikes in greywacke-rich zones and sills in shale-rich zones, reactivation along the Nixon-Fork fault forming NNE trending fractures in the dike and sill package followed by several phases of hydrothermal fluids, which produced the district mineralogy. As the dikes and sills cool, the hydrothermal fluids are pushed into the NNE trending fractures and precipitate quartz. This first quartz phase (V2a) is enriched in trace As, Ba, Fe, Li, Mg, Rb, Sn, and Ti and the open spaces within the fractures were nearly filled near Dome and partially filled in the resource area during this first event. The resource area commonly has a quartz comb texture at the fracture edges and wider open spaces compared to Dome. In contrast, quartz veins at Dome commonly contain a sugary texture and are locally open spaced. The multiple phases of rhyodacite in the district supplied the additional vein material, which fill the remaining open fracture spaces and subsequent fractures. These secondary fractures and/or microfractures formed by the cooling of igneous material and are conduits and hosts for hydrothermal fluids and minerals. Because carbonate precipitation takes place with increasing temperature, the precipitation of a relatively barren calcite phase (V4a) may reflect the influx of the second magmatic pulse. Calcite occurs as massive twinned grains that were precipitated between the first formed quartz phase and was locally replaced by sulfides. This calcite phase is only found at Dome. The base-metal-rich mineralogy (V1)

precipitated next, accompanied by the change in temperature rather than a pressure change due to the lack of platy textures or evidence of boiling of the calcite phase. This event produced tetrahedrite, sphalerite, chalcopyrite, pyrite, marcasite, and arsenopyrite, which indicate that the fluid was rich in As, Cu, Fe, S, Sb, and Zn. Tetrahedrite, sphalerite, and chalcopyrite are most common near Dome. Pyrite, marcasite, and possibly arsenopyrite are common in the resource area. The porous or rock replacement texture of pyrite and the tendency of marcasite to fill in between pyrite grains enhanced the identification of these phases in the resource area. The magma chamber sequestered Fe, S, and combines with meteoric waters from the sedimentary host rocks. The significant amount of carbonate within the resource and sulfur and oxygen isotope analyses support meteoric water input. The ensuing, most productive event in terms of gold precipitation precipitated Mn-calcite, Fe-dolomite, arsenopyrite, pyrite, realgar, and native arsenic (V3). Boiling, resulting in a change of pressure is most likely the reason for deposition of these precious-metal minerals. This event also introduced magmatic As, Fe, Mg, Mn, S, and Sb and sedimentary Fe and S into the mineralized area, locally precipitating Mg-rich chlorite within the igneous groundmass. Wide spread, platy, and locally massive Mn-calcite precipitated first followed by Fe-rich dolomite with a "grungy" appearance. The Fe-rich dolomite phase is intimately associated with arsenopyrite and locally pyrite. The youngest quartz phase (V2b) is barren and locally replaced earlier carbonate phases. The V4b event including Fe-rich calcite, tourmaline (Figs. A-50 and A-51), and fluorite (Figs. A-5 and A-52) overprinted all of the older

mineral assemblages and continued to filled open fractures in the resource area. Post-mineralization stibnite was the final hydrothermal event that locally overprinted and filled the spaces between mineral fractures and in open fracture spaces. Supergene hematite, kaolinite, and illite, locally replaced the carbonate and base- and precious-metal assemblages.

The quartz-sulfide-illite-carbonate ± kaolinite and hematite alteration assemblage is extensive in the ACMA/Lewis resource area. In contrast, the alteration styles at Dome are more focused. Sulfides in the sedimentary groundmass occur at greater depths north of Dome compared to the sulfides on top of Dome. In addition, the sulfide mineralogy occurs at shallow depths on the east and west sides of Dome. Secondary biotite is present at 33 to 70 meters at Dome and also rarely at Lewis, and hematite occurs at 123-248 meters at Dome and intensifies southward towards ACMA/Lewis. Carbonate alteration minerals are common at depths greater than 123 meters, and the sulfide mineralogy associated within veins occurs at greater than 123 meters on top of Dome and to the east. This assemblage is noted at 72 to 126 meters to the west of Dome. Kaolinite is wide spread below 195 meters. In summary, the sulfide minerals found in the groundmass and vein assemblages, and carbonate, kaolinite and locally biotite, are all present at greater depths to the east and north of Dome compared to the west. These alteration patterns at Dome suggest a NE source direction for the hydrothermal fluids and possibly a magma chamber that ultimately was responsible for the mineralizing fluids in the district.

Higher temperatures, greater ore formation depth, thicker vein widths, local potassic alteration, and the presence of hornfelsing found at Dome support the alteration evidence in that Dome was spatially closer to the magmatic source than was the ACMA/Lewis district. An increase in hematite, carbonate, As, and Hg concentrations, and lighter δD and $\delta^{18}O$ values from Dome to ACMA/Lewis could suggest a shallower more distal emplacement of the ACMA/Lewis district compared to Dome.

5.2 Exploration Implications

Based on this and other studies, NH_4-illite is a strong indicator of gold in the resource area. In addition, Mn-calcite ± ankerite are also guides to higher gold grades. Unfortunately, these exploration tools are not useful at the currently uneconomic Dome prospect. Piekenbrock *et al.* (2003) constructed a map illustrating corridors of clay alteration with respect to gold grade. Additional mapping at 50 meter elevation intervals completed during this study demonstrated that the mineral corridors proposed by Piekenbrock *et al.* (2003) do occur in the Lewis-Queen areas where dikes are dominant. In contrast, these corridors were not clearly observed in the sill dominant ACMA area. There, gold tends to parallel the sill orientation with a NNE trend in the 400 zone where RDXL dikes occur. This and previous studies suggest that the rhyodacite intrusions will continue to be good targets for exploration; however, NH4-illite and Mn-calcite can guide on a smaller scale to more specific high grade zones.

5.3 Conclusions

The study of carbonate mineralogy, geochemistry, and argillic alteration completed during this project has demonstrated, with the addition of previous studies, the genetic relationship between the >35 Moz Donlin Creek resource and the base-metal-rich Dome prospect to the NNE. The presence of a potassic alteration assemblage, mineralogical evidence of higher temperatures, hornfelsed rocks, and thicker veins compared to the resource area suggest that the Dome prospect formed closer to the large causative magmatic body at depth. Alteration patterns further suggest a magmatic source to the NE of Dome. In contrast, the lower temperature geochemical signature, smaller vein widths, lack of hornfelsed rocks, and significant amounts of low temperature illite at the resource suggest that ACMA/Lewis formed at greater distance from the heat source. A paragenetic sequence demonstrates the continuity of several quartz, sulfide, and carbonate veining events that extend from the Dome prospect to the resource area at ACMA/Lewis. Sulfur, carbon, and oxygen isotopic data from these veins overlap in the precious and base-metal districts, suggesting a similar evolution and origin for these events and therefore a genetic relationship between these two dissimilar ore deposit types. In addition, immobile element analyses indicate that the host rhyodacite intrusions that extend from Dome to ACMA/Lewis are also genetically related. As a result, this study suggests the Te-Hg-Bi-As and locally Cu-rich Dome prospect is laterally related to the As-Ag-Hg-Rb-S-Se-W-rich >35 Moz resource at ACMA/Lewis by through going quartz, sulfide, and carbonate veins within rhyodacite hosts. In addition, this study proposes that the Donlin Creek project is a high-level reduced intrusion-related

deposit. The significant correlation between the characteristics in the Donlin Creek district and these deposit types as outlined in Table 4, strongly supports this classification. These reduced ore deposit types are common in the Kuskokwim Mineral Belt and the Tintina Gold Belt in which the Donlin Creek district lies. The strong correlation shown between NH_4-illite, Mn-calcite ± ankerite and gold will aid in future exploration for large tonnage low grade gold deposits in this district and perhaps in others.

5.4 Recommendations for Future Work

The lack of carbon isotopic data for the Kuskokwim Group sediments limits the source of carbon found within the system. These new data will better define the contribution, if any, of these sedimentary rocks to the mineralizing fluids, and the changes in carbon that might have occurred from the sedimentary origins to the igneous intrusions and mineral deposits.

Szumigala (1996) showed that several zoned ore deposits within the Kuskokwim Mineral Belt have an upper level mercury signature. Donlin Creek has characteristics of the intermediate and greater depths for this deposit type but lacks the upper mercury signature. The DeCourcy mine is located SSW of Donlin Creek, and further geochemical and mineralogical studies and comparisons of these two systems may reveal their genetic or temporal relationship and further expand the lateral understanding of reduced intrusion-related gold systems.

A detailed isotopic study that evaluates sulfur, oxygen, carbon, lead, neodymium, and deuterium data from Dome to ACMA-Lewis will further the understanding of the origins and evolution of the elements associated with this laterally zoned system.

Carbonate staining methods have proven to be a useful guide to identifying higher gold zones, and staining and carbonate interpretation of more drill core may show stronger, probable locations for gold when associated with the gold-alteration interval maps shown in this study.

Collection of argillic alteration at closer than two to three meter intervals will show more specific trends and habits of gold at ACMA/Lewis. The interval used for this study does not properly represent the alteration associated with gold since gold tends to vary significantly over a two to three meter interval. A detailed clay alteration study, especially with a focus on ammonium minerals could better demonstrate the trend of gold in the resource area.

6 References

March, 2009, Red Devil Mine, Red Devil, Alaska, Alaska Department of Environmental Conservation - Spill Prevention and Response Division.

Bundtzen, T. K., and Miller, M.L., 1997, Precious-metals associated with Late Cretaceous-Early Tertiary igneous rocks of southwestern Alaska, *in* Goldfarb, R. J., and Miller, M.L., ed., Mineral Deposits of Alaska. Economic Geology, Monograph 9, p. 242-286.

Carten, R. B., Geraghty, E.P., Walker, B.M., Shannon, J.R., 1988, Cyclic Development of Igneous Features and Their Relationship to High-Temperature Hydrothermal Features in the Henderson Porphyry Molybdenum Deposit, Colorado: Economic Geology, v. 83, p. 266-296.

Decker, J., Bergman, S.C., Blodgett, R.B., Box, S.E., Bundtzen, T.K., Clough, J.G., Coonrad, W.L., Gilbert, W.G., Miller, M.L., Murphy, J.M., Robinson, M.S., and Wallace, W.K., 1994, Geology of southwestern Alaska, *in* Plafker, G., and Berg, H.C., ed., The Geology of Alaska, Geological Society of America, p. 285-310.

Drummond, S. E., and Ohmoto, H., 1985, Chemical evolution of mineral deposition in boiling hydrothermal systems: Economic Geology, v. 80, p. 126-147.

Ebert, S. W., Baker, T., and Spencer, R.J., 2003c, Fluid inclusion studies at the Donlin Creek Gold Deposit, Alaska, possible evidence for reduced porphyry-Au to sub epithermal transition, *in* Eliopoulos, ed., Mineral Exploration and Sustainable Development, August 24-28, 2003: Athens, Greece, Proceedings of the Seventh Biennial SGA Meeting, p. 263-266.

Ebert, S. W., Dodd, S., Miller, L., and Petsel, S., 2003b, The Donlin Creek Au-As-Sb-Hg Deposit, Southwestern Alaska, *in* Cluer, J. K., Price, J.G., Struhsacker, E.M., Hardyman, R.F., and Morris, C.L., ed., Geology and Ore Deposits 2000: The Great Basin and Beyond, May 15-18, 2000, Geological Society of Nevada Symposium Proceedings, p. 1069-1081.

Ebert, S. W., Miller, L., Petsel, S., Kowalczyk, P., Tucker, T.L., and Smith, M.T., 2000, Geology, mineralization, and exploration at the Donlin Creek project, southwestern Alaska: British Columbia and Yukon Chamber of Mines, v. Special 2, p. 99-114.

Ebert, S. W., Tosdal, R., Goldfarb, R., Dodd, S., Petsel, S., Mortensen, J., and Gabites, J., 2003a, The 25 million ounce Donlin Creek Gold Deposit, Southwest Alaska: a possible link between reduced porphyry Au and sub-epithermal Au-As-Sb-Hg mineralization in Regional Geologic Framework and deposit specific exploration models for intrusion-related gold mineralization, Yukon and

Alaska [CD-ROM], *in* Ebert, S., ed., The Mineral Deposit Research Group, University of British Columbia, Special Publication 3.

Flanigan, B., Freeman, C., McCoy, D., Newberry, R., and Hart, C, 2000, Paleo-reconstruction of the Tintina Gold Belt – Implications for Mineral Exploration, The Tintina Gold Belt: concepts, exploration, and discoveries, Special 2, British Columbia and Yukon Chamber of Mines, Cordilleran Roundup, January 2000.

Goldfarb, R., Hart, C., Miller, M., Miller, L., Farmer, G.L., and Groves, D., 2000, The Tintina Gold Belt – A global perspective, The Tintina gold belt: concepts, exploration, and discoveries, Special 2, British Columbia and Yukon Chamber of Mines, Cordilleran Roundup, January 2000.

Goldfarb, R. J., and Miller, M.L., 1997, Metallogenic Evolution of Alaska: Economic Geology, Monograph 9, p. 4-34.

Goldfarb, R. J., Ayuso, R., Miller, M.L., Ebert, S.W., Marsh, E.E., Petsel, S.A., Miller, L.D., Bradley, D., Johnson, C., and McClelland, W., 2004, The Late Cretaceous Donlin Creek Gold Deposit, Southwestern Alaska: Controls on Epizonal Ore Formation: Economic Geology, v. 99, p. 643-671.

Goldfarb, R. J., Baker, T., Dube, B., Groves, D.I., Hart, C.J.R., Gosselin, P., 2005, Distribution, Character, and Genesis of Gold Deposits in Metamorphic Terranes, Economic Geology 100th Anniversary Volume, p. 407-450.

Gray, J. E., Gent, C.A., Snee, L.W., and Wilson, F.H., 1997, Epithermal mercury-antimony and gold-bearing vein lodes of southwestern Alaska: Economic Geology, Monograph 9, p. 287-305.

Hanson, K., G. S. M., Allard, S., Wortman, G., and Kozak, A., April 1, 2009, Donlin Creek Gold Project, Alaska, USA, NI-43-101 Technical Report, AMEC, p. 222.

Hart, C. J. R., 2007, Reduced intrusion-related gold systems: Geological Association of Canada, Mineral Deposits of Canada: A synthesis of major deposit types, district metallogeny, the evolution of geological provinces and exploration methods, Special Publication no 5, p. 95-112.

Hillier, D., 2007, Variability Mineralogy of Donlin Creek Ores, AMTEL internal report 07/17 for Barrick Gold Corporation.

Hitzman, M. W., 1999, Routine staining of drill core to determine carbonate mineralogy and distinguish carbonate alteration textures: Mineralium Deposita v. 34, p. 794-798.

Kirschner, C. E., 1994, Sedimentary Basins of Alaska, *in* Plafker, G., and Berg, H.C., ed., the Geology of Alaska, G-1, Boulder Colorado, Geological Society of America, the Geology of North America.

Lang, J. R., Baker, T., Hart, C.J.R., and Mortensen, J.K., 2000, An exploration model for intrusion-related gold systems: Society of Economic Geology Newsletter, v. 40, p. 1, 6-15.

MacNeil, K. D., 2009, The timing and structural evolution of the Donlin Creek gold deposit, southwest Alaska, master's thesis, University of British Columbia.

McCrea, J.M., 1950, On the isotope chemistry of carbonates and a paleotemperature scale: Journal of Chemical Physics, v. 18, p. 849-857.

Miller, M. L., Bradley, D.C., Bundtzen, T.K., and McCelland, W., 2002, Late Cretaceous through Cenozoic strike-slip tectonics of southwestern Alaska: The Journal of Geology, v. 110, p. 247-270.

NovaGold, April 8, 2010, Donlin Creek Property, http://www.novagold.com/section.asp?pageid=3359.

Piekenbrock, J. R., 2002, Status of Technical Studies – Donlin Creek Project, Unpublished internal report, p. 16.

Piekenbrock, J. R., and Petsel, S.A., 2003, Geology and Interpretation of the Donlin Creek Gold Deposits: Juneau, Alaska, NovaGold Resources Inc., p. 58, unpublished report.

Silberling, N. J., Jones, D.L., Monger, J.W.H., Coney, P.J., Berg, H.C., Plafker, G., 1994, Lithotectonic Terrane Map of Alaska and Adjacent Parts of Canada, *in* Plafker, G., and Berg, H.C., ed., The Geology of Alaska, G-1: Boulder Colorado, Geological Society of America, The Geology of North America.

Sillitoe, R. H., and Thompson, J.F.H., 1998, Intrusion-related vein gold deposits: types, tectono-magmatic settings, and difficulties of distinction between orogenic gold deposits: Resource Geology, v. 48, p. 237-250.

Szumigala, D. J., 1996, Gold Mineralization Related to Cretaceous-Tertiary magmatism in West-Central Alaska – A Geochemical Model and Prospecting Guide for the Kuskokwim Region, *in* Coyner, A. R., and Fahey, P.L., ed., Geology and Ore Deposits of the American Cordillera, April, 1995: Reno/Sparks, NV, Geological Society of Nevada Symposium Proceedings, p. 1317-1340.

Szumigala, D. J., Dodd, S.P., and Arribas, A., Jr., 1999, Geology and gold mineralization at the Donlin Creek prospects, southwestern Alaska, Professional Report 119, Alaska Division of Geological and Geophysical Survey, p. 91-115.

Thompson, T. B., 2007, Petrography of the DC06-series core samples, Donlin Creek, Alaska, Barrick-Donlin Creek Joint Venture internal report.

Wahrhaftig, C., 1994, Physiographic Divisions of Alaska, *in* Plafker, G., and Berg, H.C., ed., the Geology of Alaska, G-1: Boulder Colorado, Geological Society of America, The Geology of North America.

7 Appendix A: Photomicrographs

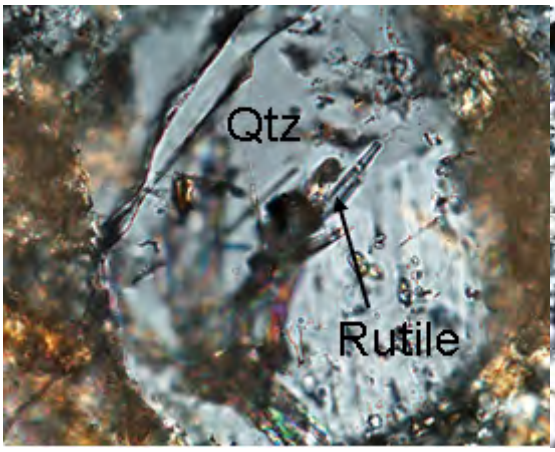

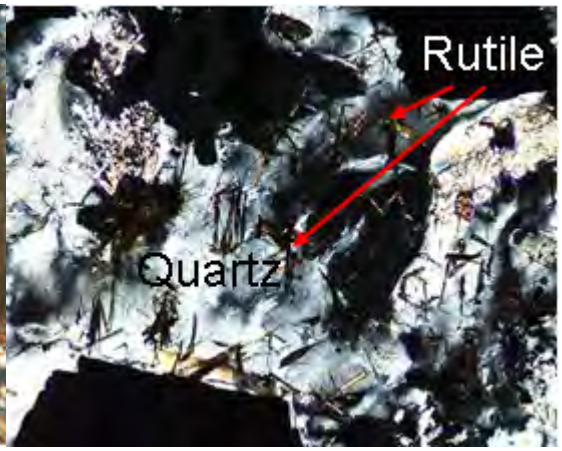

Figure A 1. Left photomicrograph showing magmatic quartz grain with syngenetic rutile located near Dome. Field of view (FOV) = 0.43mm, crossed-polarized light (XPL)
Figure A 2. Right photomicrograph showing magmatic quartz grain with syngenetic rutile located near Dome. FOV = 2.2mm, XPL

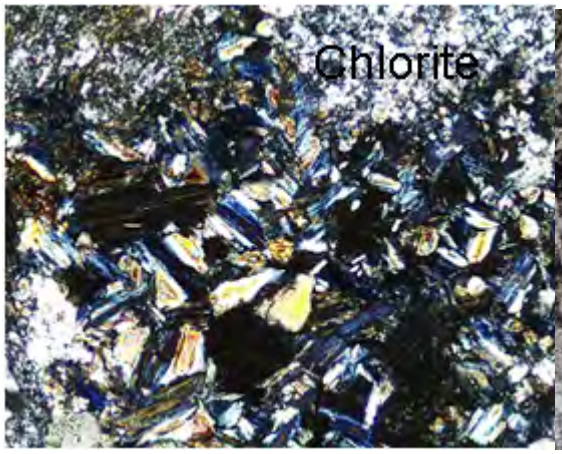

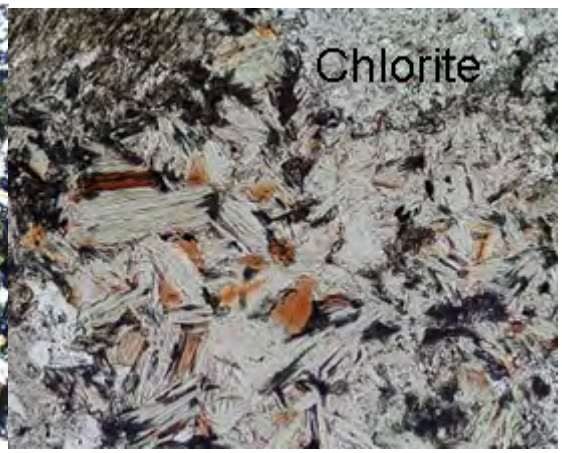

Figure A 3. Photomicrographs of Mg-rich chlorite found north of Dome. Left, FOV= 2.2mm, XPL; right, FOV = 2.2mm, plane-polarized light (PPL).

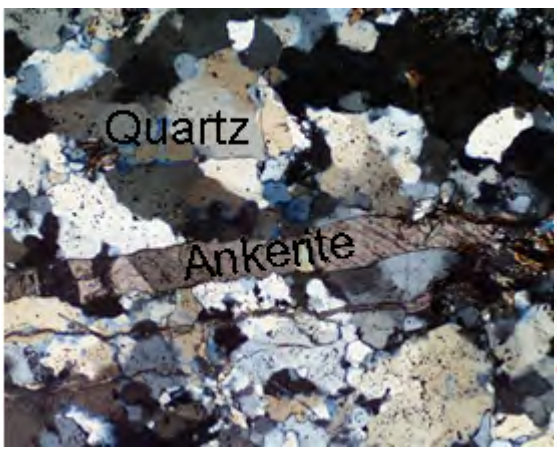

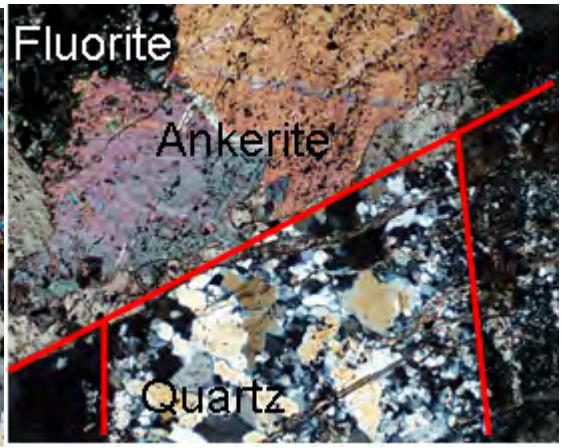

Figure A 4. Left: Earliest quartz vein phase with a sugary texture with an overprinting ankerite veinlet observed north of Dome, FOV = 4.4mm, XPL.
Figure A 5. Right: Same quartz phase overprinted by ankerite and fluorite vein located north of Dome, FOV = 4.4mm, XPL.

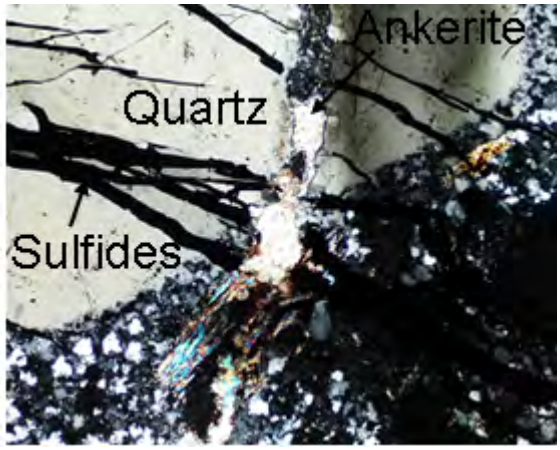

Figure A 6. Left: Comb textured quartz from the first quartz phase filled in by ankerite located on Dome, FOV = 4.4mm, XPL.
Figure A 7. Right: Groundmass quartz grain overprinted by sulfide stringers and subsequently by ankerite found at Quartz, FOV = 4.4mm, XPL.

Figure A 8. Large groundmass quartz grain overprinted by pyrite and marcasite in the Quartz district, FOV = 4.4mm, left = XPL, right = reflected light.

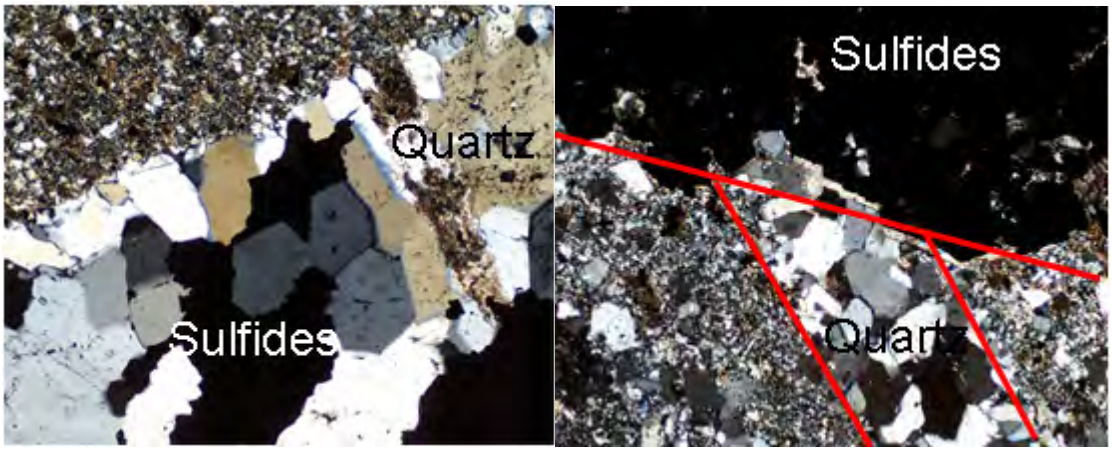

Figure A 9. A sugary textured quartz vein with sulfides filling in between grains and overprinting this phase found to the north and east of Dome, both FOVs are 4.4mm and XPL.

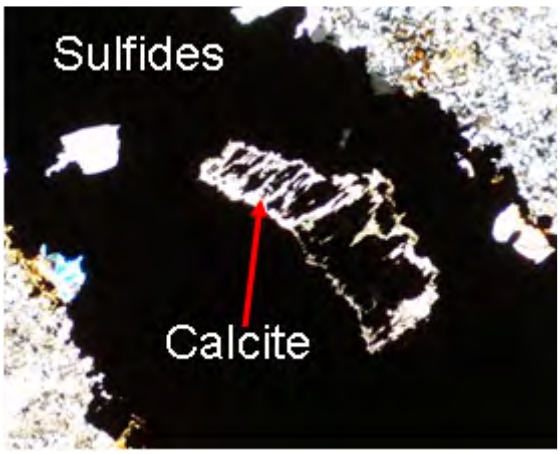

Figure A 10. A pre-sulfide calcite phase observed on Dome, FOV = 4.4mm, XPL.

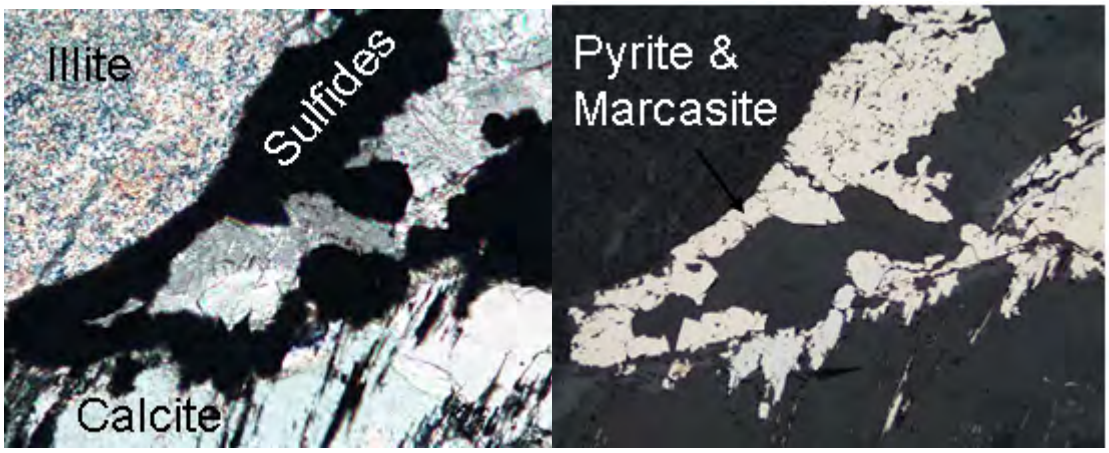

Figure A 11. Pyrite and marcasite replacing calcite along grain boundaries on the east side of Dome, FOV = 1.1mm, left is XPL and right is reflected light.

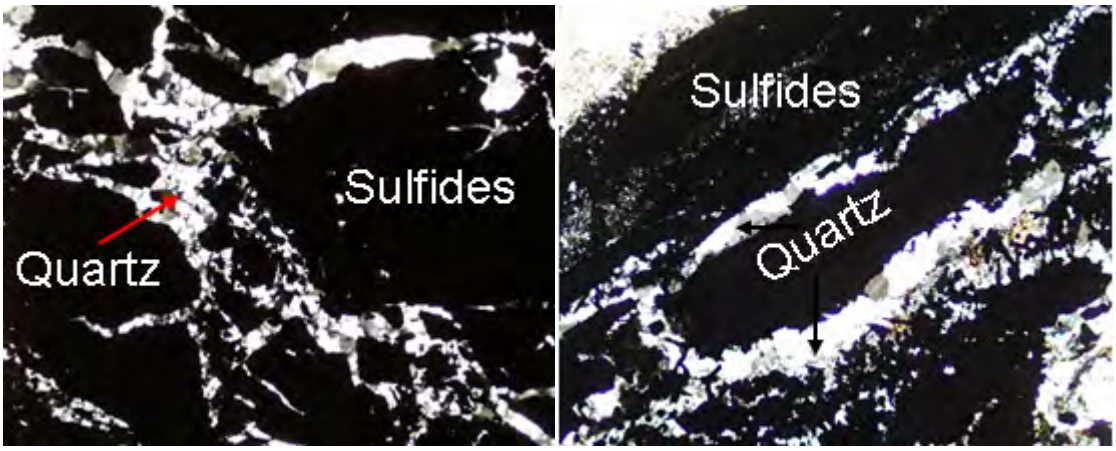

Figure A 12. Post sulfide quartz phase infilling between sulfide grains, left: located west of Dome, FOV = 4.4mm, XPL; right: found in ACMA, FOV = 2.2mm, XPL.

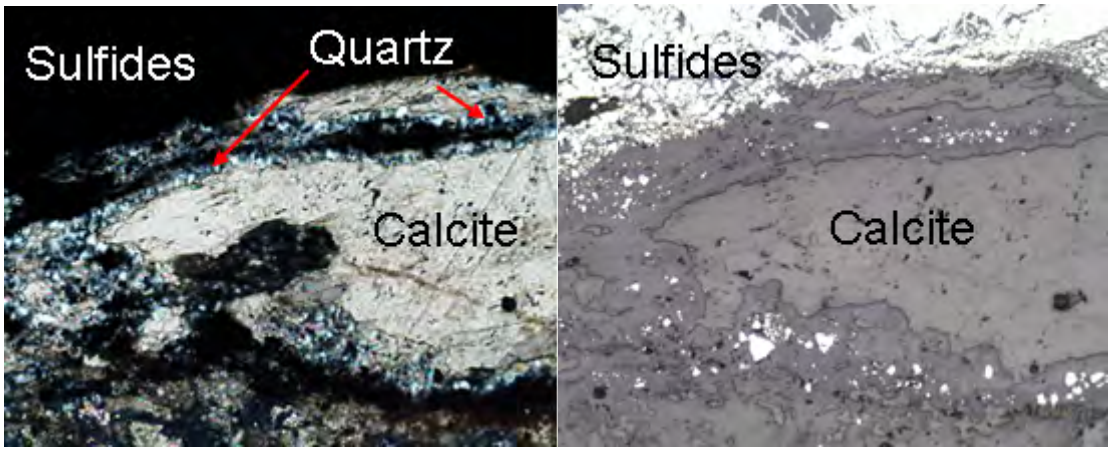

Figure A 13. Early stage carbonate phase surrounded by sulfides ± Fe-dolomite. A late quartz phase forms around carbonate grain boundaries, located in the Quartz district, FOV = 2.2mm, left photograph is XPL and right is reflected light.

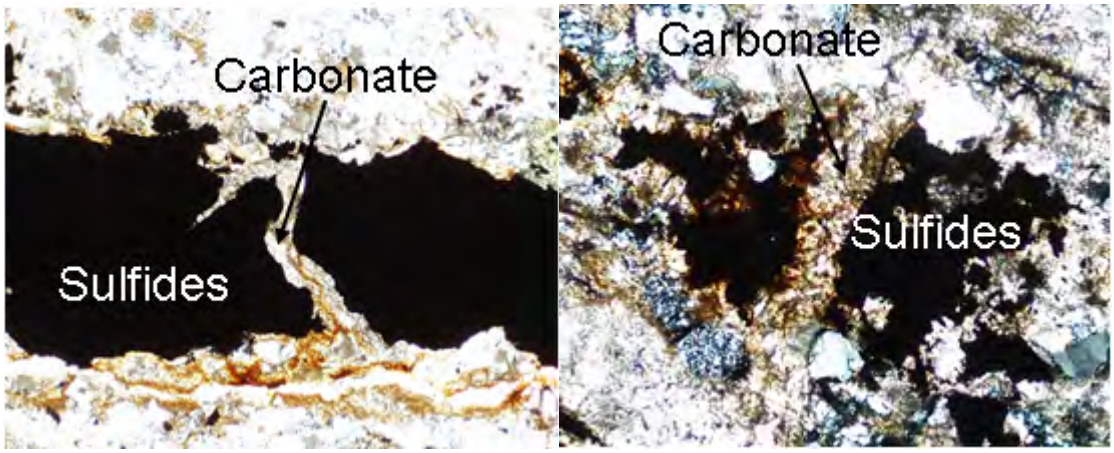

Figure A 14. Carbonate phase cutting sulfide phase found to the north of Dome and in the Lewis area, photograph on the left has a FOV = 2.2mm and is XPL; right has a FOV = 4.4mm and is also XPL.

Figure A 15. Carbonate phase that broke up pyrite and marcasite grains in the Quartz district, FOV = 4.4mm, XPL and reflected light.

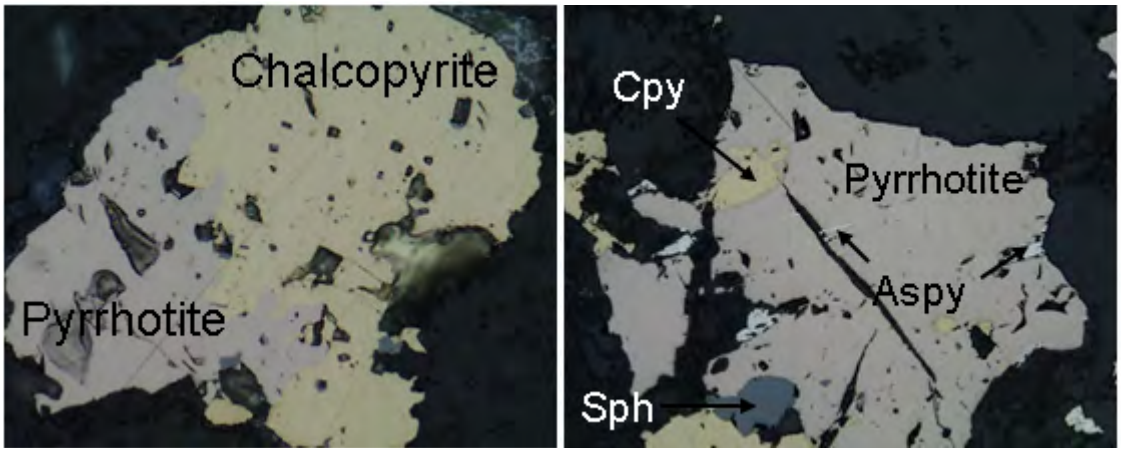

Figure A 16. Co-precipitated pyrrhotite and chalcopyrite located to the north of Dome, FOV = 0.43mm, reflected light.

Figure A 17. Right: co-precipitated pyrrhotite and chalcopyrite, overprinting of sphalerite and the replacement of pyrrhotite by arsenopyrite found to the north of Dome, FOV = 1.1mm, reflected light.

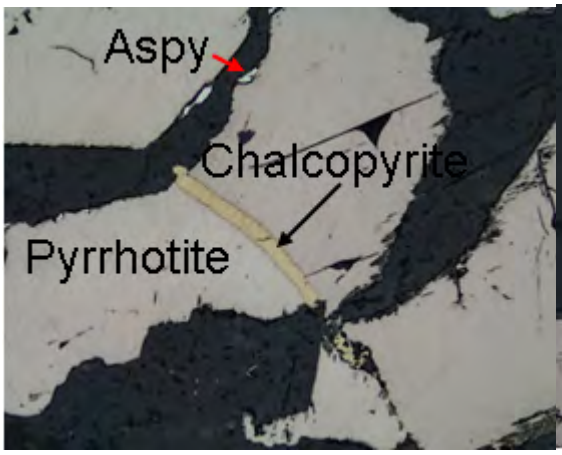

Figure A 18. Left: chalcopyrite overprinting pyrrhotite and the formation of arsenopyrite at the grain boundary found north of Dome, FOV = 1.1mm, reflected light.
Figure A 19. Right: pyrrhotite being replaced by arsenopyrite found to the east of Dome, FOV = 1.1mm, reflected light.

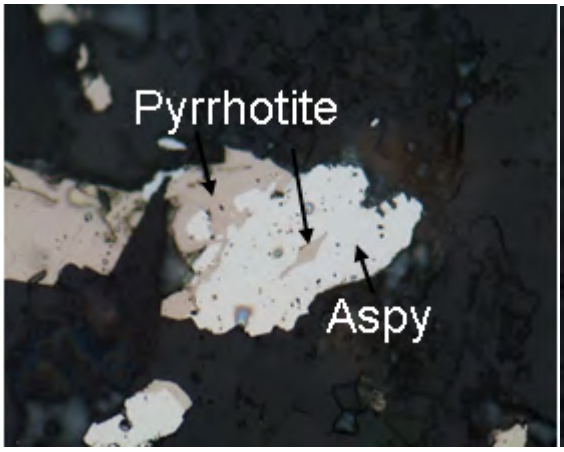

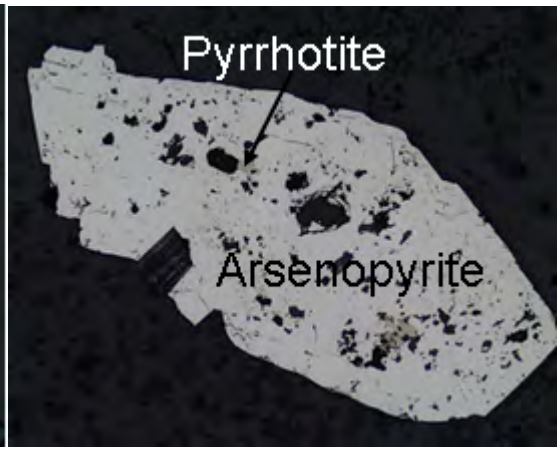

Figure A 20. Replacement of pyrrhotite by arsenopyrite both located to the north of Dome, left FOV = 0.43, reflected light; right FOV = 2.2mm, reflected light.

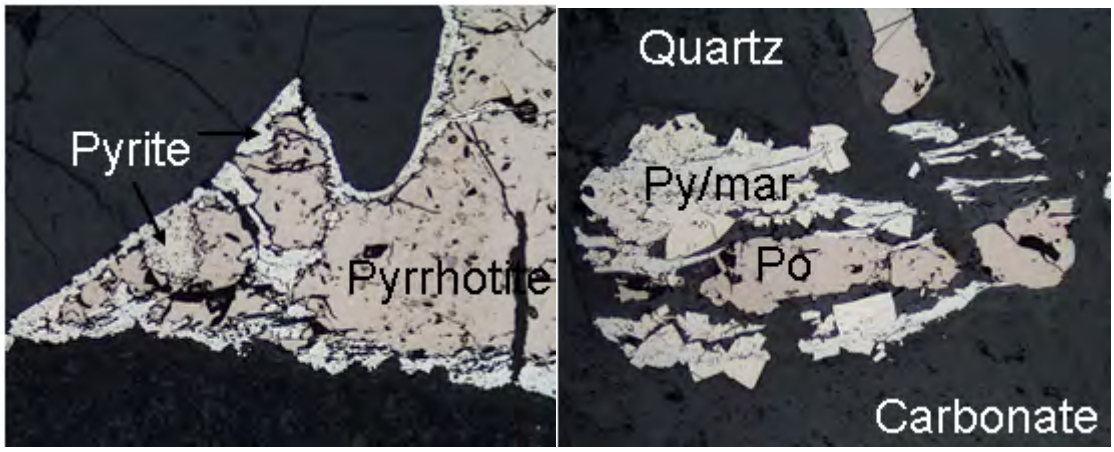

Figure A 21. Pyrite ± marcasite forming at the edges of pyrrhotite grains located to the north and east of Dome, left FOV = 2.2mm, reflected light; right FOV = 2.2mm, reflected light.

Figure A 22. Left: pyrrhotite grains that formed between euhedral quartz grains. Pyrite formed at the opposite pyrrhotite grain boundary, FOV = 1.1mm, reflected light.
Figure A 23. Right: porous pyrite forming around and locally replacing arsenopyrite grain with few remaining blebs of pyrrhotite, FOV = 1.1mm, reflected light.

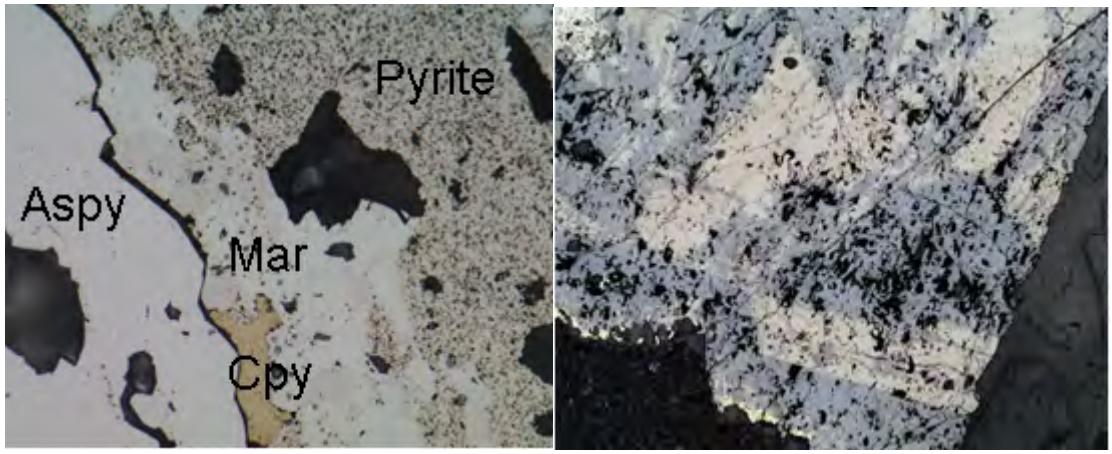

Figure A 24. Left: Blocky arsenopyrite grain in contact with chalcopyrite, marcasite and sooty pyrite, FOV = 1.1mm, reflected light.

Figure A 25. Right: partially relict euhedral tetrahedrite overprinted by sphalerite with chalcopyrite disease, east side of Dome, FOV = 4.4mm, reflected light.

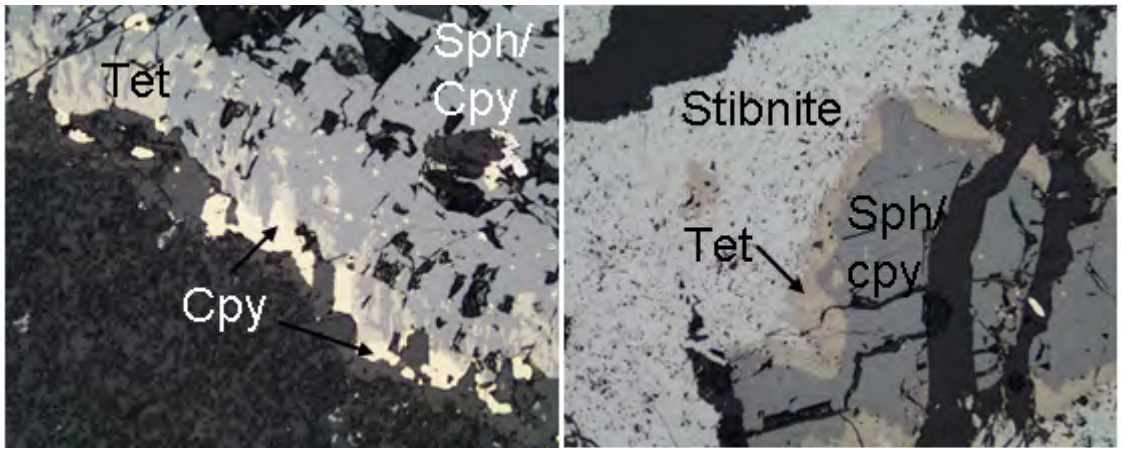

Figure A 26. Left: tetrahedrite overprinted by sphalerite with chalcopyrite disease, chalcopyrite forms at the grain boundary, east side of Dome, FOV = 1.1mm, reflected light.

Figure A 27. Right: tetrahedrite overprinted by sphalerite with chalcopyrite disease and in contact with and possibly the replacement of tetrahedrite by stibnite, west side of Dome, FOV = 1.1mm, reflected light.

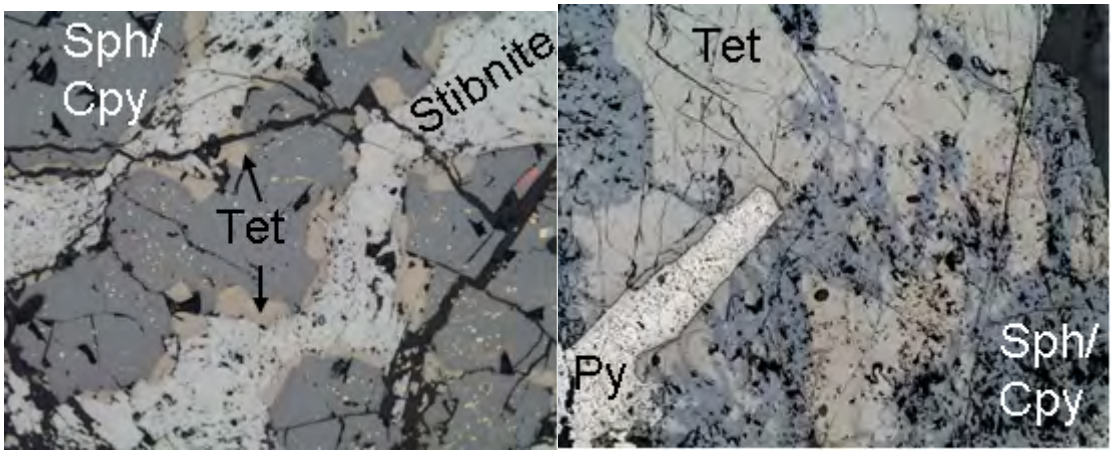

Figure A 28. Left: tetrahedrite replaced by sphalerite with chalcopyrite disease on the west side of Dome. Tetrahedrite is then replaced by stibnite, FOV = 1.1mm, reflected light.
Figure A 29. Right: Same relationship between sphalerite/chalcopyrite and tetrahedrite on the east side of Dome with the subsequent formation of pyrite, FOV = 2.2mm, reflected light.

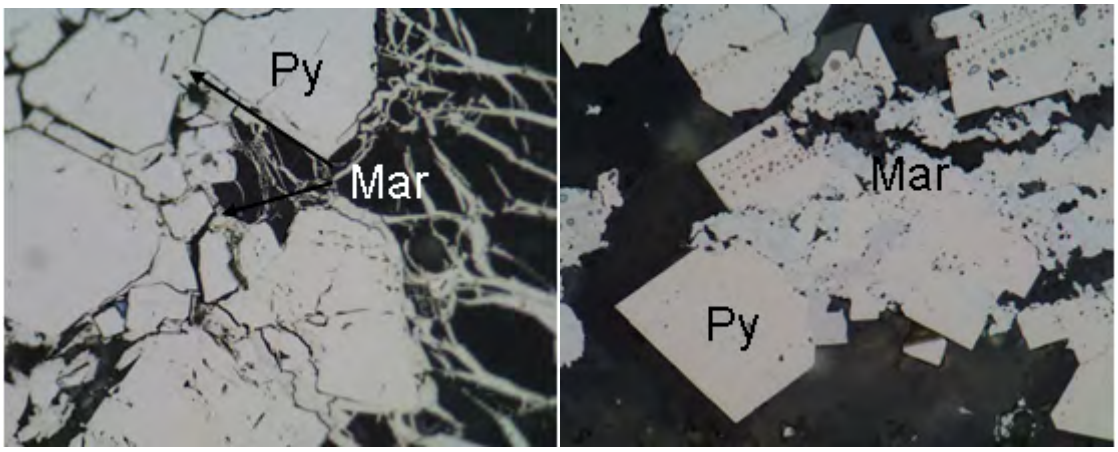

Figure A 30. Euhedral to subhedral pyrite cemented together by marcasite, left located at Quartz, FOV = 0.43mm, reflected light; right located on Lewis, FOV = 0.43mm, reflected light.

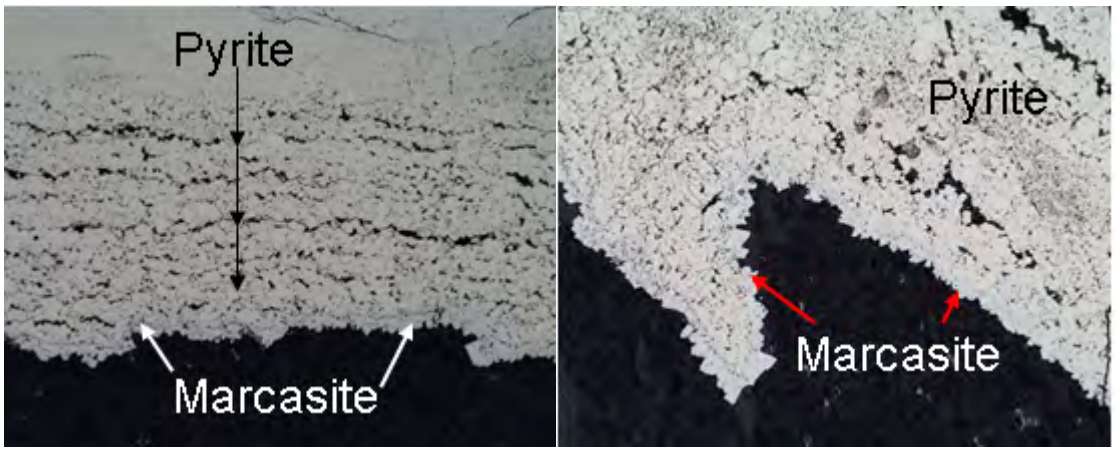

Figure A 31. Pyrite replacing original lithology at Dome and rimmed at the margin by marcasite, left = FOV = 4.4mm, reflected light; right FOV = 2.2mm, reflected light.

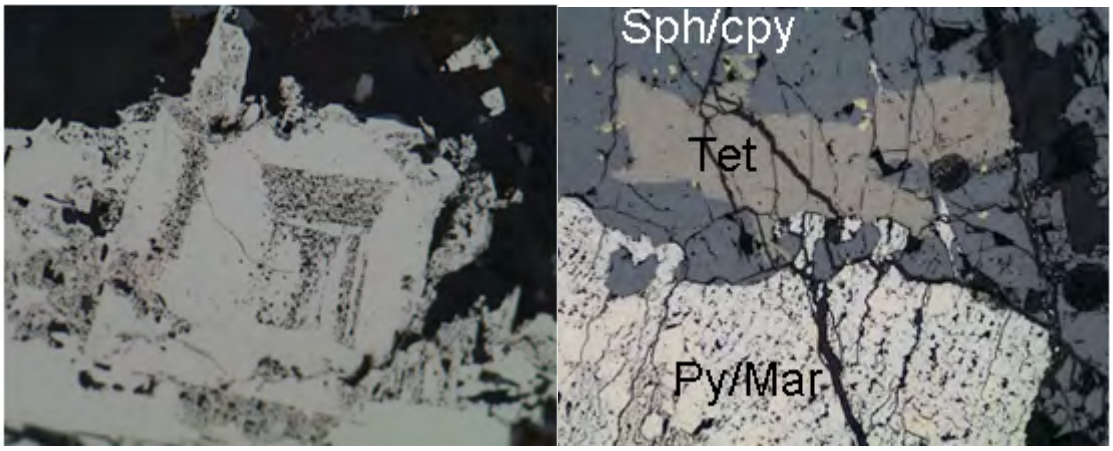

Figure A 32. Left: zoned pyrite found in the Lewis area, FOV = 0.43mm, reflected light.
Figure A 33. Right: Tetrahedrite replaced by sphalerite with chalcopyrite disease observed to the west of Dome, FOV = 1.1mm, reflected light.

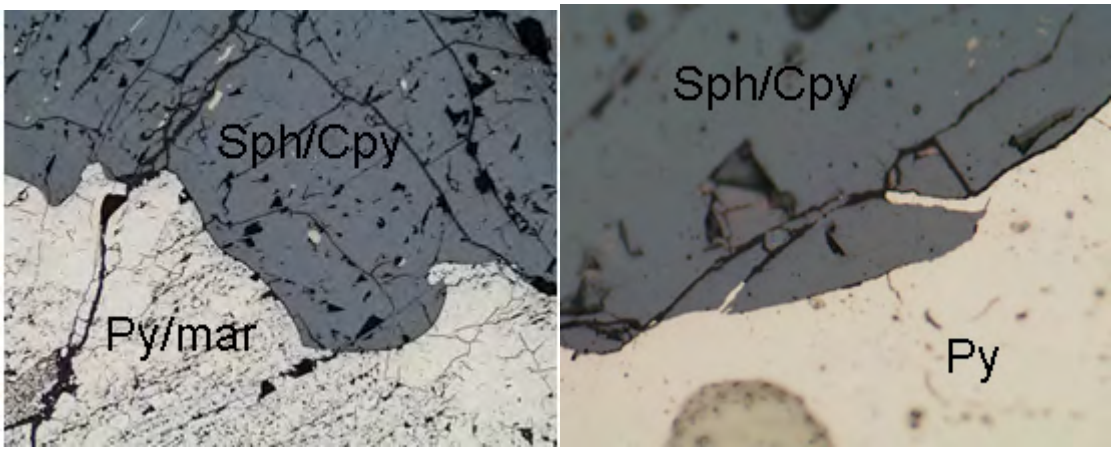

Figure A 34. Sphalerite with chalcopyrite disease being overprinted by pyrite ± marcasite observed west of Dome, FOV = 2.2mm on the left and 0.43mm on the right, both are reflected light images.

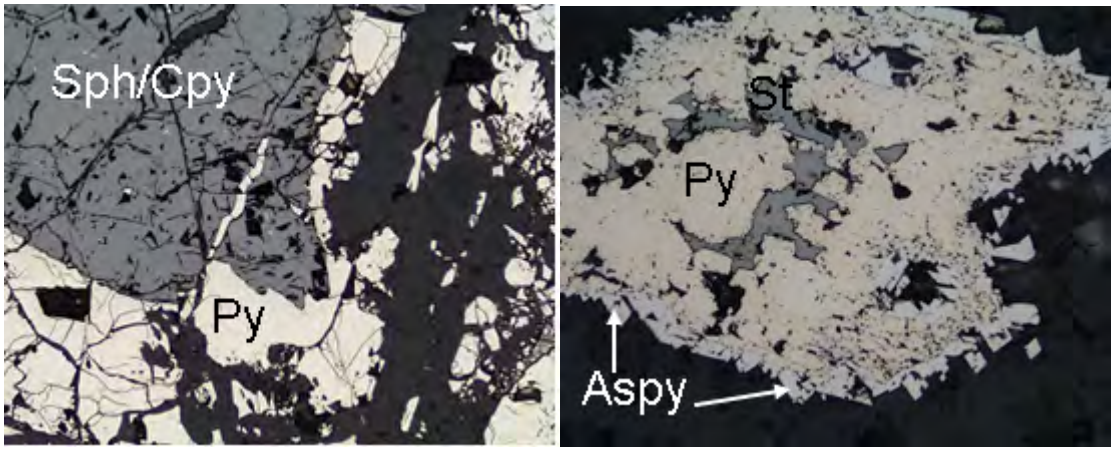

Figure A 35. Left: sphalerite with chalcopyrite disease being replaced by pyrite on the west side of Dome, FOV = 2.2mm, reflected light.
Figure A 36. Right: pyrite ± marcasite with stibnite in ACMA, FOV = 1.1mm, reflected light.

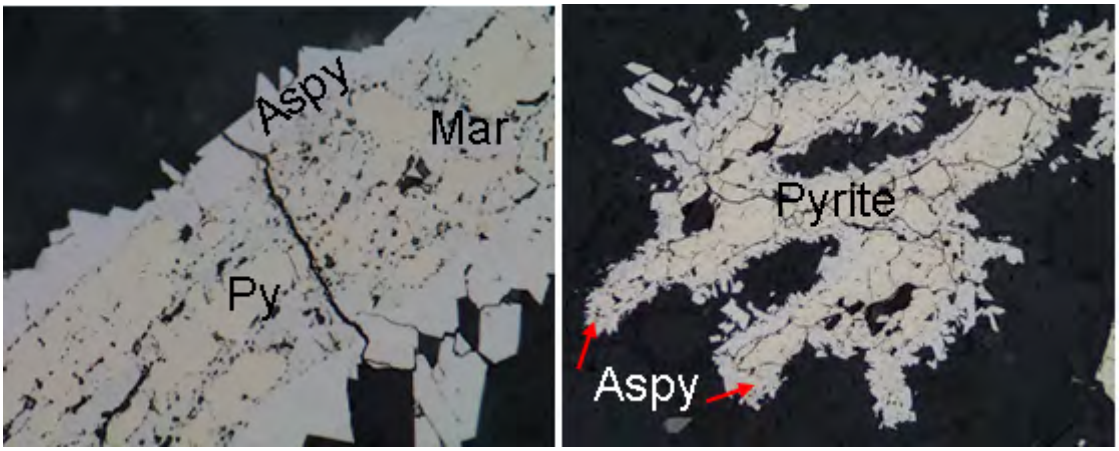

Figure A 37. Pyrite ± marcasite rimmed by euhedral arsenopyrite grains found at Lewis, FOV = 0.43mm on the left and 1.1mm on the right, reflected light.

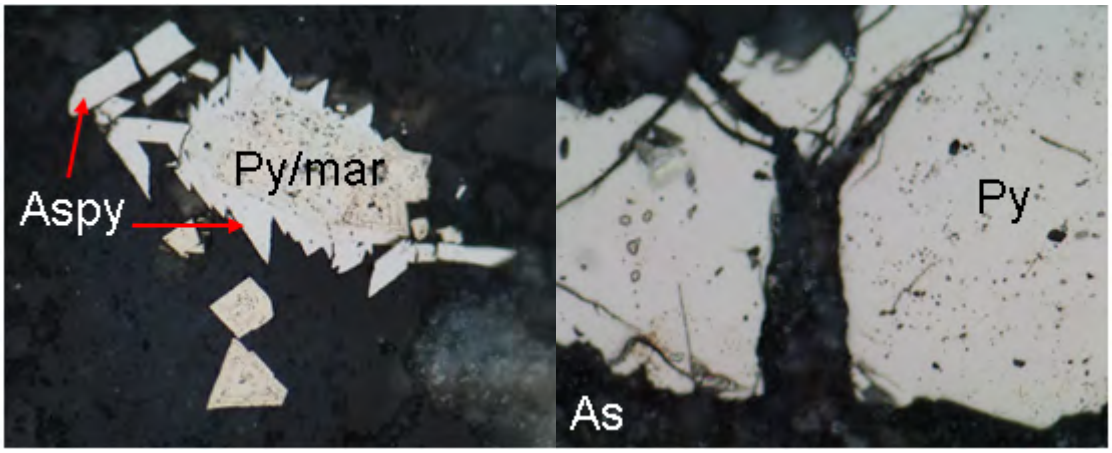

Figure A 38. Left: zoned pyrite and marcasite rimmed by euhedral arsenopyrite in Queen, FOV = 0.43mm, reflected light.

Figure A 39. Right: pyrite cut by native arsenic to the west of Dome, FOV = 0.43mm, reflected light.

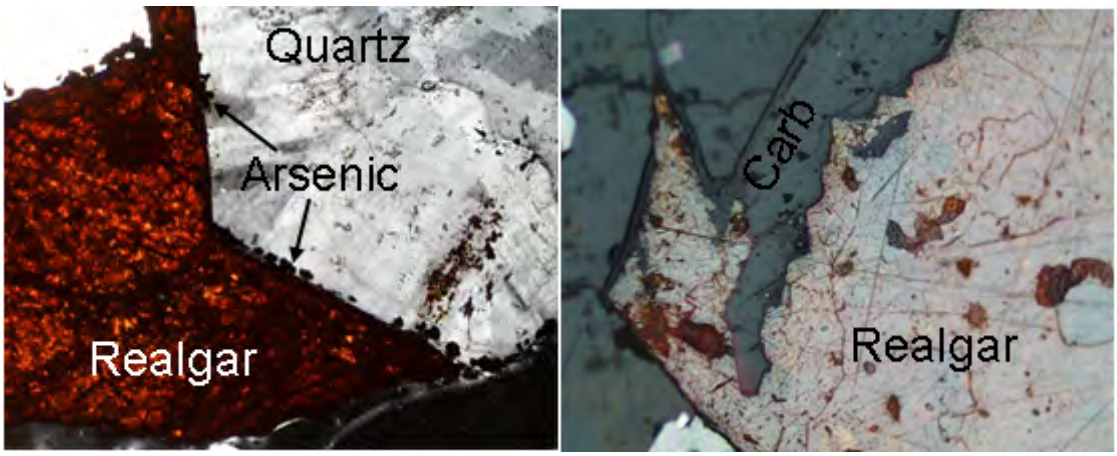

Figure A 40. Left: realgar filling in between euhedral quartz grains found in ACMA. Note the very fine grained blebs of native arsenic at the edges of the quartz grain, FOV = 4.4mm, XPL.
Figure A 41. Right: realgar being cut by carbonate also found in ACMA, FOV = 1.1mm, reflected light.

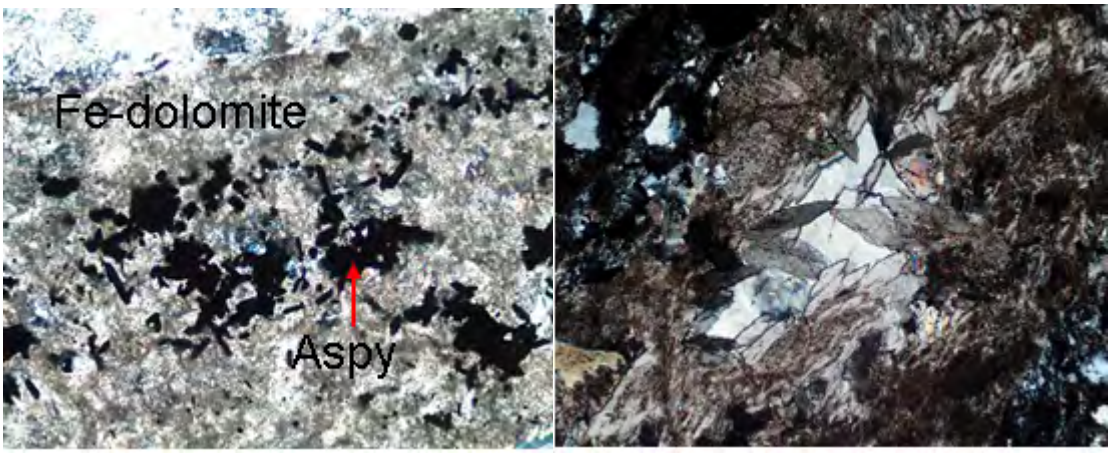

Figure A 42. Left: very fine grains of arsenopyrite within Fe-dolomite found in Lewis, FOV = 2.2mm, XPL.
Figure A 43. Right: grungy Fe-dolomite replacing platy Mn-calcite with quartz in between, FOV = 4.4mm, XPL.

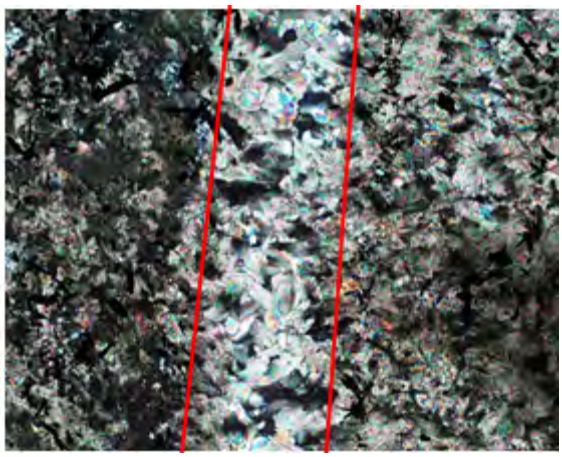

Figure A 44. Red lines separate the Mn-calcite in the center of the red lines from the Fe-dolomite to the left and right of the photomicrograph. Fe-dolomite is intimately associated with very fine grains of arsenopyrite, FOV = 4.4mm, XPL.

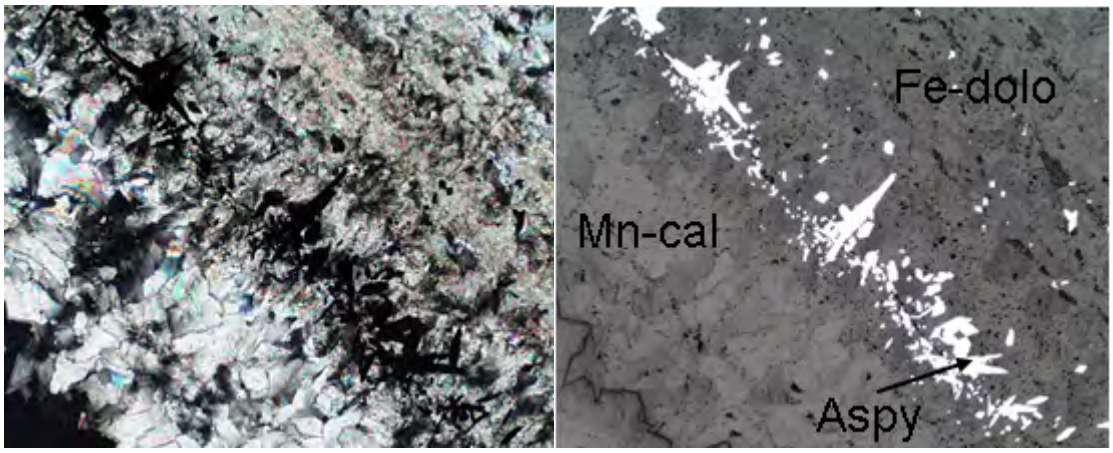

Figure A 45. Photomicrographs illustrating the association of Fe-dolomite and arsenopyrite next to Mn-calcite, FOV = 4.4mm, XPL and reflected light.

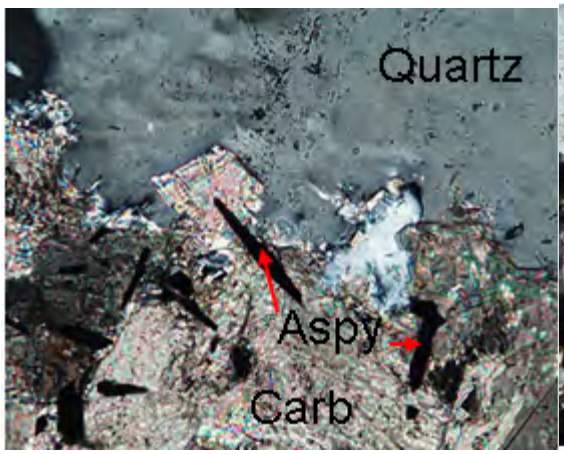

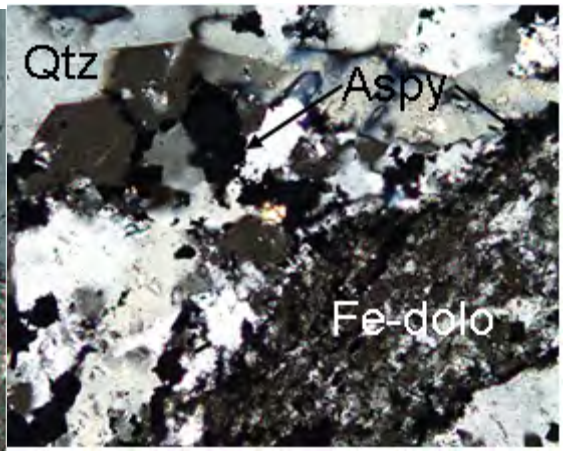

Figure A 46. Left: carbonate associated with arsenopyrite in contact with quartz, FOV = 4.4mm, XPL.

Figure A 47. Right: Fe-dolomite and arsenopyrite in between grains of quartz, FOV = 1.1mm, XPL.

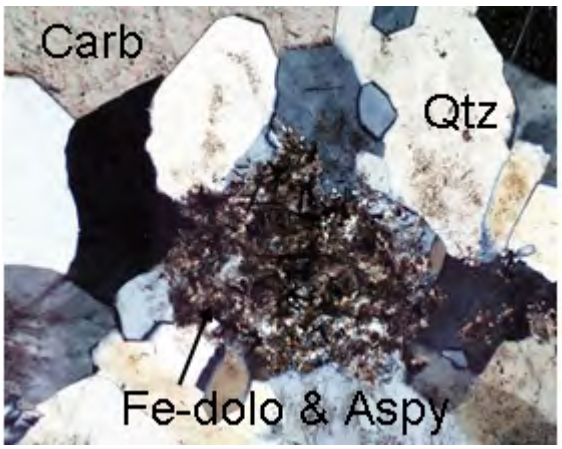

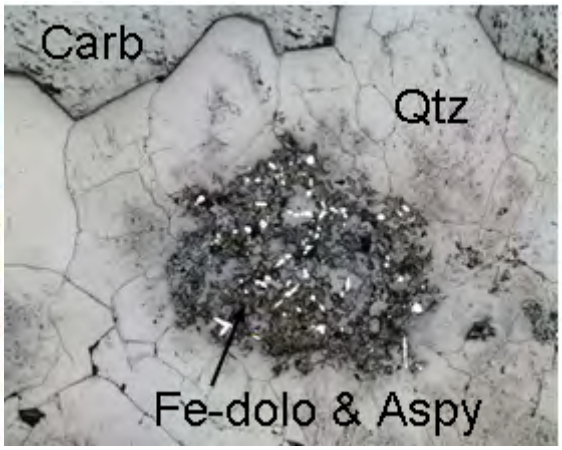

Figure A 48. Fe-dolomite and arsenopyrite surrounded by quartz grains, FOV = 4.4mm, XPL and reflected light.

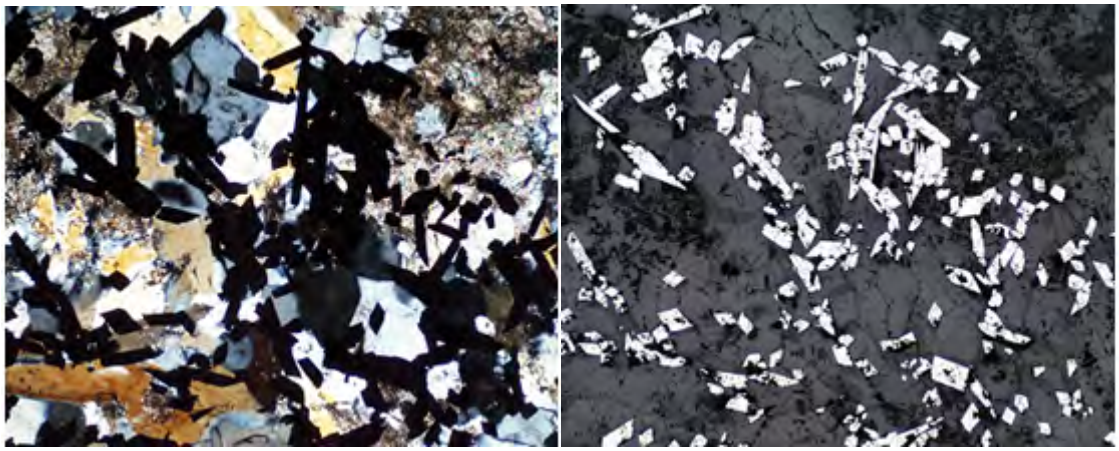

Figure A 49. Arsenopyrite grains between quartz grains, FOV = 4.4mm, XPL and reflected light.

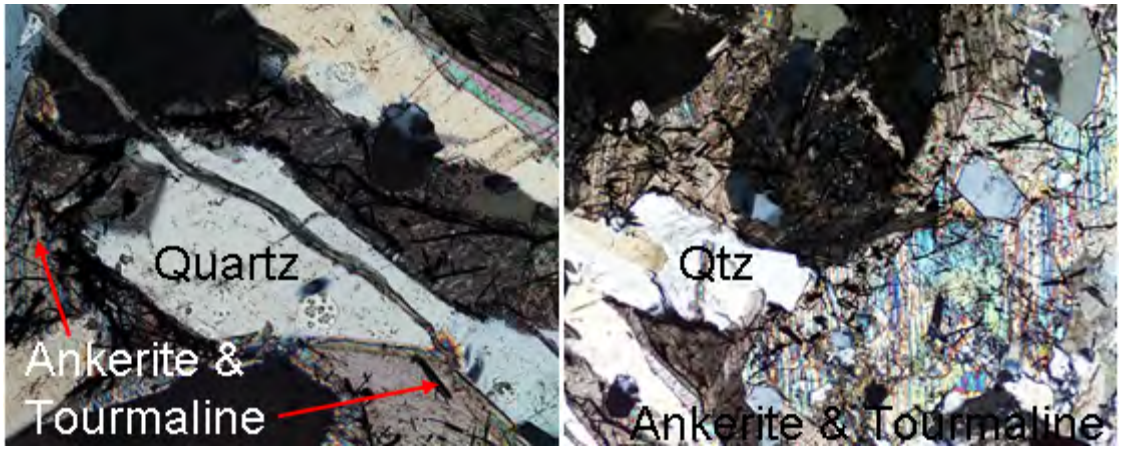

Figure A 50. Ankerite with tourmaline forming between and cross cutting quartz grains to the west of Dome, FOV = 2.2mm and 4.4mm, XPL.

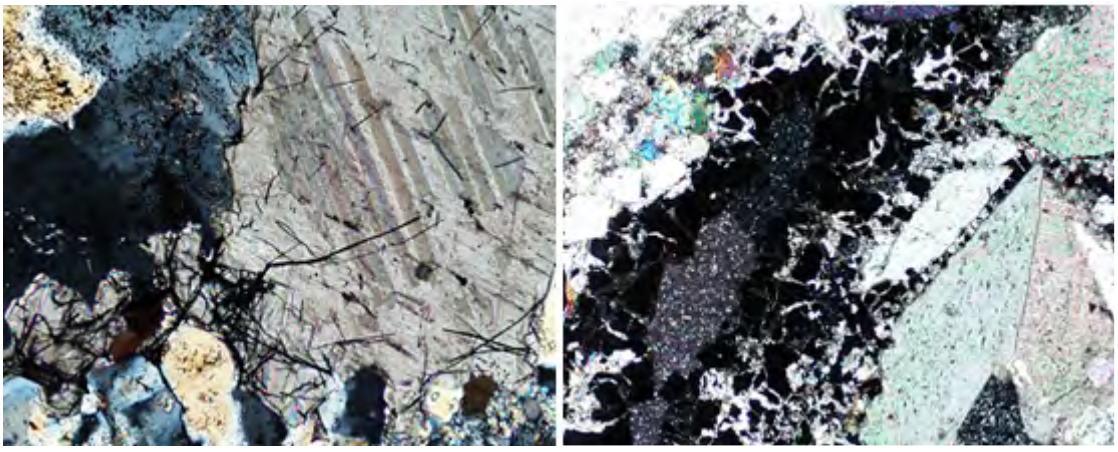

Figure A 51. Left: ankerite and needle-like tourmaline forming between quartz grains in ACMA, FOV = 2.2mm, XPL.
Figure A 52. Right: fluorite cutting ankerite north of Dome, FOV = 4.4mm, XPL.

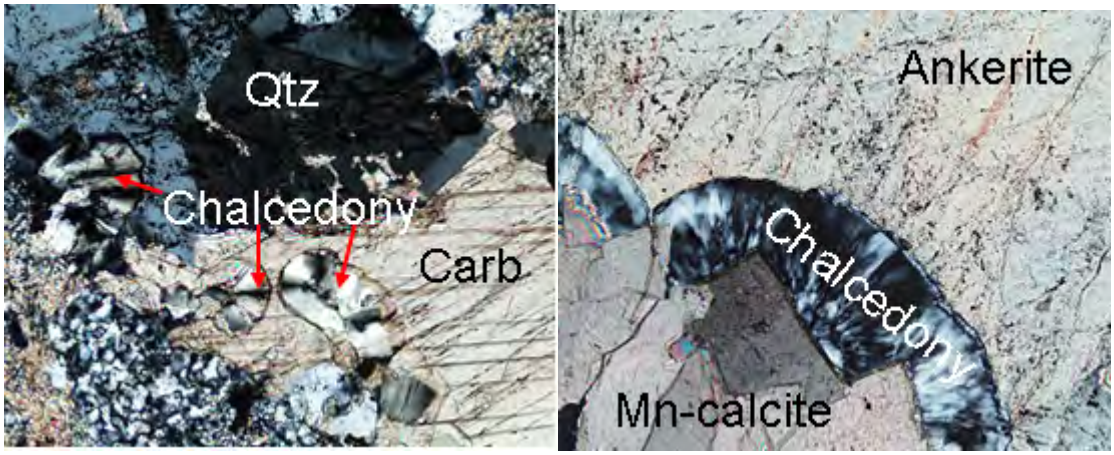

Figure A 53. The formation of chalcedony in and in between carbonate phases found north of Dome, FOV = 2.2mm, XPL.

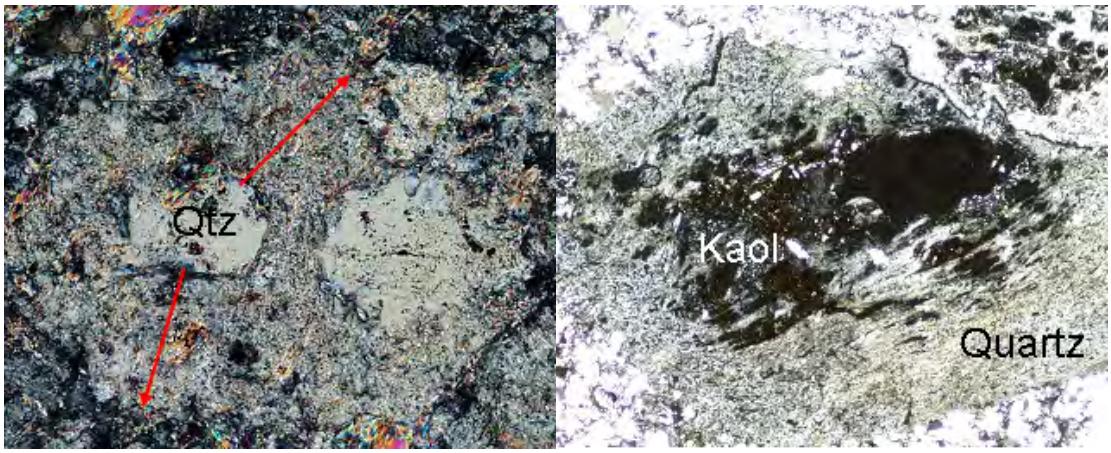

Figure A 54. Significant resorption of quartz grains ± kaolinite alteration found in and near ACMA suggesting greater changes in pressure, FOV = 2.2mm and 4.4mm, XPL.

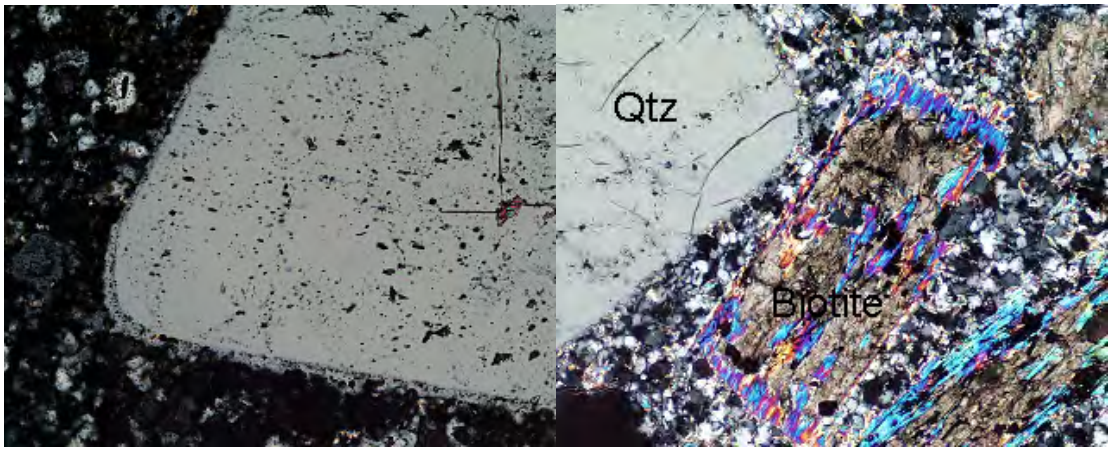

Figure A 55. Minor amounts of resorption on edges of quartz grains within the groundmass in both photomicrographs located near Dome demonstrating a smaller change in pressure compared to the resource area.
Figure A 56. Photo on the right also shows carbonate and illite alteration of primary biotite. FOV = 4.4mm, XPL.

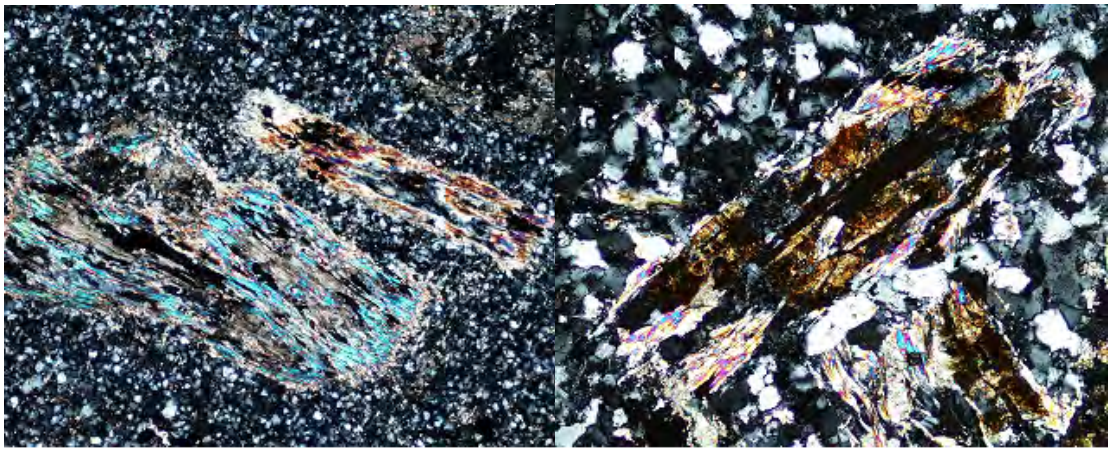

Figure A 57. Relict biotite grains showing illite, carbonate, and locally hematite alteration within a siliceous groundmass near Dome, FOV = 4.4mm and 2.2mm, XPL.

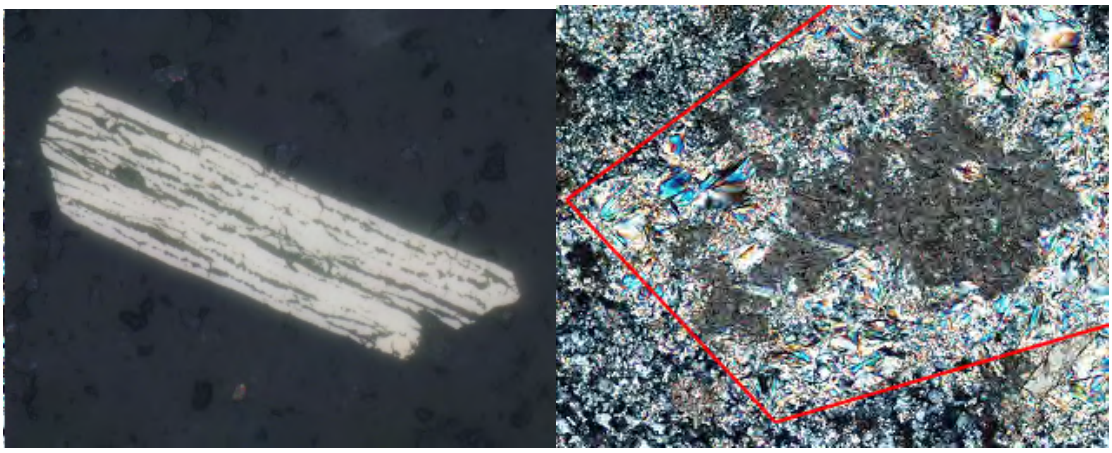

Figure A 58. Left: total replacement of primary biotite by pyrite and marcasite, FOV = 0.43mm, reflected light.
Figure A 59. Right: replacement of feldspar by illite and carbonate, FOV = 2.2mm, XPL.

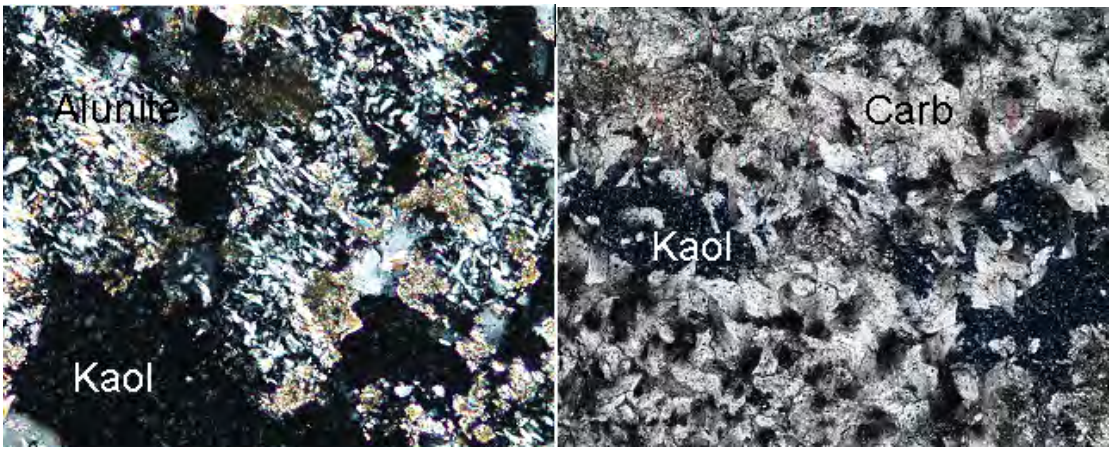

Figure A 60. Left: alunite and kaolinite replacement of primary feldspar grains located in ACMA, FOV = 1.1mm, XPL.
Figure A 61. Right: carbonate and kaolinite within veins, FOV = 4.4mm, XPL.

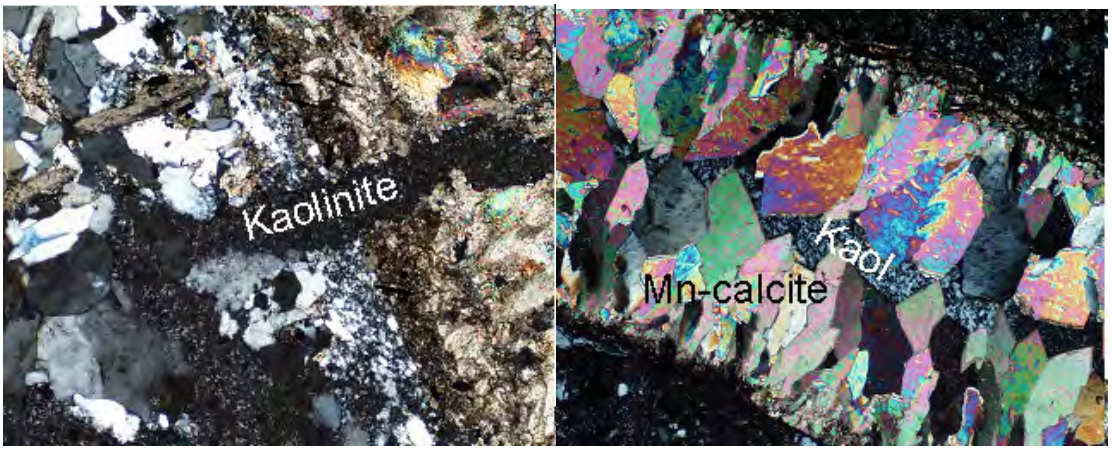

Figure A 62. Kaolinite overprinting and filling in between quartz and carbonate grains found throughout the district, FOV = 4.4mm, XPL.

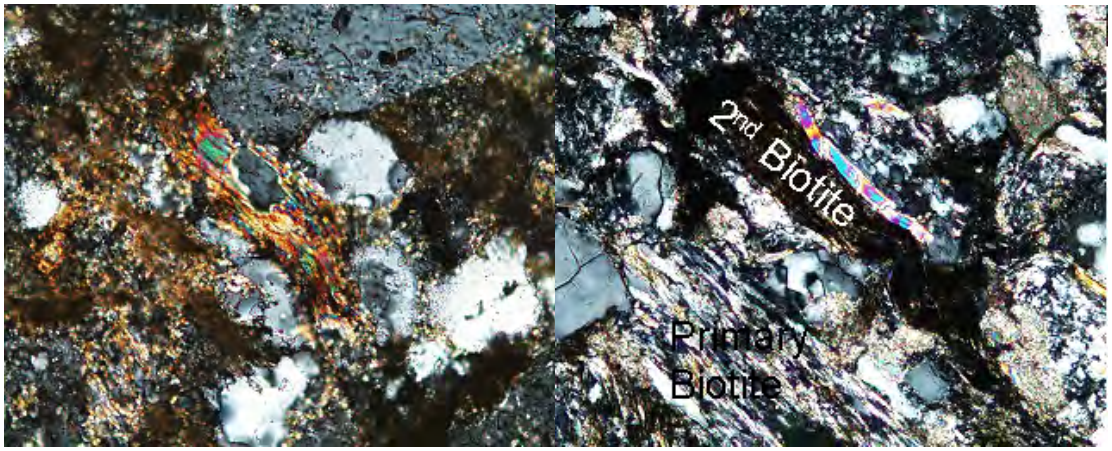

Figure A 63. Secondary biotite observed forming around quartz grains found at Dome and at Lewis, FOV = 1.1mm, XPL.

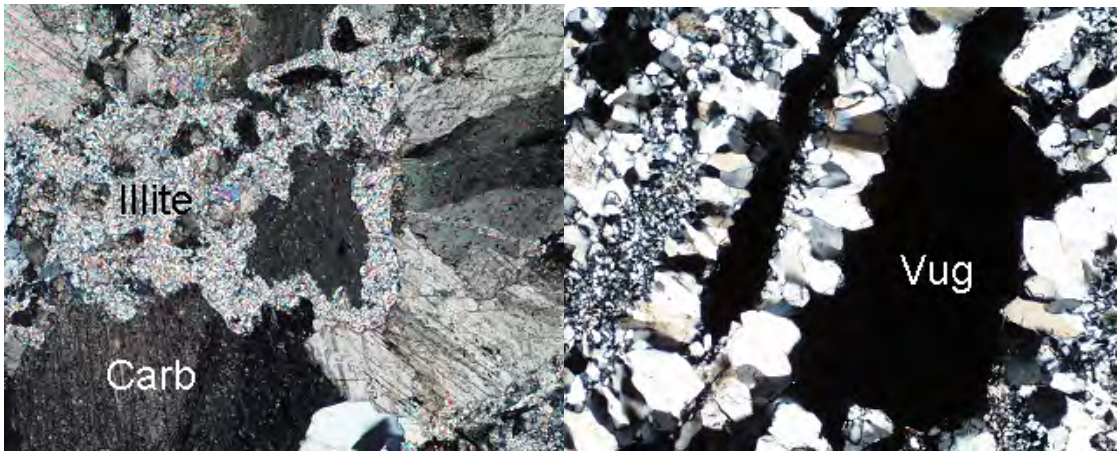

Figure A 64. Illite overprinting and forming between carbonate grains in ACMA, FOV = 4.4mm, XPL.

Figure A 65. Vuggy silica found to the west of Dome, FOV = 4.4mm, XPL.

8 Appendix B: Megascopic Vein Relationships

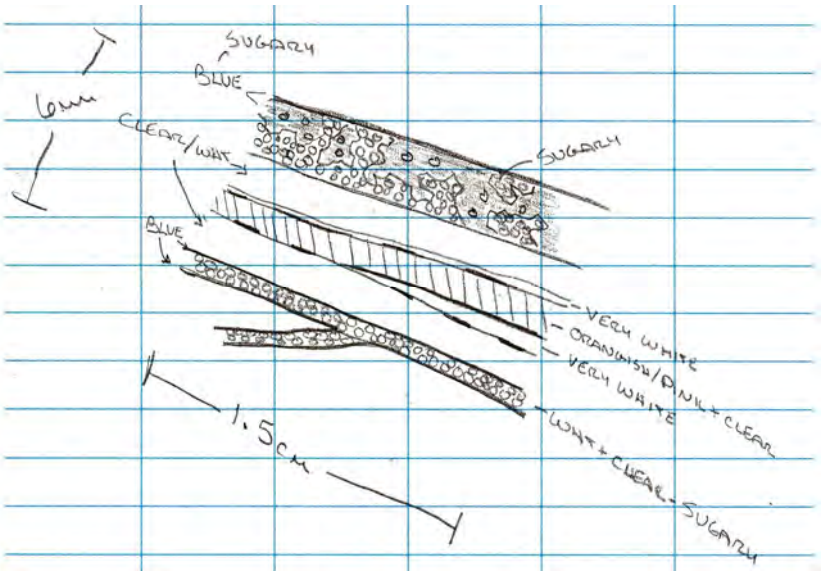

Figure B 1. Drawing illustrating several stages of veins located north of Dome in drill hole DC00-582. Sequence located nearest the outer edge of the vein consists of sugary quartz (small circles) with ankerite (blue). The middle vein phase noted as clear/white, is interpreted as a massive carbonate phase that does not react with the staining solutions. The phase in the center labeled orange/pink to clear is also a carbonate phase and is locally rimmed by a "very white" vein phase interpreted to be quartz. This sample sits within a two meter sample interval that assays 0.095 g/t Au.

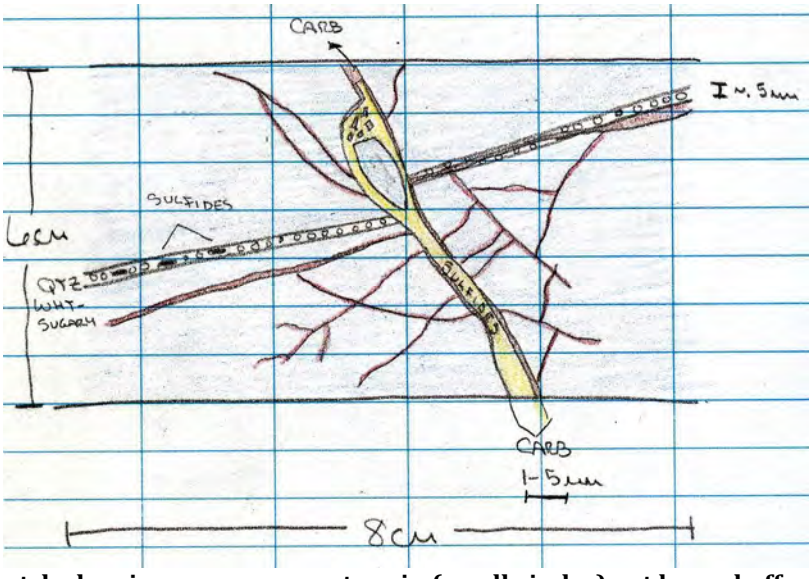

Figure B 2. Sketch showing a sugary quartz vein (small circles) cut by and off set by a sulfide-rich vein (yellow) within a sedimentary host rock located in drill hole DC00-582 north of Dome. Calcite stringers locally line the quartz and sulfide-rich veins and megascopically appear to be overprinted by the sulfide vein. The 3 m wide sample from which this sample came contained assays of 0.125 g/t Au.

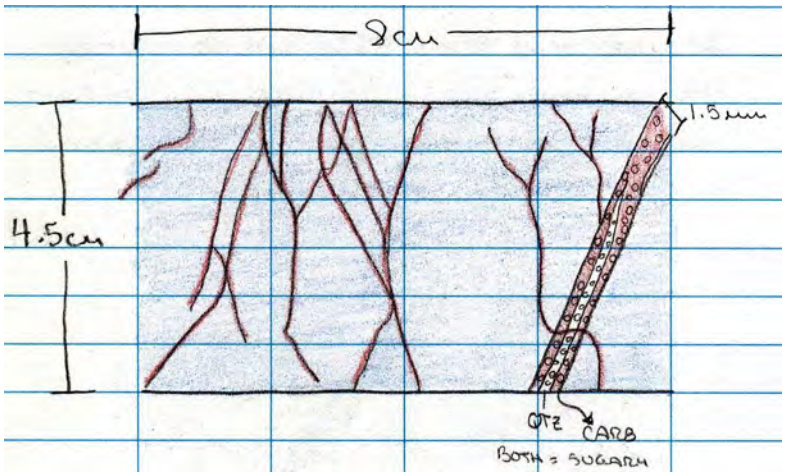

Figure B 3. Sketch showing calcite veinlets cutting sugary quartz- (small circles) calcite vein. Three meter sample interval assays at 0.17 g/t Au. This sample is from drill hole DC97-393 to the east of Dome.

Figure B 4. Sketch of sulfide-rich veinlets (yellow) that were cut and offset by calcite and ankerite-rich veins containing minor sulfides. Phenocrysts observed around these vein and veinlets locally are replaced by calcite, rimmed by ankerite, weathered out, and replaced by kaolinite. Sample interval located in the Quartz district (drill hole DC97-385) assays 0.02 g/t Au.

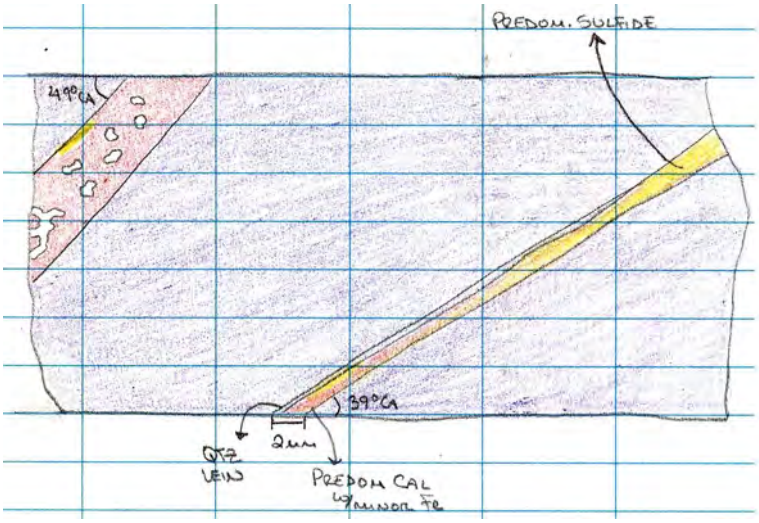

Figure B 5. The vein in the upper left hand corner consists predominantly of calcite with inclusions of quartz and minor sulfides. Vein on the right consists of a mix of sulfides (yellow) and calcite locally rimmed by a quartz stringer veinlet. Sample is located in drill hole DC07-1680 located to the north of Queen; assay runs 0.84 g/t Au.

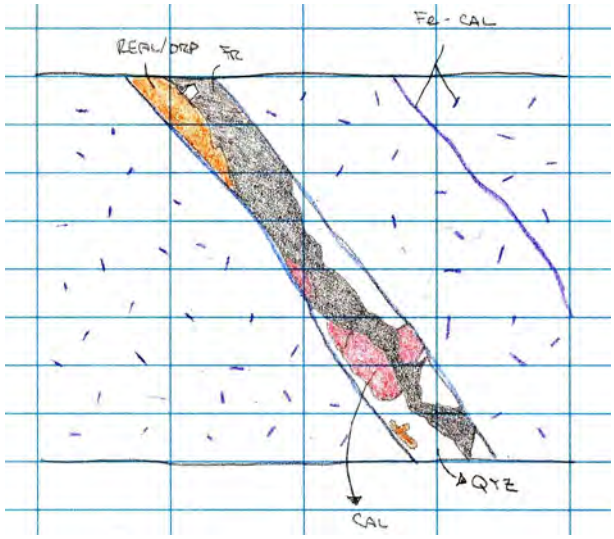

Figure B 6. Sketch of a sample that contains a 7mm quartz- (white) realgar- (orange) calcite (red) vein within an intrusive unit. Phenocrysts and stringer veinlet are stained blue (ferroan). The grey color within the center of the vein represents a major fracture. This sample is located in drill hole DC08-1702 in ACMA and the interval assays at 5.86 g/t Au.

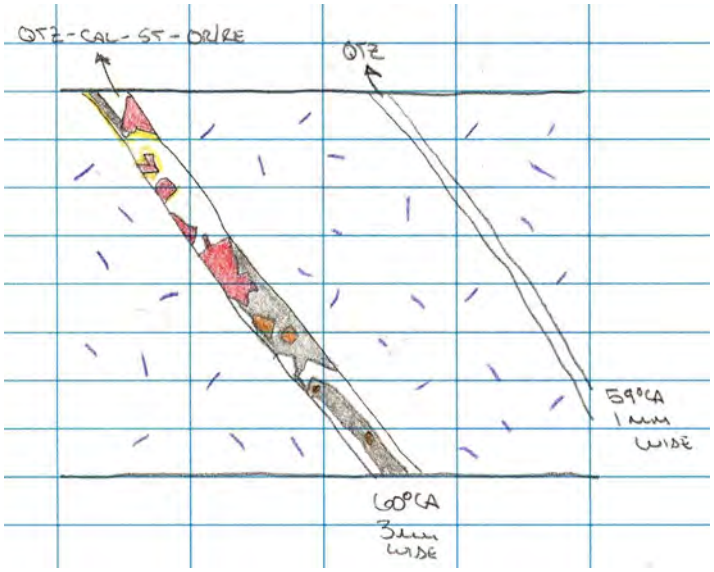

Figure B 7. Sketch of an igneous sample that contains Fe-rich carbonate alteration of the phenocrysts and 2 mm veinlets consisting of quartz-nonferroan carbonate (red)-realgar±stibnite and quartz from left to right. The grey color in the veinlet on the left represents open space. It is interpreted the quartz, which locally occurs with a euhedral shape, precipitated first followed by realgar and/or nonferroan carbonate. The 2 meter sample interval is located in drill hole DC08-1702 in ACMA and assays 11.2 g/t Au.

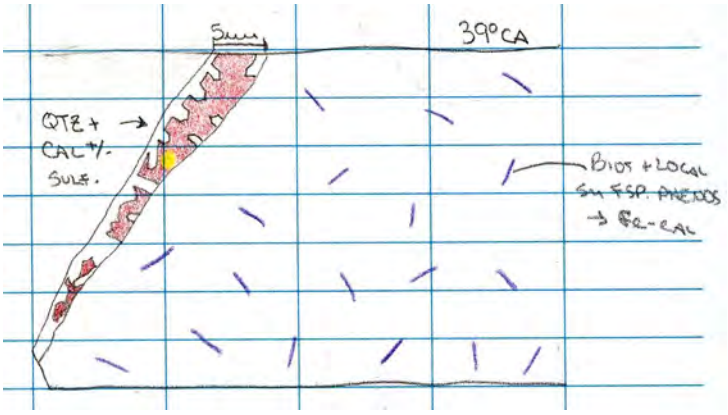

Figure B 8. Sketch showing euhedral quartz grains that line the outer edges of this predominantly nonferroan carbonate 5 mm wide vein. Locally, sulfides (yellow) occur within the carbonate phase. This igneous sample is located in drill hole DC08-1702 in ACMA and assays 5.69 g/t Au.

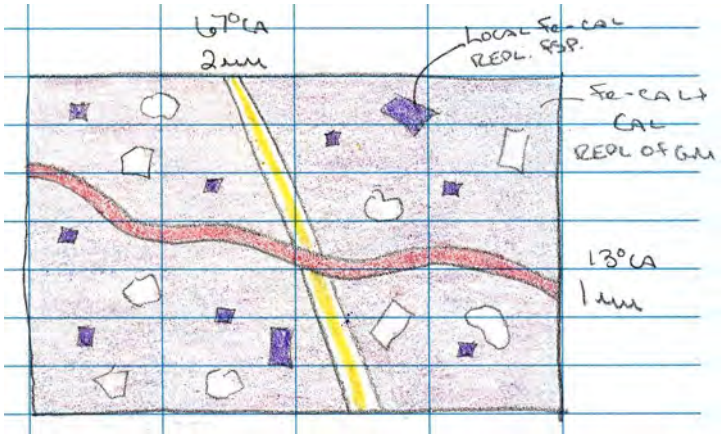

Figure B 9. Sketch showing a quartz-sulfide-rich, 2 mm veinlet (white and yellow) that was cut by a 1mm nonferroan carbonate veinlet (red). The carbonate staining of this igneous host rock is not well represented in this illustration. Purple stain dominates the groundmass representing ankerite. Locally the relict feldspar phenocrysts were replaced by ferroan carbonate (blue). This sample is located in ACMA in drill hole DC08-1693 and assays 0.66 g/t Au.

9 Appendix C: Correlation Models

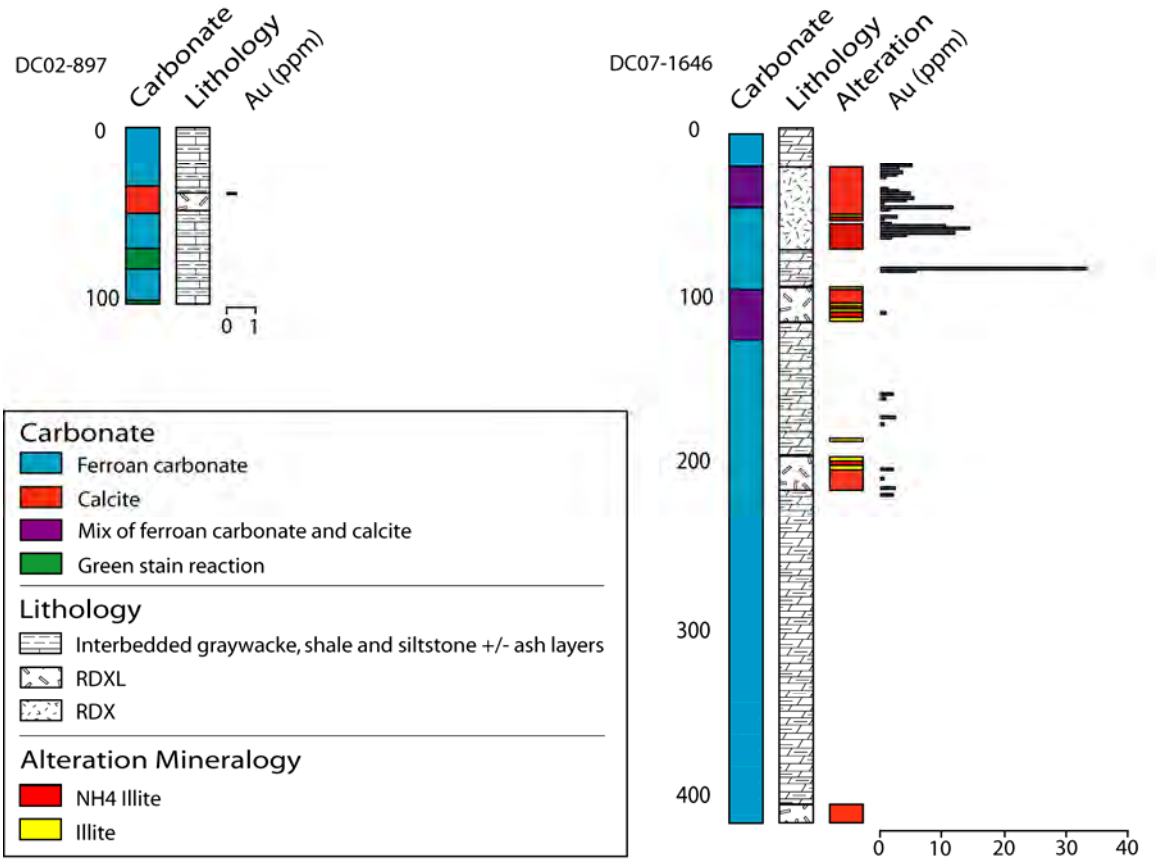

Figure C 1. Diagrams illustrating the correlation between carbonate alteration minerals, host-rock lithology, argillic alteration minerals, where available, and gold in ppm. These drill holes are located on the west side of ACMA.

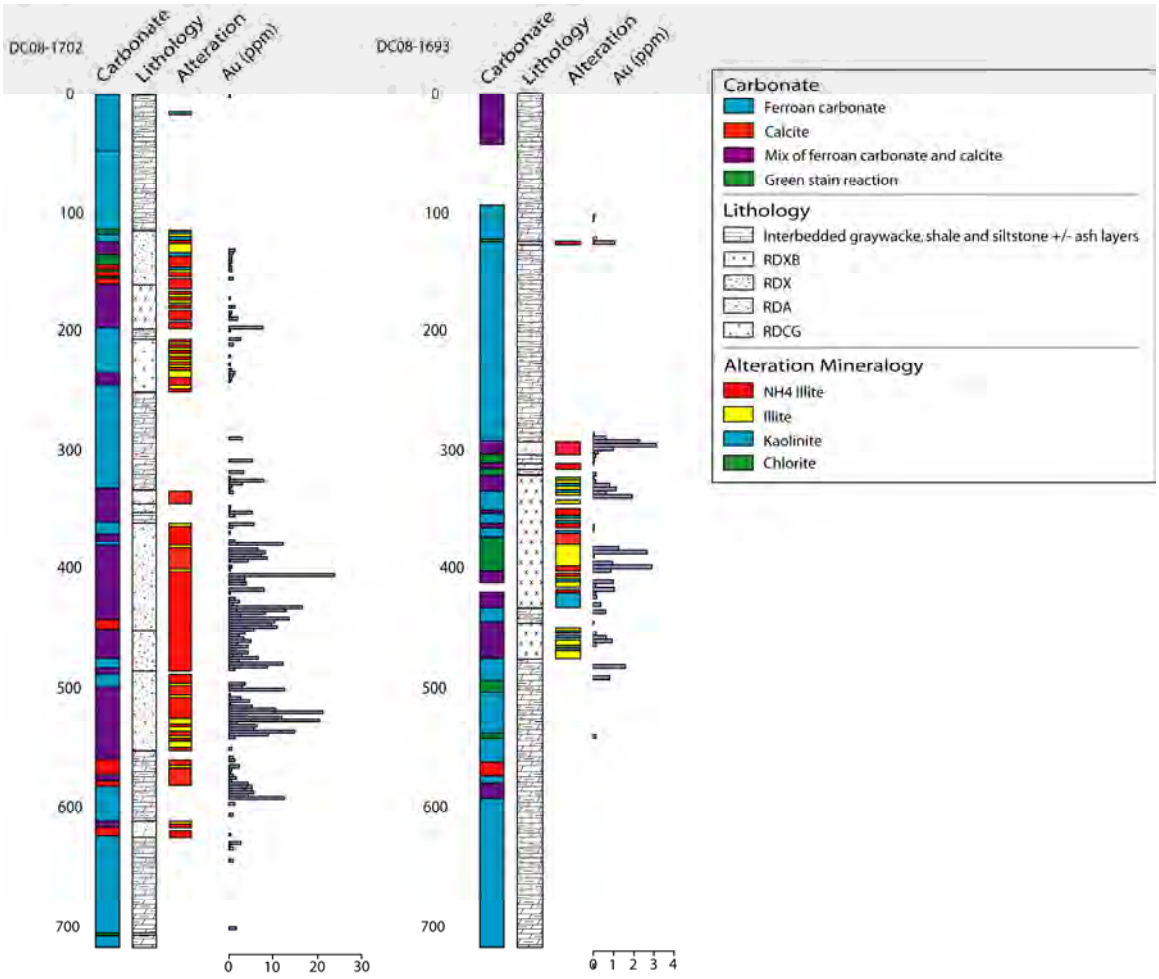

Figure C 2. Diagrams showing the correlation between carbonate alteration minerals, host rock lithology, argillic alteration minerals, and gold in ppm. These drill holes are located in ACMA.

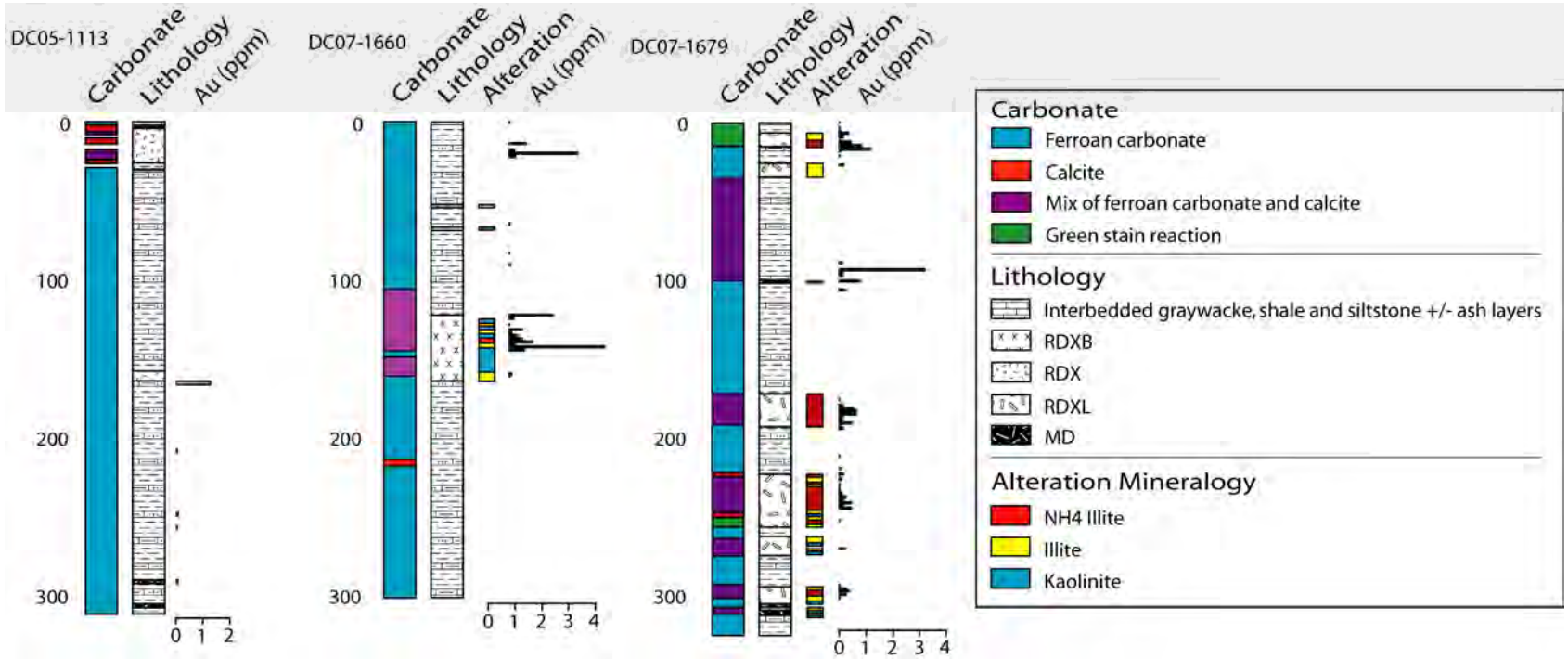

Figure C 3. Drill holes at Queen exhibiting a local association with carbonate alteration minerals, host rock lithology, argillic alteration minerals, where available, and gold in ppm.

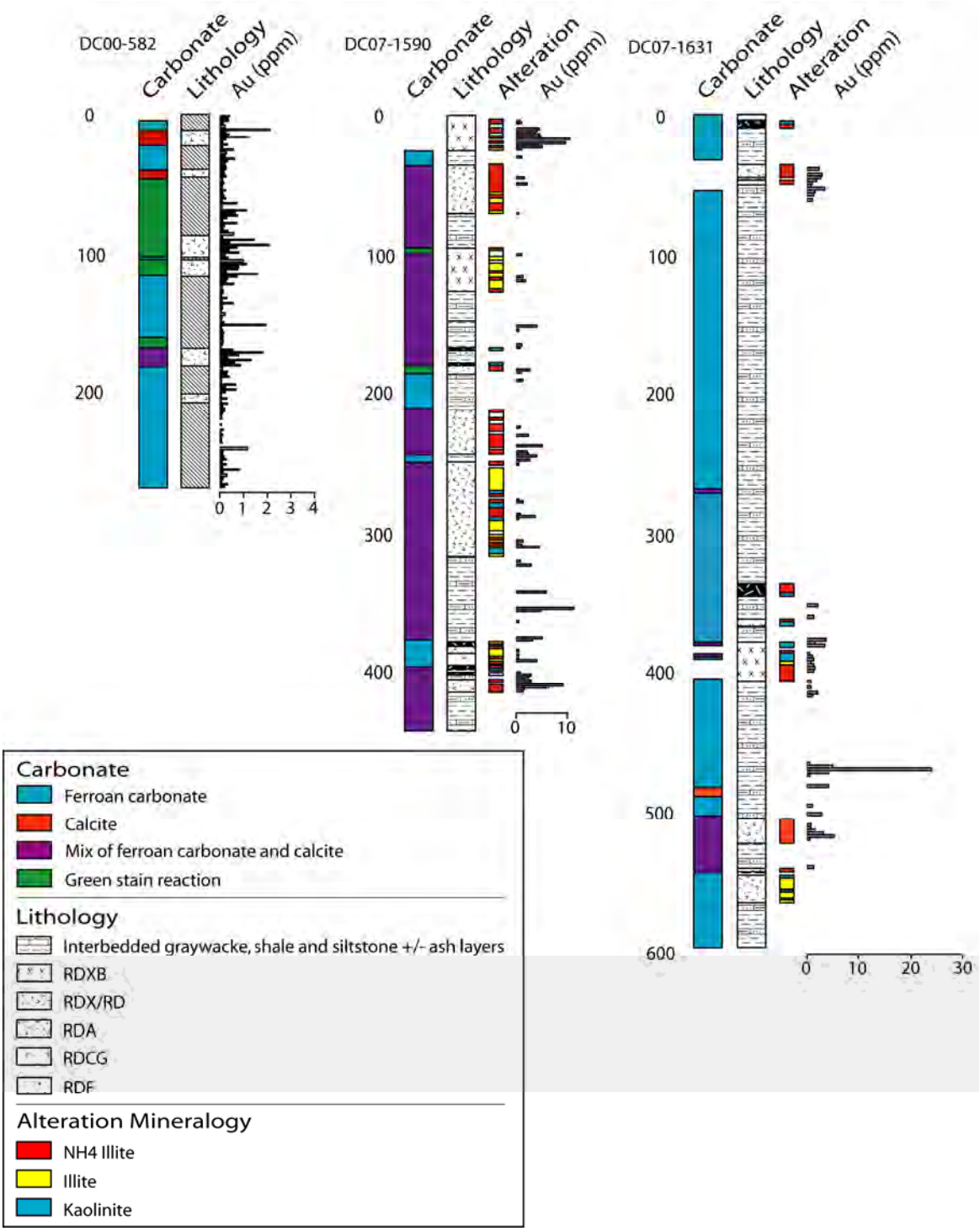

Figure C 4. Drill holes parallel to the intrusive trend extending north of Dome to Lewis. These diagrams show the correlation between carbonate alteration minerals, host rock lithology, argillic alteration minerals, and gold in ppm.

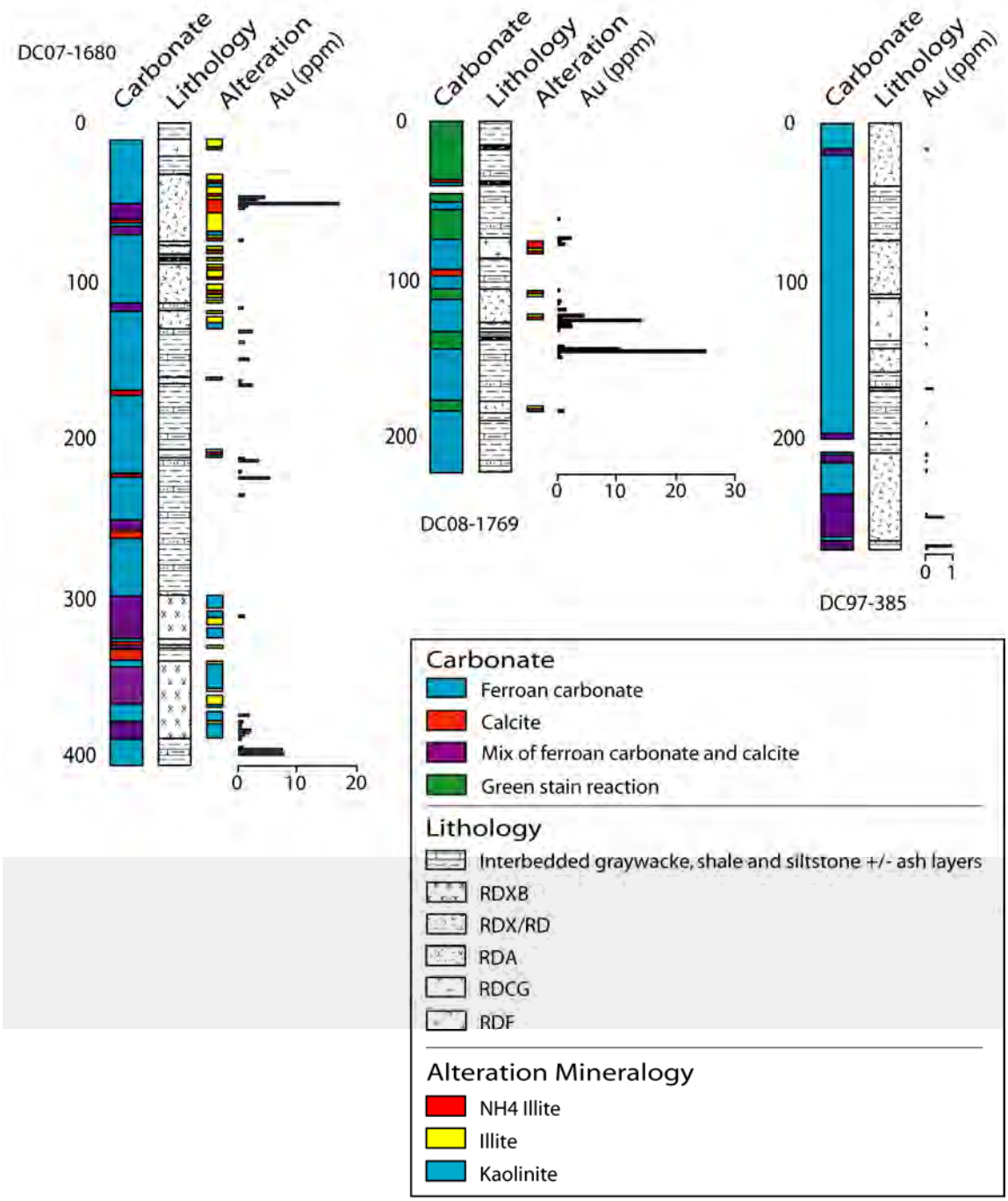

Figure C 5. Drill holes located within the Snow and Quartz districts comparing carbonate alteration minerals, host rock lithology, argillic alteration minerals, where available, and gold in ppm.

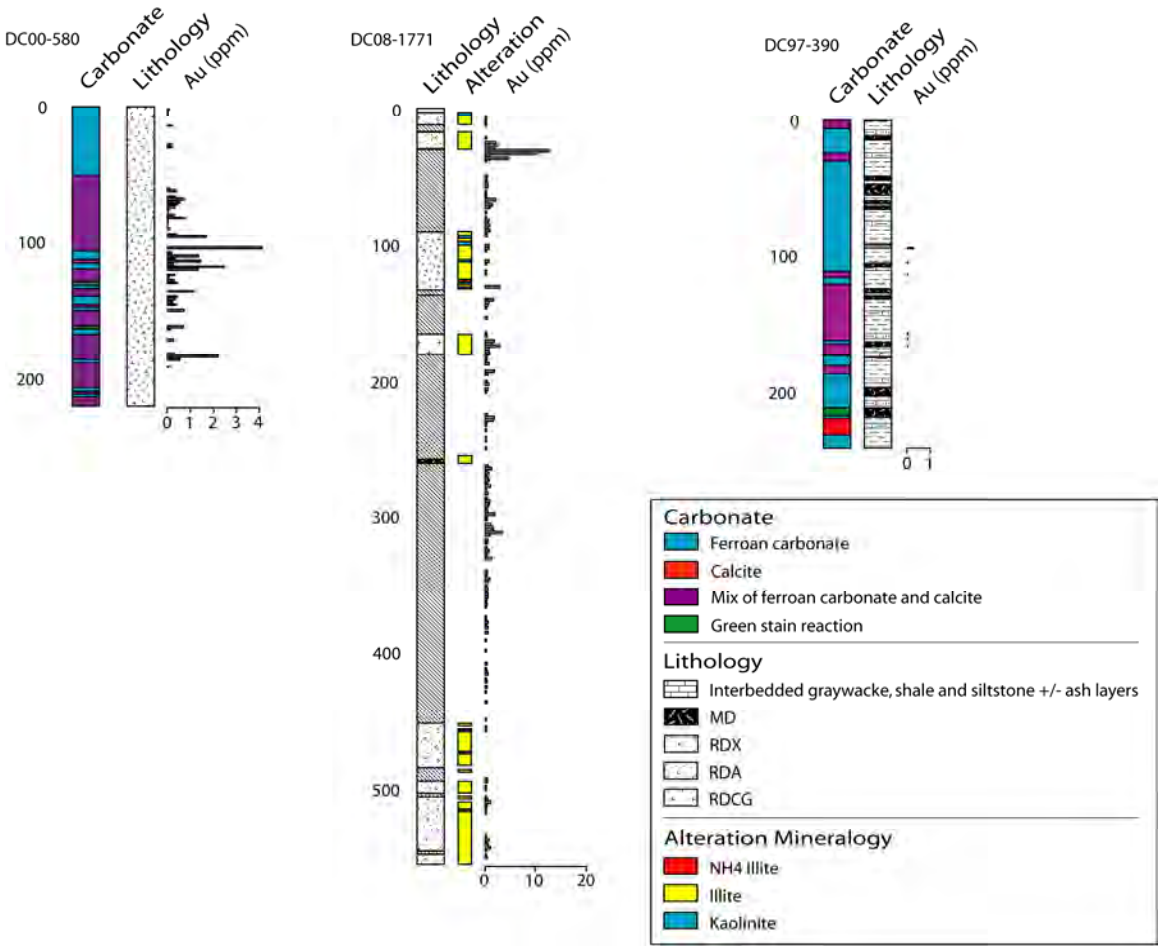

Figure C 6. Drill holes at Dome located on a line perpendicular to the igneous trend showing the comparison between carbonate alteration minerals, where available, host rock lithology, argillic alteration minerals, and gold values in ppm.

10 Appendix D: Ordinary Kriging Methods of Gold and Clay Alteration Maps

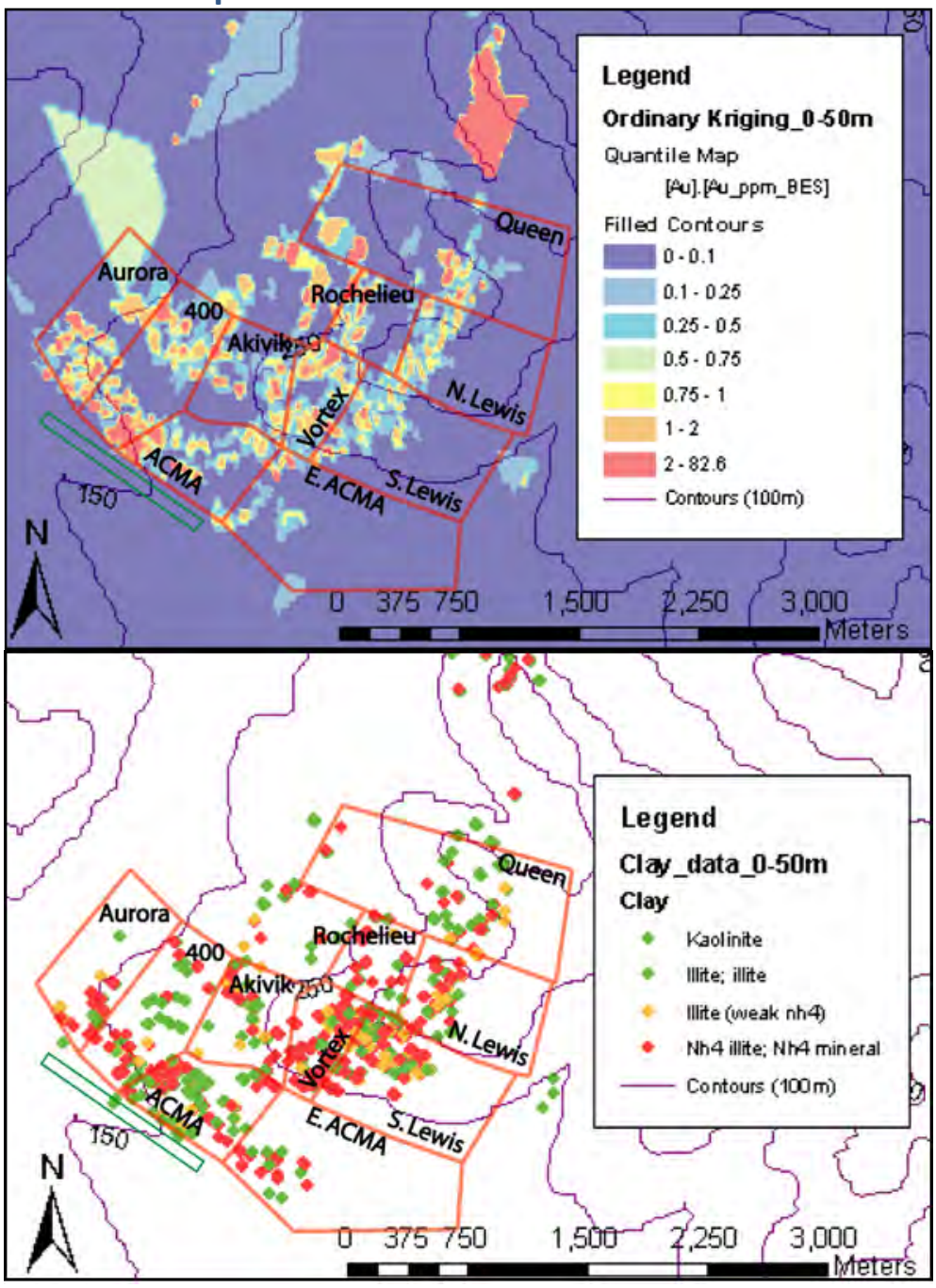

Figure D 1. The top map shows ordinary kriging methods of gold and the bottom map shows clay alteration both at depths of 0 to 50 meter elevations. Models shown in Appendix C illustrate the correlation of Au with NH_4-illite. Piekenbrock *et al.* (2003) defined Au and NH_4-illite trend to the NNE. These maps also demonstrate this trend that appears to not extend beyond the Queen prospect. The ten prospects within the resource area are outlined in red and modified from MacNeil (2009). The NE trend to the west of Rochelieu and north of Akivik and the 400 zones is a relatively new prospect that follows RDXL dikes.

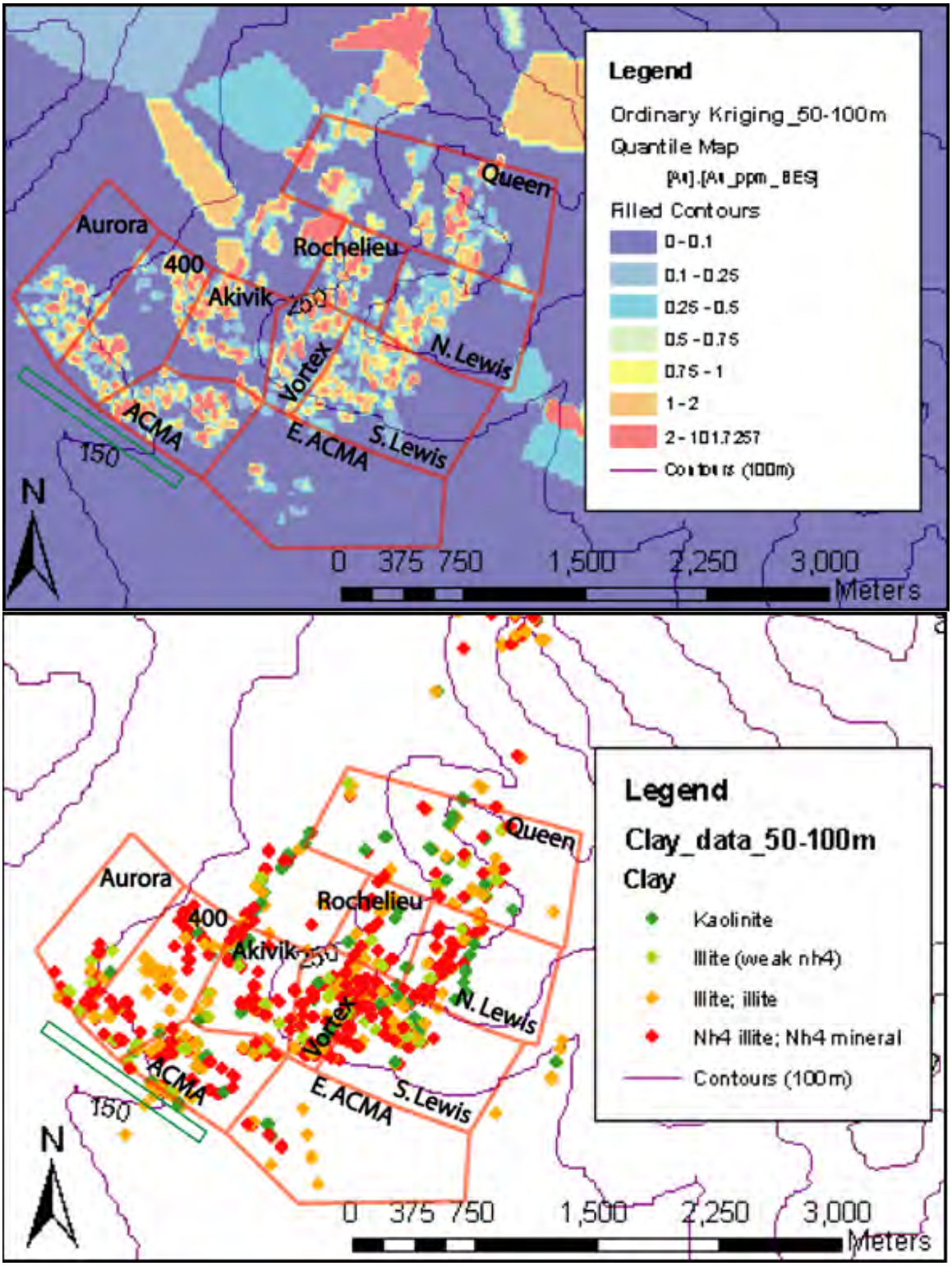

Figure D 2. Ordinary kriging methods of gold and clay alteration maps at elevation 50 to 100 meters showing the correlation between NH_4-illite and Au.

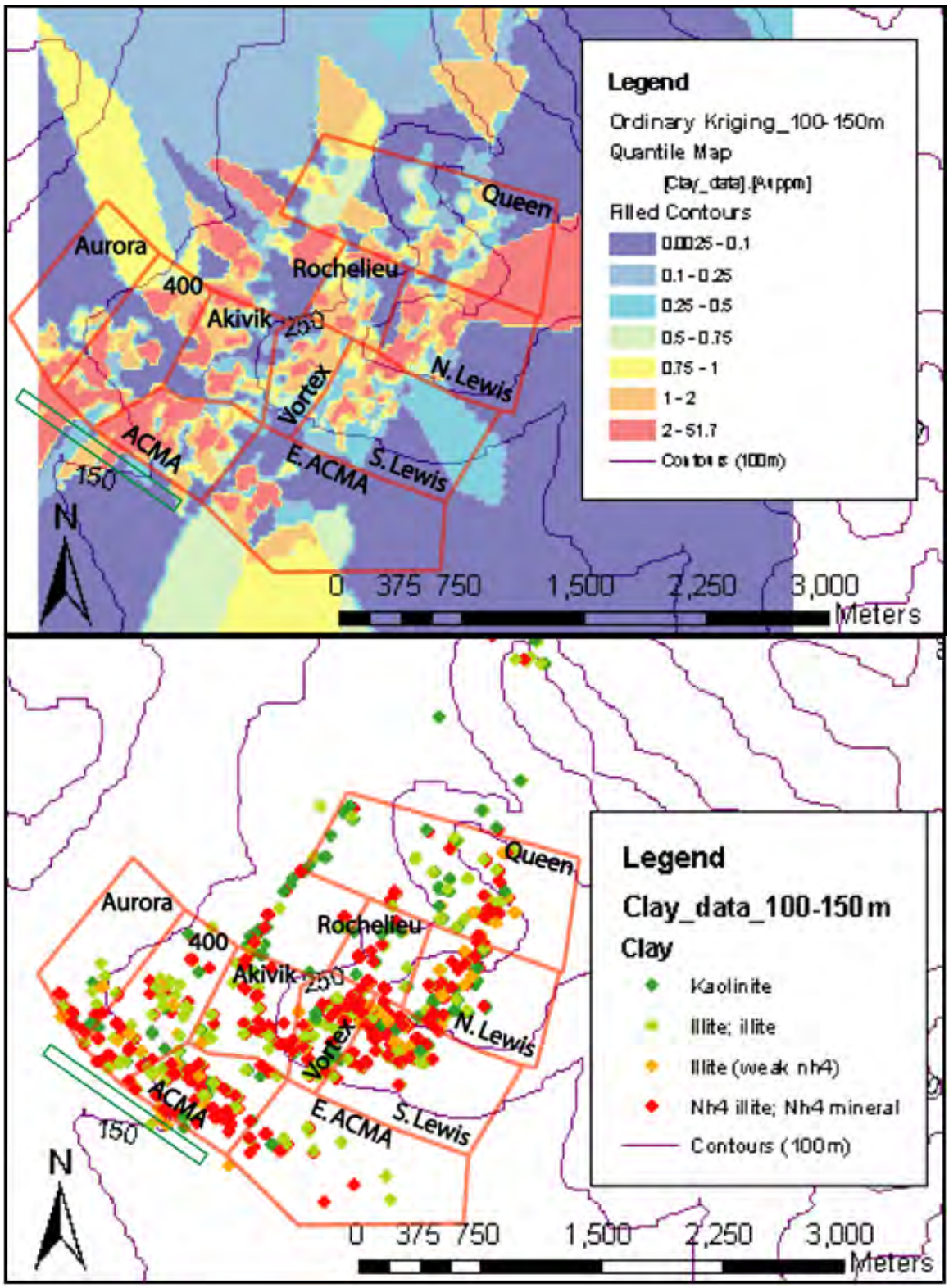

Figure D 3. Maps showing ordinary kriging methods of gold and clay alteration at elevation 100-150 meters.

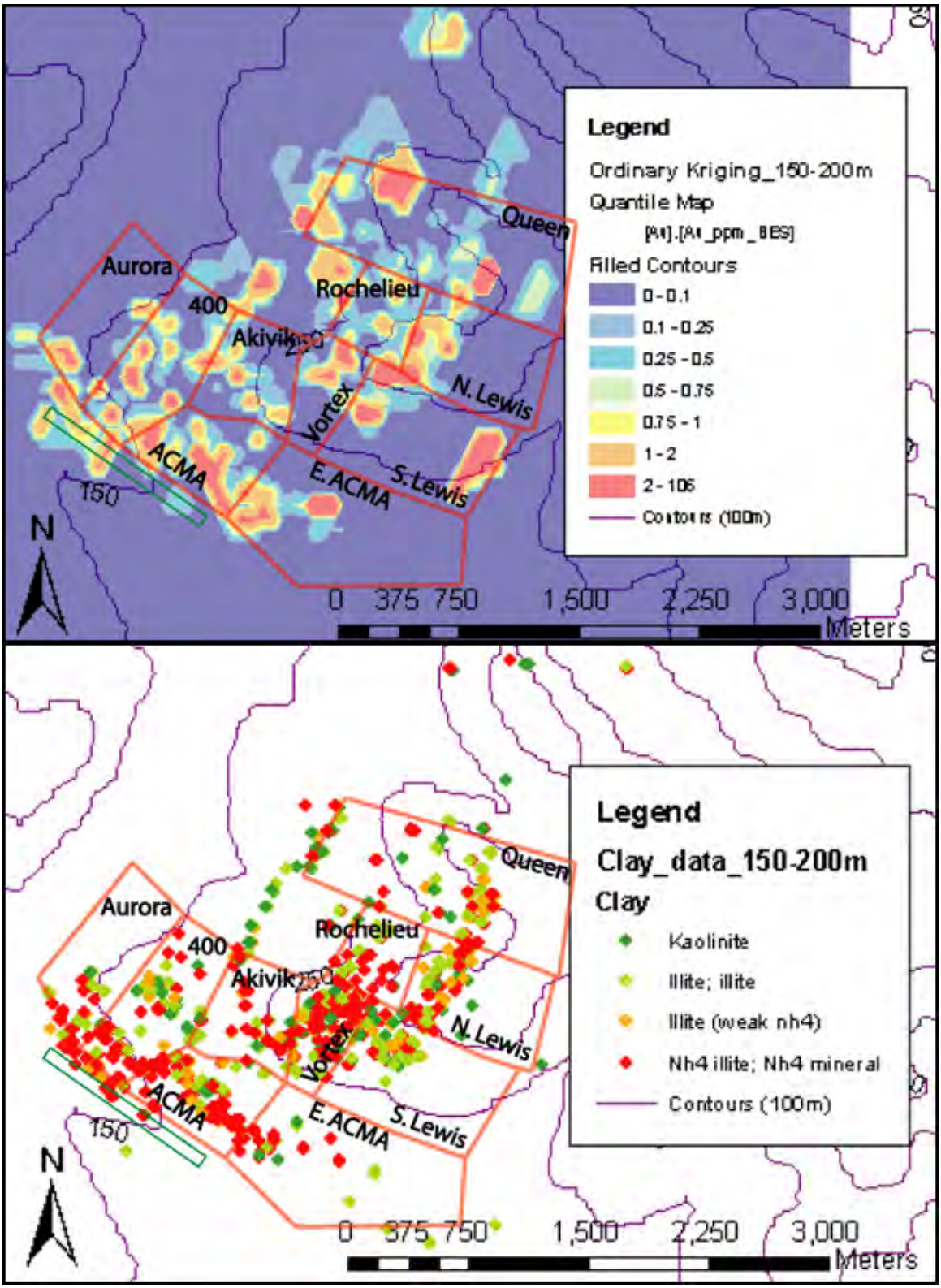

Figure D 4. Elevation maps at 150 to 200 meters showing ordinary kriging of gold and clay alteration.

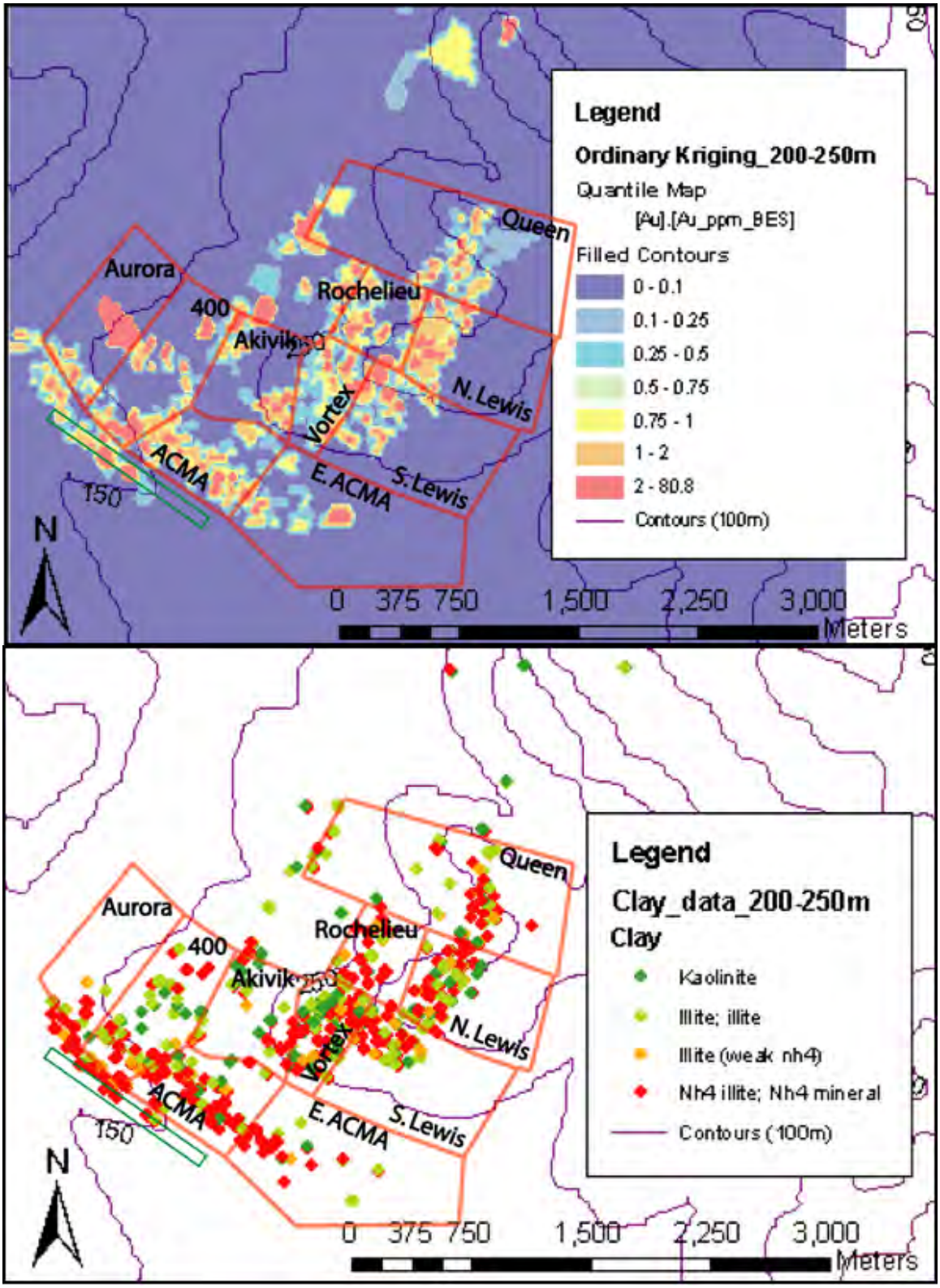

Figure D 5. Maps illustrating the correlation of ordinary kriging methods of gold and clay alteration at depths of 200-250.

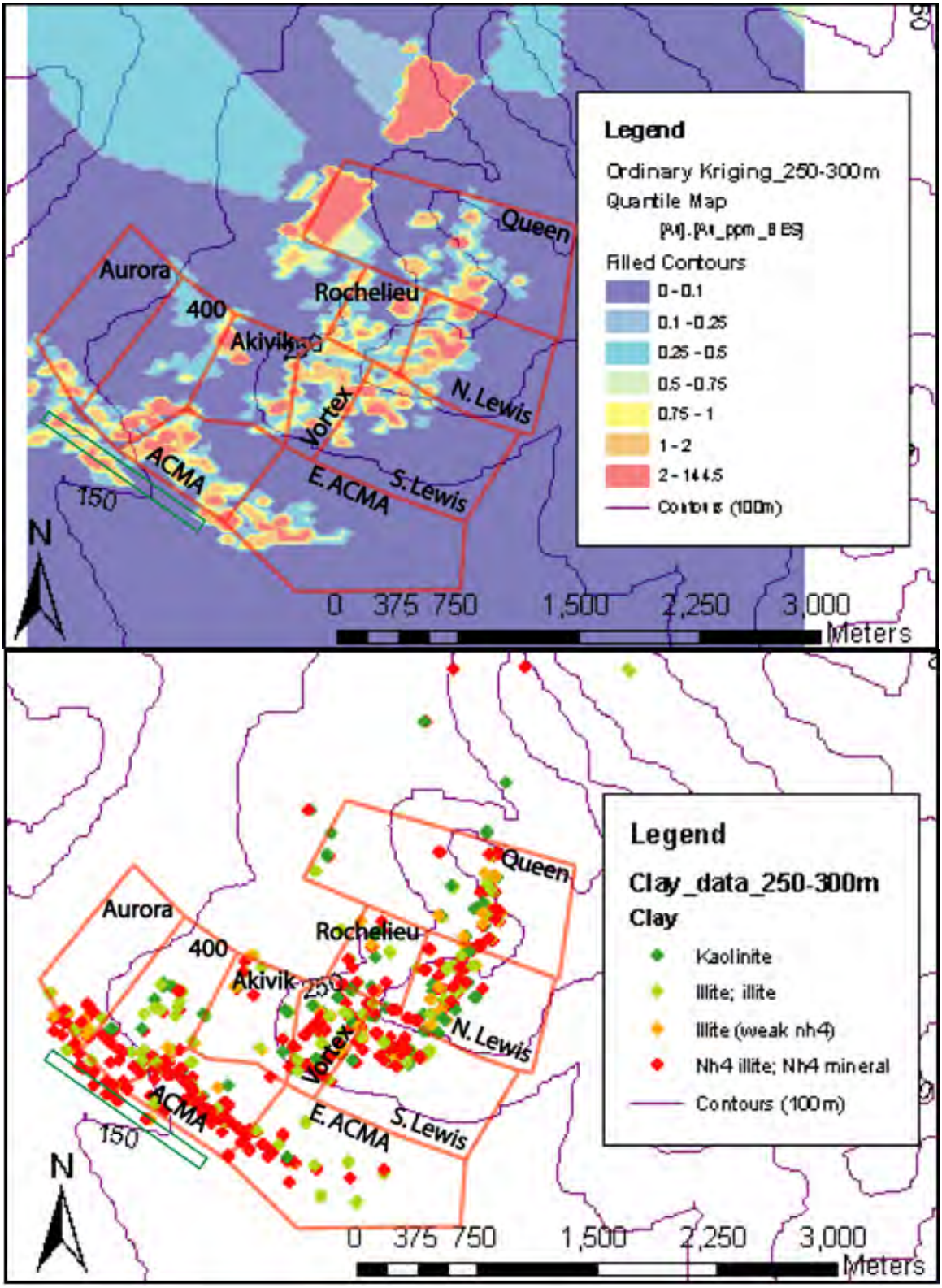

Figure D 6. Maps at depths of 250 to 300 meters showing the association of NH_4-illite and high gold grades.

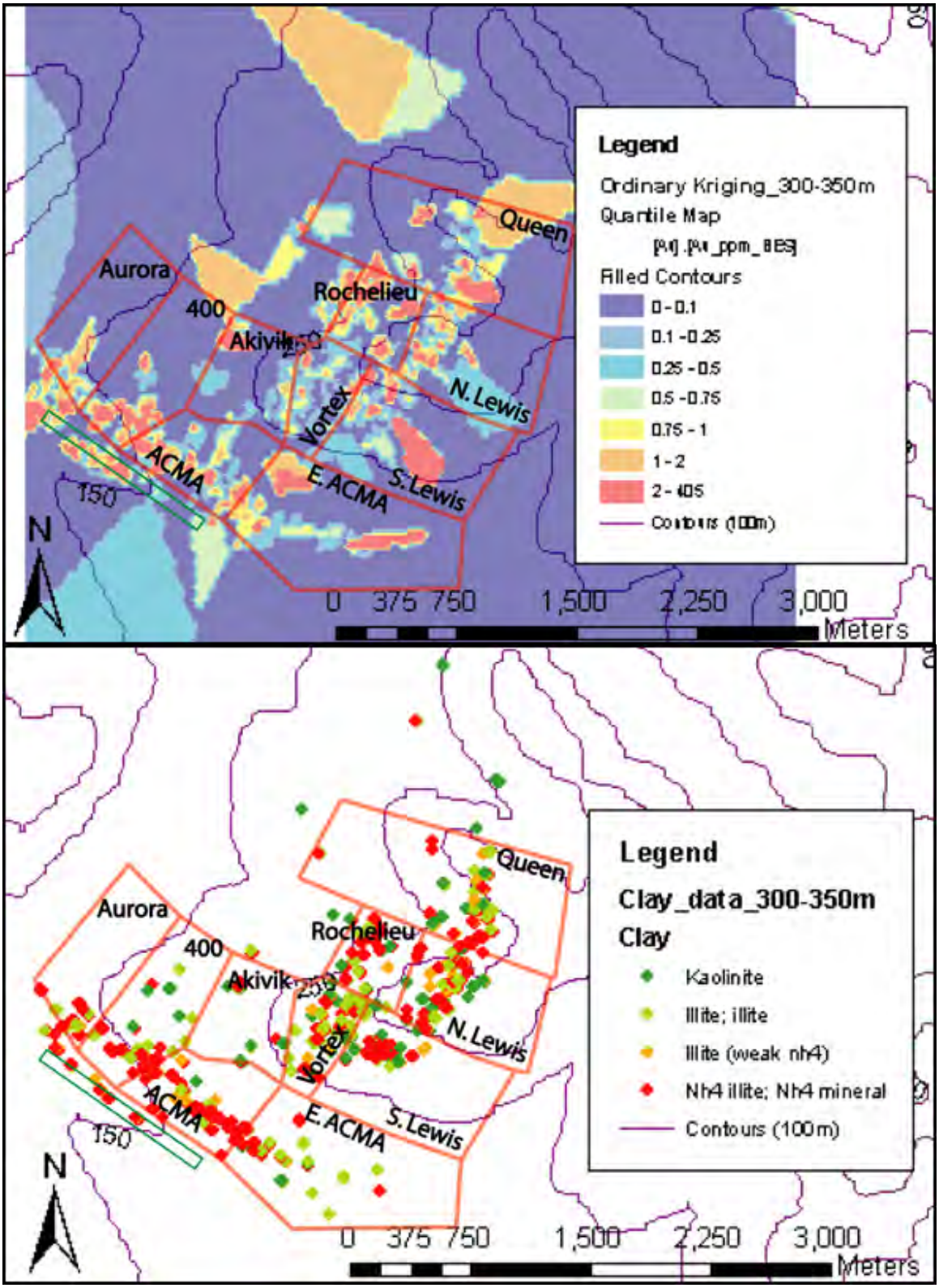

Figure D 7. Maps at depths of 300-350 meters where the amount of gold grade first appears to decrease.

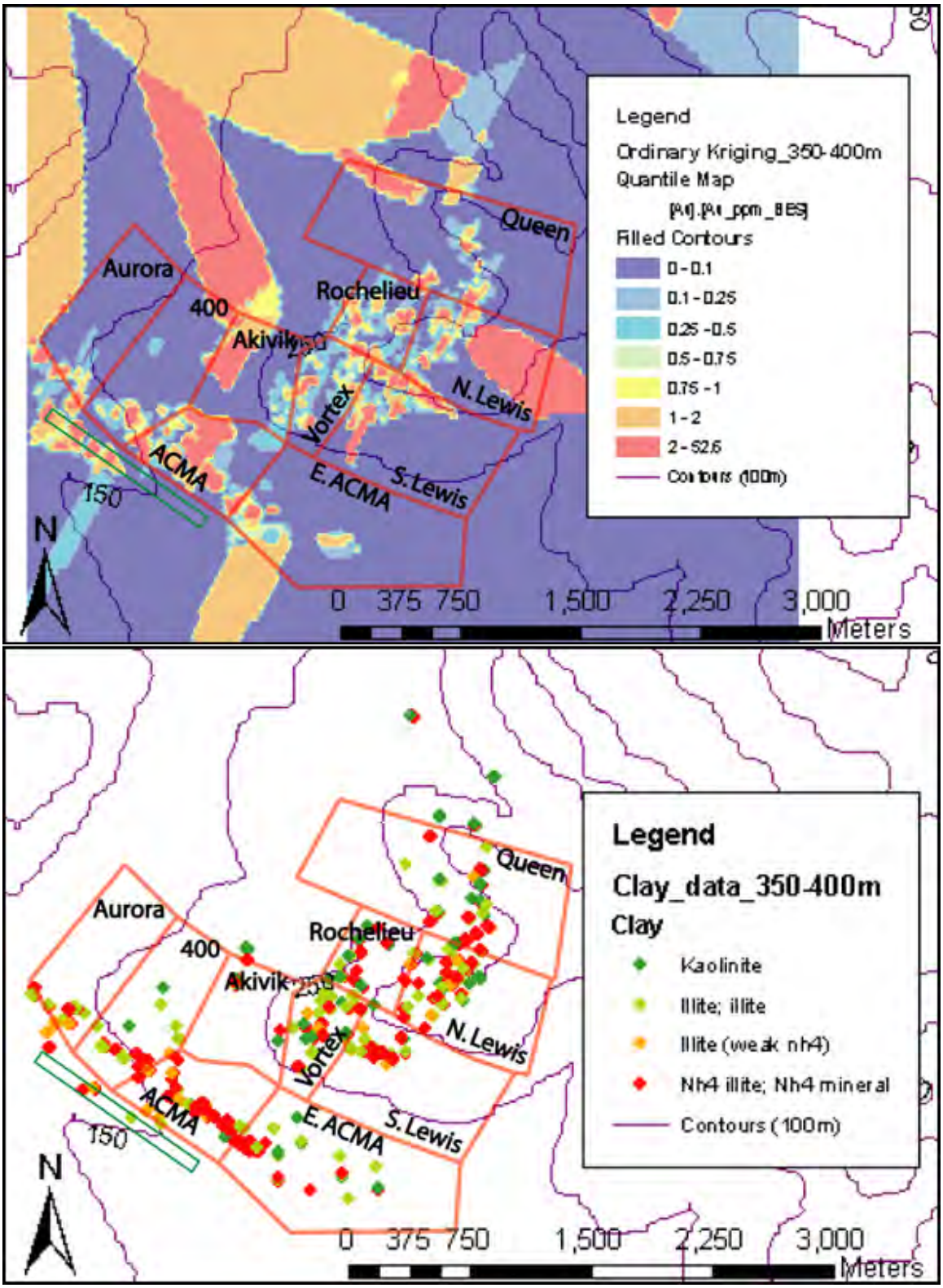

Figure D 8. Maps at depths of 350 to 400 meters illustrating kriging methods of gold and clay alteration minerals. Kriging methods show higher gold grade (red and orange) on the left side of the map; however, drill hole assay results do not agree.

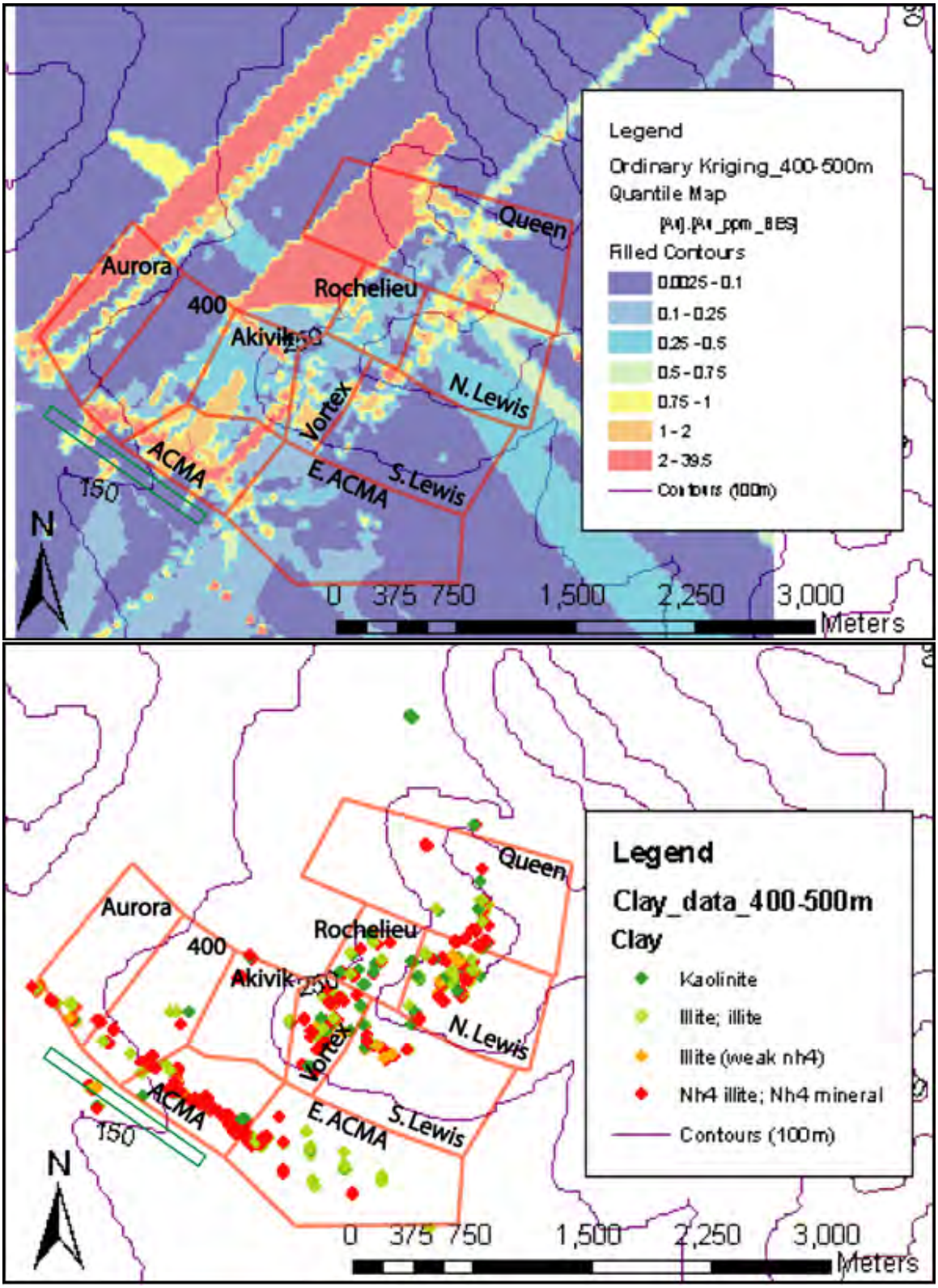

Figure D 9. Maps at depths of 400-450 meters of gold kriging methods and clay alteration minerals. Kriging illustrates strong gold trends extending to the NE and to the SE, which reflect the rhyodacite dikes and sills in the resource area.

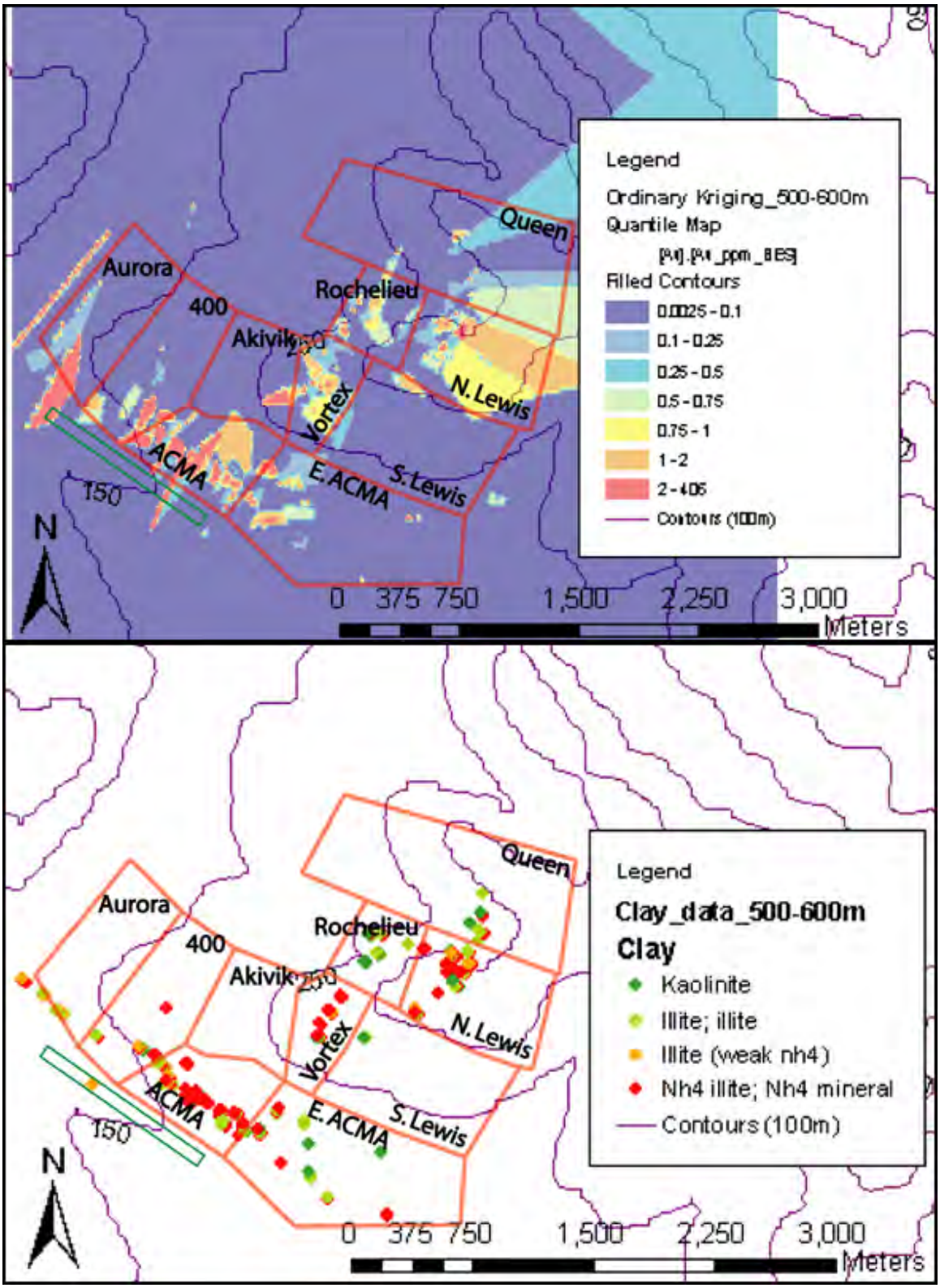

Figure D 10. Maps at depths of 500 to 600 meters showing fewer high gold grade zones trending to the NE and SE.

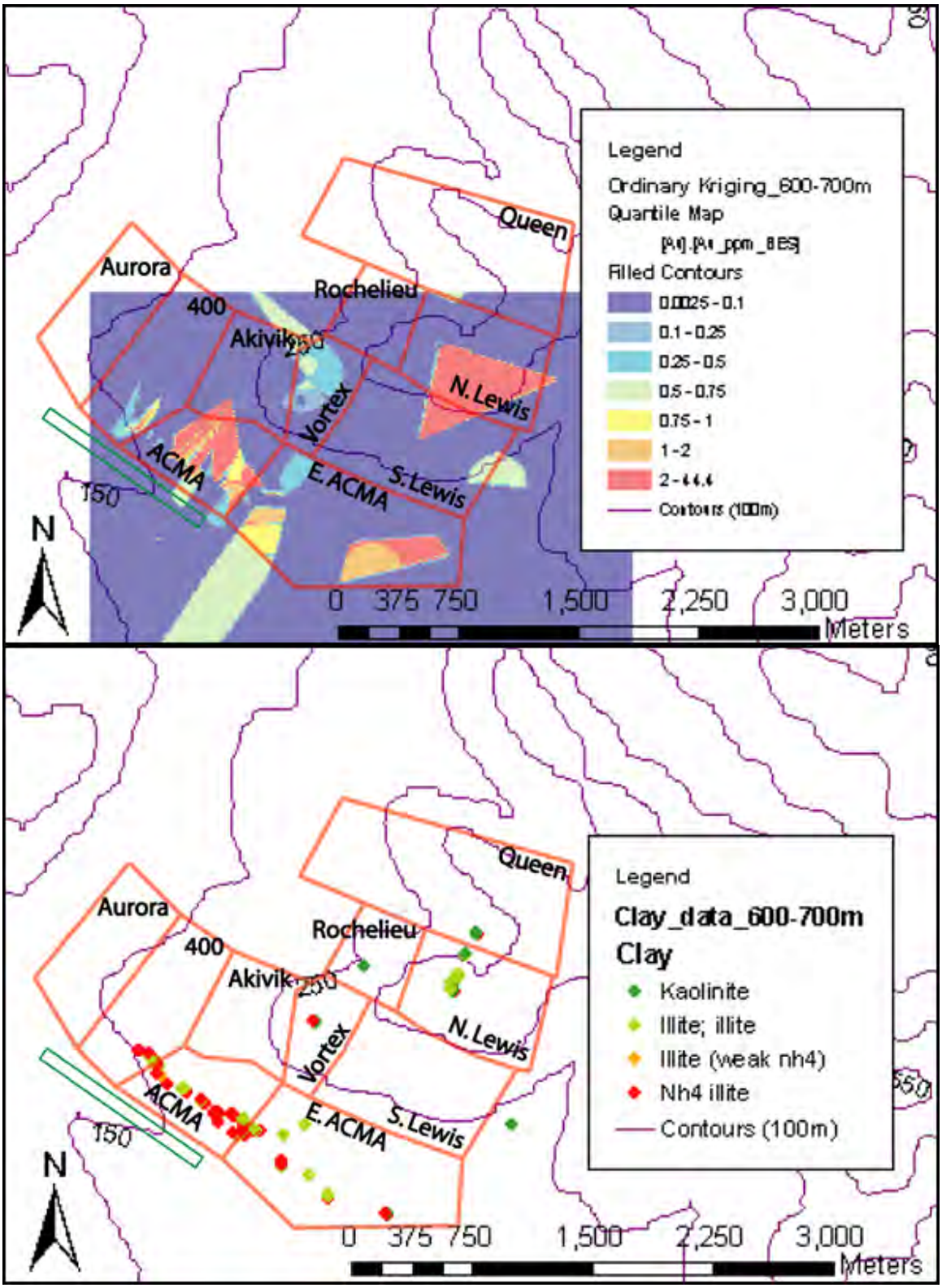

Figure D 11. Fewer drill holes at depths of 600 to 700 meters limits the gold versus clay alteration minerals data comparison available throughout the resource area.

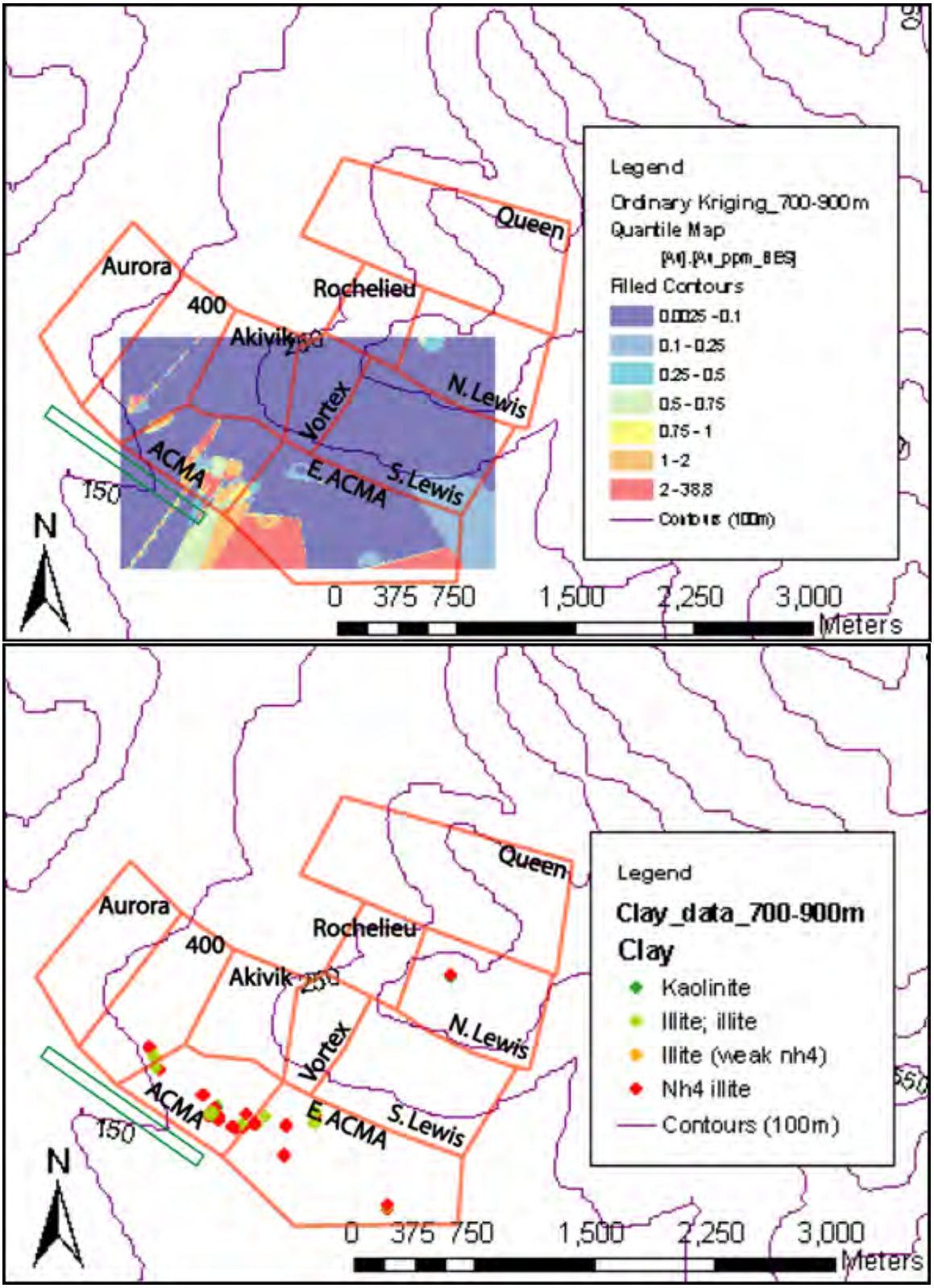

Figure D 12. Maps illustrating gold and clay alteration minerals at depths >700 meters.

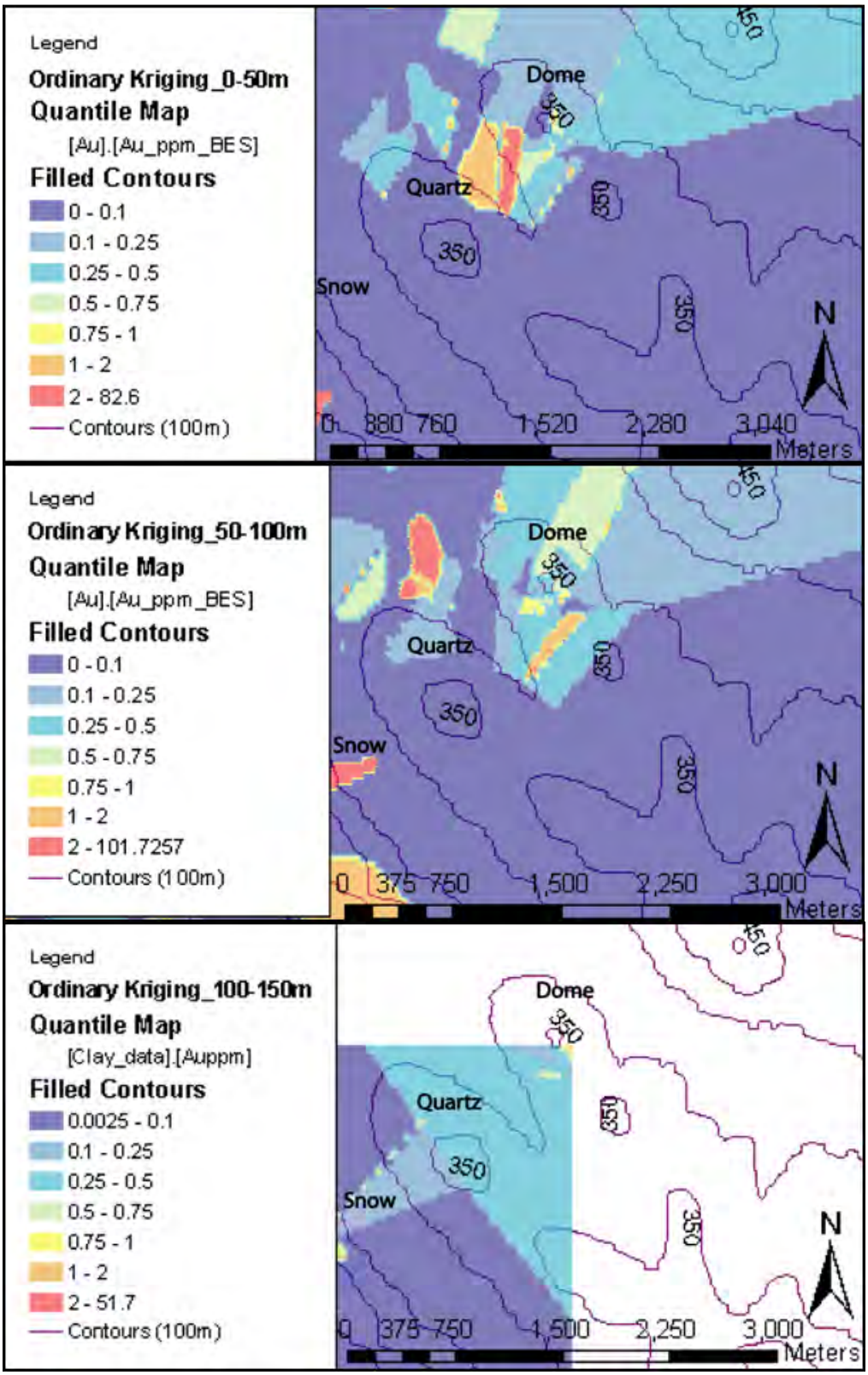

Figure D 13. Maps at depths of 0-50, 50-100, and 100-150 meters illustrating ordinary kriging methods of gold in the Dome, Quartz and Snow districts. Note the patchy gold appearance.

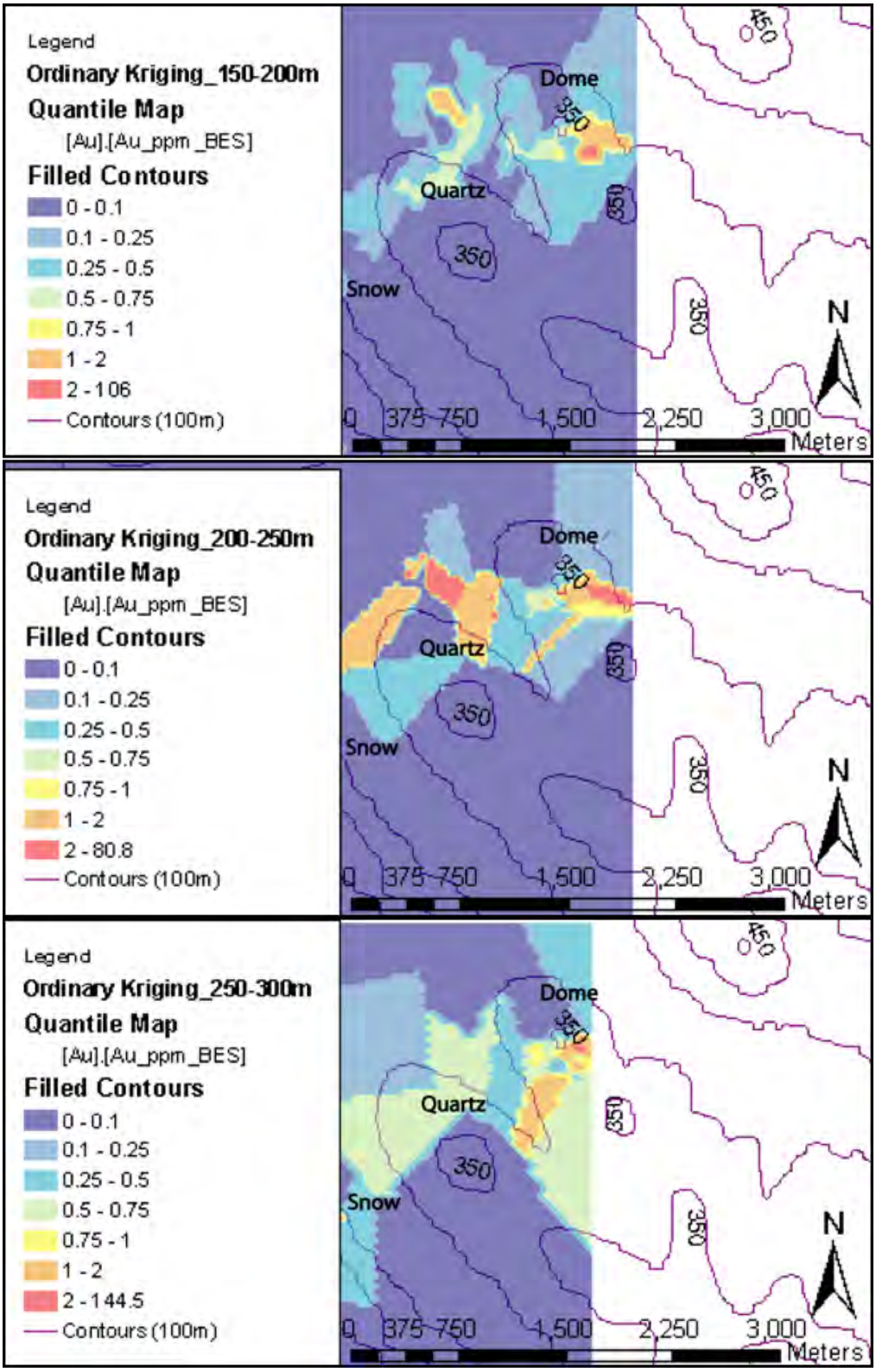

Figure D 14. Maps at depths of 150-200, 200-250, 250-300 meters showing the ordinary kriging methods at the Dome, Quartz, and Snow zones.

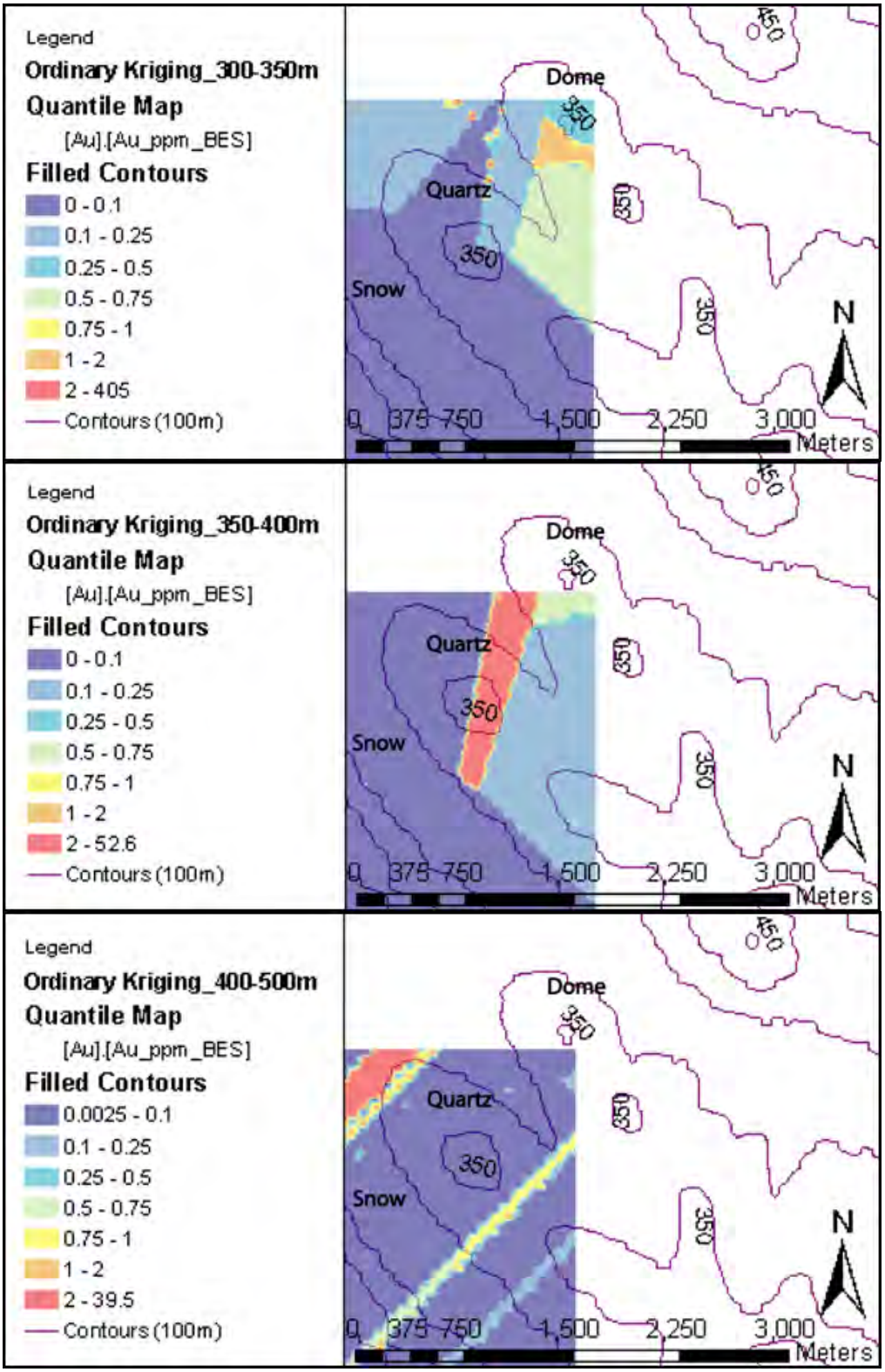

Figure D 15. Maps at 300-350, 350-400, and 400-500 meters showing the random occurrence of gold in the Dome, Quartz, and Snow areas.

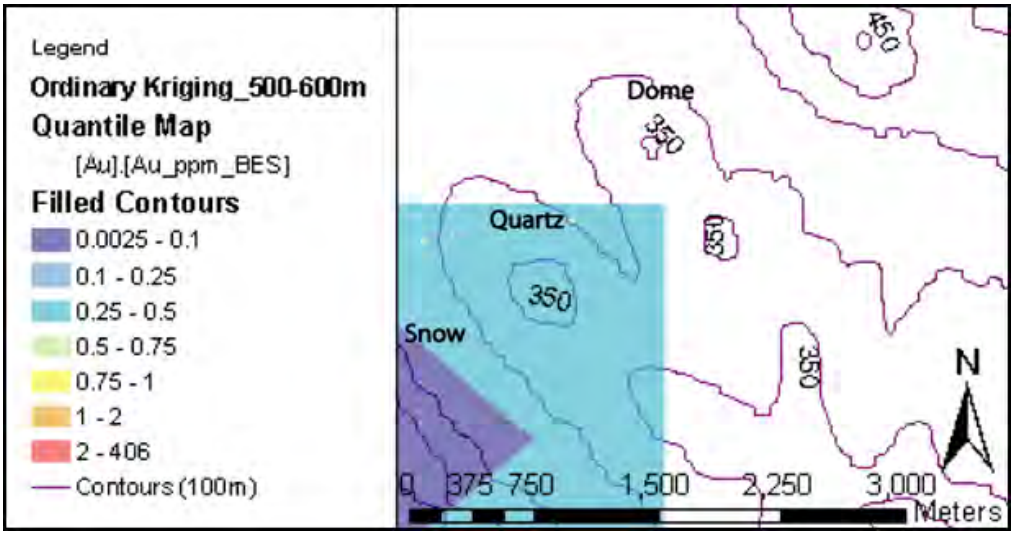

Figure D 16. Ordinary kriging methods of gold at depths of 500 to 600 meters below the surface in the Dome, Quartz, and Snow areas.